1-1-1980

Near-time-optimal stabilization of tank turrets.

David Alfred Haessig

NEAR-TIME-OPTIMAL STABILIZATION OF TANK TURRETS

by

David Alfred Haessig, Jr.

A Thesis

Presented to the Graduate Committee

of Lehigh University

in Candidacy for the Degree of

Master of Science

in

Mechanical Engineering

Lehigh University

1981

This thesis is accepted and approved in partial fulfillment of the requirements for the degree of Master of Science.

11 Dec 1980
(date)

Professor in Charge

Chairman of the Department

ACKNOWLEDGEMENTS

My association with Dr. Forbes T. Brown has been tremendously rewarding in terms of educational content and personal satisfaction. During this association, he has advised and assisted me in this research effort. I have grown to appreciate the expertise which accompanies his guidance and am indebted for the time and interest he has invested in me. For this I offer him my sincere thanks.

I am also grateful to Dr. Stanley H. Johnson for his confidence in me which was of great help during the preliminary stages of the project.

Financial support from the U.S. Army under contract DAAK 10-78-C-0368 is gratefully acknowledged.

The patience of my wife and parents who encouraged me in spite of the time taken from them is very much appreciated. My thanks to all of them for their support.

TABLE OF CONTENTS

List of Figures vi

List of Tables ix

Abstract 1

1. INTRODUCTION 3

2. SYSTEM MODELING 7

2.1 Reference Frames 8
2.2 Hull Equations 8

2.21 Angular Momentum Computations 13
2.22 Position Vectors 15
2.23 Acceleration Calculations 17

2.3 Matrix Formulation 20
2.4 Turret and Gun Equations 22
2.5 Models of the Hydraulic Gun Drives 28

2.51 Conventional Controllers 30

2.6 Model Linearization 35

3. TIME OPTIMAL CONTROL 40

3.1 The Switching-Time Method 45
3.2 Application to the Hydraulic System 47

3.21 Elevation Time Optimal Control 50
3.22 Traverse Time Optimal Control 55

3.3 A Nonlinear Gun Position Observer 59
3.4 Application to the Electric System 67

3.41 Incorporation of Measurement Noise 74

4. RESULTS 78

4.1 Hydraulic System with Conventional Control 80
4.2 Hydraulic System with Time Optimal Control 83
4.3 Electric System with Time Optimal Control 90

5. DISCUSSION 105

5.1 Conclusions and Recommendations 112

List of References 118

Appendix A: Symbol List and Parameter Values 119

Appendix B: Hydraulic System with Stochastic Optimal Control 128

Appendix C: Electric System with Conventional Control 130

Appendix D: Electric System with Stochastic Optimal Control 132

Vita 136

LIST OF FIGURES

1.1	Nominal Gun Position	5
2.1	Main Reference Frames	9
2.2	Rotating Reference Frames	10
2.3	Turret-Gun CG (D) and Turret CG(B) Positions	24
2.4	Elevation Hydraulic Gun Drive System	31
2.5	Traverse Hydraulic Gun Drive System	32
2.6	Simplified Conventional Elevation Controller	33
2.7	Conventional Traverse Time Optimal Controller	34
2.8a	Lim Function	37
2.8b	Pressure Differential Magnitude, P_L, and P_{LMN}	37
2.9	Simplified Elevation Hydraulic Gun Drive System	39
3.1	Bang-bang Control	42
3.2	Switching Curve	44
3.3	Elevation Gun Dynamics - Hydraulic Drive	51
3.4	Elevation Time Optimal Control	56
3.5	Nonlinear Observer Reference Frames	61
3.6	Nonlinear Gun Position Observer	65
3.7	Elevation Gun Dynamics - Electric Drive	72
3.8	Traverse Gun Dynamics - Electric Drive	73
4.1	Right-Side Ground Input	79
4.2	Hull Pitch and Roll Angles, Conventional Control, Linear and Nonlinear Models, Hydraulic Gun Drives	81

4.3	Hull Yaw Angle and Vertical Position, Conventional Control, Linear and Nonlinear Models, Hydraulic Gun Drives	82
4.4	Traverse (VIN) and Elevation (ELVV) Controller Outputs, Conventional Control, Nonlinear Model, Hydraulic Gun Drives	84
4.5	Absolute Traverse and Elevation Pointing Errors, Conventional Control, Linear and Nonlinear Models, Hydraulic Gun Drives	85
4.6	Elevation Controller Output, Time Optimal Elevation Control, 10 V. Saturation Voltage, Hydraulic Gun Drives	86
4.7	Absolute Traverse and Elevation Pointing Errors, Time Optimal Elevation Control, 10 V. Saturation Voltage, Hydraulic Gun Drives	88
4.8	Absolute Traverse and Elevation Pointing Errors, Time Optimal Elevation Control, 1 V. Saturation Voltage, Hydraulic Gun Drives	89
4.9	Elevation Controller Output, Time Optimal Control, Noise-free Case, Electric Gun Drives	92
4.10	Traverse Controller Output, Time Optimal Control, Noise-free Case, Electric Gun Drives	93
4.11	Absolute Traverse and Elevation Pointing Errors, Time Optimal Control, Noise-free Case, Electric Gun Drives	95
4.12	Traverse and Elevation Rate Gyro Measurements, Time Optimal Control, Noise-free Case, Electric Gun Drives	96
4.13	Hull Pitch and Roll Angles, Time Optimal Control, Electric Gun Drives	98
4.14	Hull Yaw Angle and Vertical Position, Time Optimal Control, Electric Gun Drives	99

4.15	Elevation Controller Output, Time Optimal Control, Noise-added Case, Electric Gun Drives	100
4.16	Traverse Controller Output, Time Optimal Control, Noise-added Case, Electric Gun Drives	101
4.17	Absolute Traverse and Elevation Pointing Errors, Time Optimal Control, Noise-added Case, Electric Gun Drives	102
4.18	Traverse and Elevation Rate Gyro Measurements, Time Optimal Control, Noise-added Case, Electric Gun Drives	103
B1	Traverse (VIN) and Elevation (ELVV) Controller Outputs, Stochastic Optimal Control, Hydraulic Gun Drives	128
B2	Absolute Traverse and Elevation Pointing Errors, Stochastic Optimal Control, Hydraulic Gun Drives	129
C1	Traverse (TQEL) and Elevation (TQEL) Controller Outputs, Conventional Control, Electric Gun Drives	130
C2	Absolute Traverse and Elevation Pointing Errors, Conventional Control, Electric Gun Drives	131
D1	Hull Pitch and Roll Angles, Stochastic Optimal Control, Electric Gun Drives	132
D2	Hull Yaw Angle and Vertical Position, Stochastic Optimal Control, Electric Gun Drives	133
D3	Traverse (TQTR) and Elevation (TQEL) Controller Outputs, Stochastic Optimal Control, Electric Gun Drives	134
D4	Absolute Traverse and Elevation Pointing Errors, Stochastic Optimal Control, Electric Gun Drives	135

LIST OF TABLES

1. Measurement-Noise-Sequence Variances 77

2. Summary Comparison of Control Systems 104

Abstract

Modern control theory is applied to a dynamic model of the M60 tank to investigate possible enhancement of its fire-on-the-move capability. Conventional analog controllers based on classical control theory, currently in use, are inadequate for firing while moving. Recent studies directed toward the application of stochastic optimal control have shown considerable theoretical potential, but have not addressed certain important practical problems [2]. In this thesis, a computationally practical control scheme is presented which attains high performance using simple time optimal controllers and an atypical nonlinear observer.

Conventional, stochastic optimal, and time optimal control schemes are compared on the basis of their ability to minimize deviations from the desired gun position. In each case, electric and hydraulic gun drive systems are considered. When employing the electric gun drives, the gun pointing errors of the conventional case are reduced by a factor of 15 with the stochastic optimal scheme and between factors of 42 and 16 with the time optimal scheme. The smaller time optimal reduction factor occurs when significant measurement noise is added. Similar but not so impressive results are achieved when employing the hydraulic gun drives.

The proposed time optimal control scheme eliminates the problems inhibiting the use of the stochastic optimal control scheme by assuming simple models which neglect hull motion. Consequently, only a few state variables are needed for control. A nonlinear observer which estimates only the gun pointing errors is developed for this purpose; other needed variables are directly measured. This time optimal scheme is fully implementable, but at a possibly excessive cost in terms of wear,noise and power consumption. A hybrid control scheme is suggested which combines the stochastic and time optimal schemes to eliminate their individual drawbacks while retaining high performance.

1. Introduction

Conventional on-board stabilization systems for the M60 tank fail to provide the ability to fire accurately while on the move. The absolute pointing angle of the main gun is disturbed by the motion of the tank over rough ground. An ideal stabilization system would exert control torques on the gun to precisely cancel out the disturbance torques. Thus the gunner would not need to compensate for changes in the gun orientation, and the on-board balistic computer, which is designed to keep the gun of a moving tank on target, would perform its job unhindered. Modern optimal control methods have been applied in previous related studies concerned with the design of a disturbance accommodating stabilization system of this type [1,2]. These studies have produced a linear-quadratic stochastic optimal control scheme which dramatically improves the performance of the stabilization system over that of the conventional control, but requires a presently impractical increase in control system complexity. The object of this study is to develop a simple, computationally practical control scheme using time optimal control theory, and to investigate its potential for improved fire-on-the-move performance.

The proposed time optimal control scheme is compared with the stochastic optimal and conventional control schemes through

simulation on a digital computer, using the dynamic model of the tank derived in Chapter 2. In all cases the tank is moving straight ahead at 8.5 m/s (~19 mph) over rough terrain that is about as severe as a very bumpy dirt road (see Fig. 4.1). The position of the gun is initiated at 30 degrees in absolute elevation and 45 degrees in absolute traverse as shown in Fig. 1.1. Gun pointing errors are measured as deviations from this starting position.

The application of time optimal and stochastic optimal control theory leads to control schemes which are very different, both internally and operationally. For example, the stochastic optimal scheme contains a dynamic model of the tank and ground contour under the tread, enabling it to predict the current and future disturbances plus the gun pointing errors and select an accommodating proportional control. The resulting performance is very impressive, much better than conventional control, but the control system is very complex, making the stochastic optimal control scheme practically unrealizable. The time optimal scheme takes another approach, seeking not to eliminate the disturbance torques but to correct the gun position errors which result by using maximum-effort control. It contains a dynamic model of the turret and gun only, which neglects the motion of the hull. Therefore, detailed knowledge

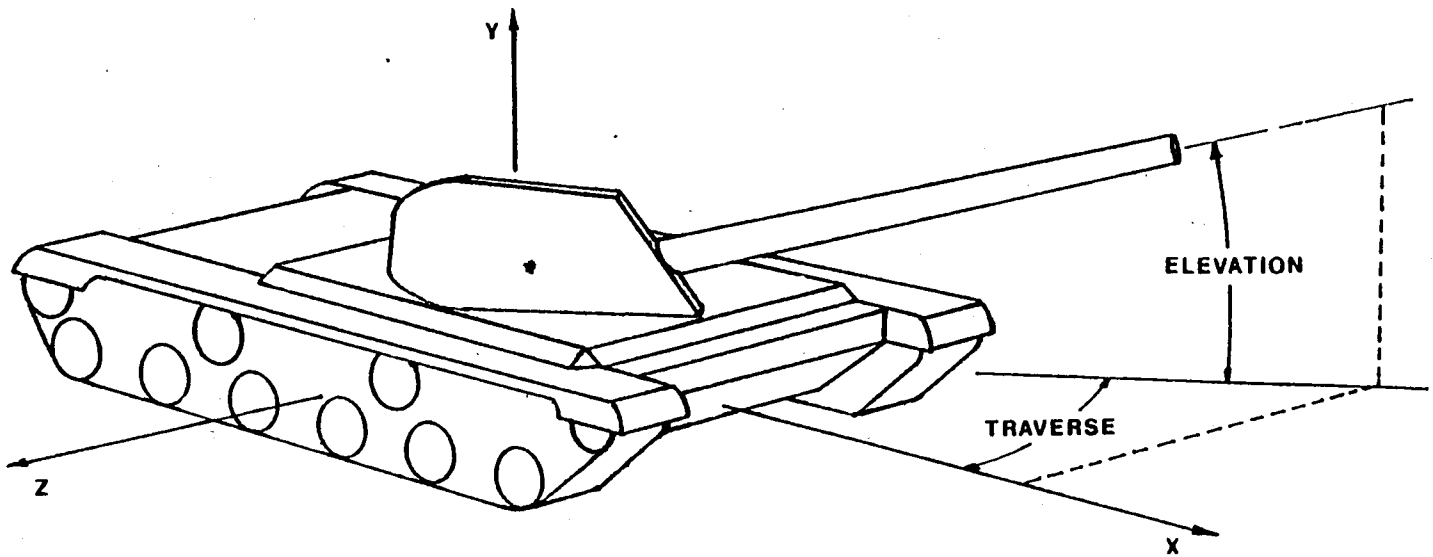

Fig. 1.1 Nominal Gun Position

of the state of the tank and ground contour is not required, greatly simplifying the observer. A nonlinear observer which estimates only the gun pointing errors has been developed for this purpose. The other needed variables, such as gun space rates, are measured directly. The complete time optimal control scheme which follows is developed in Chapter 3 and compared to the stochastic optimal and conventional control schemes with respect to structure and performance in Chapters 4 and 5.

Unfortunately, the strict implementation of time optimal control causes high levels of noise, vibration, power consumption and life-shortening wear. Stochastic optimal control is gentle in comparison, but is currently barred from use by its complexity, particularly its need to adapt to changing gun position and tank speed [2]. Each scheme therefore has very different but complimentary strong and weak points. A hybrid scheme which combines the two to eliminate their individual impediments and retain high performance is proposed in Chapter 5. This scheme has been theoretically developed but not tested.

2. SYSTEM MODELING

A nonlinear model of a tank rolling over rough terrain has been developed to facilitate the design and simulated testing of proposed control schemes. This model assumes that the tank is moving at a constant velocity over continuous hard ground. The development in Sections 2.1 to 2.4 along with the resulting equations noted in Ref. [2] includes a complete derivation of the equations of motion based on conservation of linear and angular momentum. It applies to both the hydraulic and electric gun drive tanks, but is used only for the hydraulic. The model employed with the electric drives is approximately equivalent (see Ref. [2]), but excludes the nonlinear coupling between the hull, turret, and gun incorporated in the new model by the matrix formulation of Section 2.3

Models of the hydraulic gun drives and conventional controllers are discussed in Sections 2.5 and 2.51. Finally, Section 2.6 addresses the model linearizations which precede the design of the time optimal controllers.

The electric gun drives are modeled as non-dynamic torque motors which are linear except for speed and load saturation. These models and the conventional electric drive controllers are discussed in Ref. [1].

2.1 Reference Frames

Two main reference frames are employed in the model: an inertial frame of fixed orientation, Oxyz, and a rotating frame, $Gx_hy_hz_h$, that is fixed to the tank with its origin located at the vehicle c.g. (see Fig. 2.1). It is assumed (1) that the tank pivots about a point labeled T which is fixed with respect to the rotating axes and defined by the intersection of the y_h axis and the torsion bar plane, and (2) that point T is constrained to move vertically and coincides with O when the tank is in its equilibrium position.

Three other reference frames also assist in the angular momentum computations which are described in Section 2.2. These frames, labeled $Ax_Ay_Az_A$, $Bx_By_Bz_B$, and $Cx_Cy_Cz_C$, are fixed to the hull, turret, and gun respectively with their origins at the c.g. of the body to which they are attached (see Fig. 2.2).

2.2 Hull Equations

The differential equations governing hull motion are derived using the fundamental equations shown below which relate the time derivatives of linear and angular momentum to external forces and moments, respectively:[1]

$$m\,\bar{a} = \Sigma F \qquad (2.1)$$

[1] the bar signifies that this acceleration is at the mass center G.

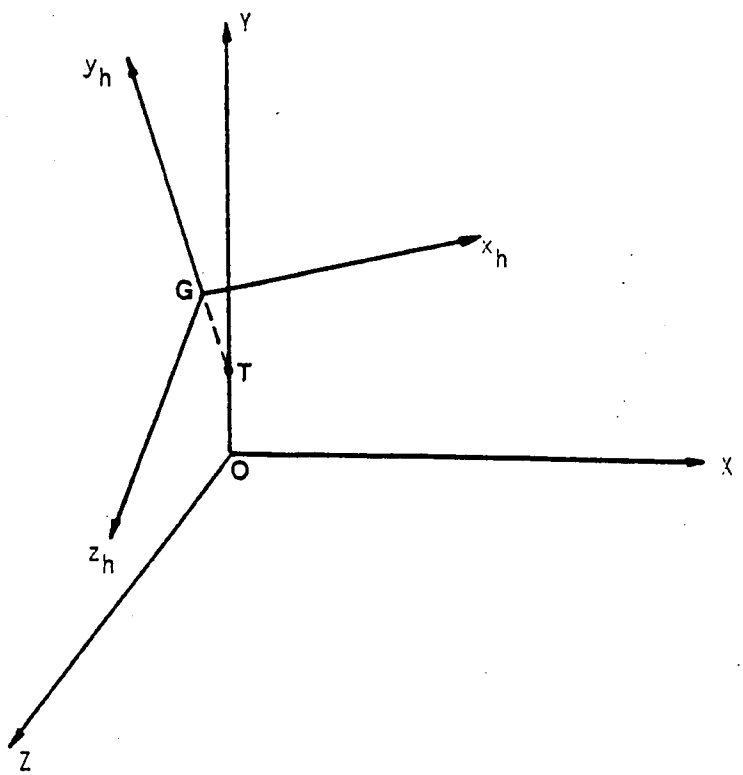

Fig. 2.1 Main Reference Frames

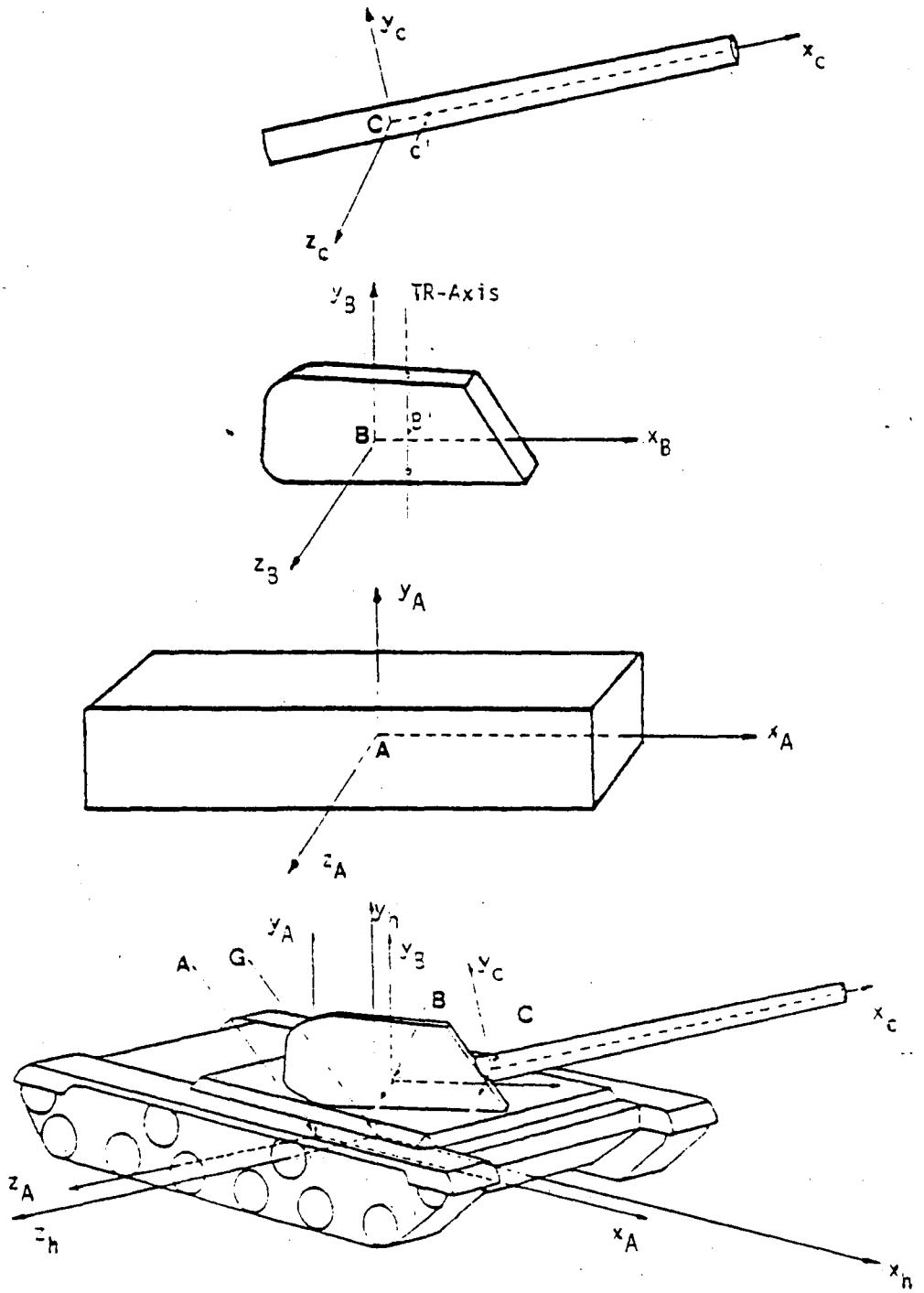

Fig. 2.2 Rotating Reference Frames

$$\dot{H}_G = \Sigma M_G \qquad (2.2)$$

In the present case the external forces and moments result only from the suspension reactions, F_s, and gravity, g. Since the suspension forces are assumed to act vertically, equation (2.1) reduces to

$$m_v \ddot{Y}_H = \Sigma F_s - m_v g \qquad (2.3)$$

where $\ddot{Y}_H$ is the vertical acceleration of the mass center, and m_v is the vehicle mass.

Equation (2.2), on the other hand, requires an expression for the vehicle angular momentum, H_G. H_G is calculated by summing the angular momenta of the hull, turret, and gun about point O, yielding H_O, and then solving for H_G using equation (2.4). This equation relates the angular momentum of a rigid body about its mass center to its angular momentum about a fixed point, O.

$$H_O = r_G \times m \bar{v} + H_G \qquad (2.4)^1$$

Therefore,

$$H_G = H_h + H_t + H_g - r_G \times m_v \bar{v} \qquad (2.5)$$

---

[1] All position vectors are defined with respect to point O.

where H_h, H_t, and H_g are the hull, turret, and gun angular momenta about point O, respectively.

Equation (2.4) is also used to calculate H_h, H_t, and H_g. For a concise illustration, consider the main gun. In this case

$$H_g = r_C \times m_g \bar{v}_C + (H_g)_C \tag{2.6}$$

where $(H_g)_C$ is the gun angular momentum about its mass center, C. During the application of equation (2.2) the time derivative of H_g is evaluated, which is

$$\dot{H}_g = \dot{r}_C \times m_g \bar{v}_C + r_C \times m_g \dot{\bar{v}}_C + (\dot{H}_g)_C \tag{2.7}$$

The first term in this equation is zero:

$$\dot{r}_C \times m_g \bar{v}_C = \bar{v}_C \times m_g \bar{v}_C = 0 \tag{2.8}$$

The last term is the time derivative of $(H_g)_C$ with respect to a frame of fixed orientation:

$$(\dot{H}_g)_C = \frac{d}{dt} [J_g \omega_{gy_C} \underline{j} + J_g \omega_{gz_C} \underline{k}] \tag{2.9}$$

To avoid the calculation of the time derivatives of the rotating unit vectors, the following fundamental equation is employed,

$$(\dot{H})_{Oxyz} = (\dot{H})_{Ox'y'z'} + \Omega \times H \tag{2.10}$$

where Ox'y'z' is a rotating frame which rotates with angular velocity Ω. In frame Ox'y'z' the unit vectors are constant so their time derivatives are zero. By selecting a rotating frame attached to the gun and noting that $\dot{\bar{v}} = \bar{a}$, equation (2.7) becomes

$$(\dot{H}_g)_{Oxyz} = (\dot{H}_g)_{Cx_Cy_Cz_C} + \Omega_g \times H_g + r_C \times m_g \bar{a}_C \qquad (2.11)$$

Substitution of this expression along with similar expressions for the turret and hull into equation (2.5) and then into equation (2.2) yields

$$\begin{aligned} \Sigma M_G = {} & (\dot{H}_h)_{Ax_Ay_Az_A} + \Omega_h \times H_h + r_A \times m_h a_A \\ & + (\dot{H}_t)_{Bx_By_Bz_B} + \Omega_t \times H_t + r_B \times m_t a_B \\ & + (\dot{H}_g)_{Cx_Cy_Cz_C} + \Omega_g \times H_g + r_C \times m_g a_C - r_G \times m_v a_G \end{aligned} \qquad (2.12)$$

Equation (2.12) is a vector equation governing the hull roll, yaw, and pitch angular accelerations about the rotating hull axes. It contains angular momentum terms, position vectors, and accelerations which are discussed in Sections 2.21 through 2.23.

2.21 Angular Momentum Computations

Fixing individual reference frames to the principal axes of the hull, turret, and gun simplifies the angular momentum

computations because the moments of inertia become constant and all products of inertia vanish. This simplification is illustrated by expanding the first two terms of equation (2.12) that are contributed by the turret. The angular momentum and angular velocity of the turret about point B are given as

$$(H_t)_{Bx_By_Bz_B} = J_{tx}\,\omega_{tx_B}\,\underline{i}_B + J_{ty}\,\omega_{ty_B}\,\underline{j}_B + J_{tz}\,\omega_{tz_B}\,\underline{k}_B \tag{2.13}$$

and,

$$\Omega_t = \omega_{tx_B}\underline{i}_B + \omega_{ty_B}\,\underline{j}_B + \omega_{tz_B}\,\underline{k}_B \tag{2.14}$$

Therefore,

$$(\dot{H}_t)_{Bx_By_Bz_B} = J_{tx}\,\dot{\omega}_{tx_B}\,\underline{i}_B + J_{ty}\,\dot{\omega}_{ty_B}\,\underline{j}_B + J_{tz}\,\dot{\omega}_{tz_B}\,\underline{k}_B \tag{2.15}$$

and

$$\begin{aligned}\Omega_t \times H_t = {} & (J_{tz} - J_{ty})\,\omega_{tz_B}\,\omega_{ty_B}\,\underline{i}_B \\ & + (J_{tx} - J_{tz})\,\omega_{tx_B}\,\omega_{tz_B}\,\underline{j}_B \\ & + (J_{ty} - J_{tx})\,\omega_{ty_B}\,\omega_{tx_B}\,\underline{k}_B\end{aligned} \tag{2.16}$$

These equations are written in terms of known state variables and resolved onto the rotating hull axes by applying the following two transformations:

$$(1)\quad \omega_{tx_B} = \omega_{hx}\cos TR - \omega_{hz}\sin TR \tag{2.17a}$$

$$\omega_{ty_B} = SRTR \tag{2.17b}$$

$$\omega_{tz_B} = \omega_{hz} \cos TR + \omega_{hx} \sin TR \tag{2.17c}$$

(2) $$\underline{i}_B = \underline{i} \cos TR - \underline{k} \sin TR \tag{2.18a}$$

$$\underline{j}_B = \underline{j} \tag{2.18b}$$

$$\underline{k}_B = \underline{k} \cos TR + \underline{i} \sin TR \tag{2.18c}$$

This procedure, as exemplified above, is vastly simpler than any which does not employ a rotating centroidal reference frame and is also used to expand the first two terms of equation (2.12) contributed by the hull and gun.

2.22 Position Vectors

All of the points of interest (points T, G, A, B, and C) are fixed with respect to the rotating frame attached to the body in which they are contained[1]. Therefore, any position vector, r_p, can be defined in terms of r_T, TR, and E. For example,

$$r_p = r_T + r_{p/T} \tag{2.19}$$

[1]The vehicle c.g. actually moves slightly as the turret turns because the turret c.g. does not lie precisely on the traverse axis; however, this movement is neglected and G is fixed at its nominal position.

The calculation of r_T is completely different than the other position vector calculations and therefore is shown below. Equation (2.19) is used as follows:

$$r_T = r_G + r_{T/G} \tag{2.20}$$

The vertical component of r_G is obtained by integrating equation (2.1) twice to give

$$r_G \cdot \underline{J} = Y_H + K \tag{2.21}$$

The second term, $r_{T/G}$, is a constant which is resolved onto the fixed axes, Oxyz, by the $\underline{C}$ coordinate transformation given in Appendix B2 of Ref. [2],

$$r_{T/G} = -Y_{CG}\,\underline{j} = -\,Y_{CG}\,(C_{xy}\,\underline{I} + C_{yy}\,\underline{J} + C_{zy}\,\underline{K}) \tag{2.22}$$

where Y_{CG} is the distance from point G to point T. Since point T is constrained to move vertically, the vertical component of equation (2.20) becomes

$$r_T = Y_H + K - C_{yy} \cdot Y_{CG} \tag{2.23}$$

The constant K is evaluated from the initial conditions:

$$r_T(0) = 0 \qquad Y_H(0) = 0 \qquad C_{yy}(0) = \cos(P_o) \tag{2.24}$$

Therefore,

$$K = Y_{CG} \cos(P_o) \tag{2.25}$$

and finally

$$r_T = Y_H + Y_{CG} \, (\cos(P_o) - C_{yy}) \tag{2.26}$$

Since the derivation of r_T is unique, r_A is derived below for a complete illustration.

$$r_A = r_T + r_{A/T} \tag{2.27}$$

The last term, $r_{A/T}$, is constant:

$$r_{A/T} = d_1 \, \underline{i} + d_2 \, \underline{j} + d_3 \, \underline{k} \tag{2.28}$$

The first term, r_T, is resolved onto the hull axes using the $\underline{V}$ coordinate transformation in Appendix B2 of Ref. [2],

$$r_T = r_T \, V_{xy} \, \underline{i} + r_T \, V_{yy} \, \underline{j} + r_T \, V_{zy} \, \underline{k} \tag{2.29}$$

yielding

$$r_A = (r_T \, V_{xy} + d_1)\underline{i} + (r_T \, V_{yy} + d_2)\underline{j} + (r_T \, V_{zy} + d_3)\underline{k} \tag{2.30}$$

All of position vectors which are needed are derived in this manner.

2.23 Acceleration Calculations

The calculation of the accelerations at points A, B, C, D, and G are based on the following fundamental equation:

$$a_P = a_Q + \dot{\Omega} \times r_{P/Q} + \Omega \times (\Omega \times r_{P/Q}) + 2\Omega \times (\dot{r}_{P/Q})_{Q_{xyz}} + (\ddot{r}_{P/Q})_{Q_{xyz}} \quad (2.31)$$

where P is the point of interest and Q is the origin of the rotating frame Q_{xyz}.

Equation (2.31) may be simplified in our case by selecting point Q so that $(\dot{r}_{P/Q})_{Qxyz} = (\ddot{r}_{P/Q})_{Qxyz} = 0$. This requires the definition of point B' which is located on the traverse axis at the level of the turret c.g. (see Fig. 2.3). By choosing Q so that it coincides with T when calculating a_A and a_G, and coincides with B' when calculating a_B and a_C, equation (2.31) becomes

$$a_P = a_Q + \dot{\Omega} \times r_{P/Q} + \Omega \times (\Omega \times r_{P/Q}) \quad (2.32)$$

The application of equation (2.32) to point A yields

$$a_A = a_T + \dot{\Omega} \times r_{A/T} + \Omega \times (\Omega \times r_{A/T}) \; . \quad (2.33)$$

This equation requires an expression for a_T which is derived by again applying equation (2.32), this time to point T, yielding

$$a_T = a_G + a_{T/G} \quad (2.34)$$

where

$$a_{T/G} = \dot{\Omega} \times r_{T/G} + \Omega \times (\Omega \times r_{T/G}) \; . \quad (2.35)$$

Noting that $r_{T/G} = -Y_{CG}\,\underline{j}$, and that $\Omega = \omega_{hx}\underline{i} + \omega_{hy}\underline{j} + \omega_{hz}\underline{k}$, it can be shown that

$$a_{T/G} = (a_{T/G})_x\,\underline{i} + (a_{T/G})_y\,\underline{j} + (a_{T/G})_z\,\underline{k}\,. \qquad (2.36)$$

where

$$(a_{T/G})_x = Y_{CG}(\dot{\omega}_{hz} - \omega_{hx}\omega_{hy})$$

$$(a_{T/G})_y = Y_{CG}(\omega_{hz}^2 + \omega_{hx}^2)$$

$$(a_{T/G})_z = -\,Y_{CG}(\dot{\omega}_{hx} + \omega_{hz}\omega_{hy})$$

By assumption, point T is constrained to move vertically relative to the moving inertial frame Oxyz. Therefore,

$$a_T = a_G \cdot \underline{J} + a_{T/G} \cdot \underline{J} \qquad (2.37)$$

The first term, $a_G \cdot \underline{J}$ is simply the vertical acceleration of point G, $\ddot{Y}_H$ (see equation 2.3). The second term, $a_{T/G} \cdot \underline{J}$, is derived by resolving $a_{T/G}$ onto frame Oxyz:

$$a_{T/G} \cdot \underline{J} = C_{yx}(a_{T/G})_x + C_{yy}(a_{T/G})_y + C_{yz}(a_{T/G})_z \qquad (2.38)$$

Thus,

$$a_T = \{\ddot{Y}_H + C_{yx}(a_{T/G})_x + C_{yy}(a_{T/G})_y + C_{yz}(a_{T/G})_z\}\,\underline{J}$$

Finally, the $\underline{V}$ coordinate transformation is employed to resolve a_T back onto the rotating hull axes, $G_{x_h y_h z_h}$. This transformation produces some terms such as $V_{xy}\,C_{xy}$ which are vanishingly

small and omitted. Therefore,

$$
\begin{aligned}
a_T = {} & \{\ddot{Y}_H + C_{yy}Y_{CG}(\omega_{hx}^2 + \omega_{hz}^2)\}\ V_{yy}\ \underline{i} \\
& + \{\ddot{Y}_H + C_{yx}Y_{CG}(\dot{\omega}_{hz} - \omega_{hx}\omega_{hy}) + C_{yy}Y_{CG}(\omega_{hx}^2 + \omega_{hz}^2) \\
& - C_{yz}Y_{CG}(\dot{\omega}_{hx} + \omega_{hz}\omega_{hy})\}\ V_{yy}\ \underline{j} \\
& + \{\ddot{Y}_H + C_{yy}Y_{CG}(\omega_{hx}^2 + \omega_{hz}^2)\}\ V_{zy}\ \underline{k}
\end{aligned}
\qquad (2.39)
$$

Now that a_T is specified, the components of a_A are easily derived by evaluating the cross products of equation (2.33). All acceleration calculations follow this same pattern.

2.3 Matrix Formulation

The right hand side of equation (2.12) comprises linear functions of $\dot{\underline{x}}$ and nonlinear functions of $\underline{x}$, where $\underline{x}$ represents the system state. A transferal of all nonlinear terms to the left hand side of the equation gives the following matrix formulation:

$$
\begin{bmatrix} 3 \times 6 \\ \text{Inertia Matrix} \end{bmatrix}
\begin{bmatrix} \dot{\omega}_{hx} \\ \dot{\omega}_{hy} \\ \dot{\omega}_{hz} \\ \dot{SRTR} \\ \dot{SRE} \\ \ddot{Y}_H \end{bmatrix}
=
\begin{bmatrix} \Sigma M_{sx} \\ \Sigma M_{sy} \\ \Sigma M_{sz} \end{bmatrix}
-
\begin{bmatrix} \text{Nonlinear} \\ \text{Terms} \end{bmatrix}
\qquad (2.40)
$$

This formulation is expanded by adding the turret and gun space rate equations; fourth and fifth rows, respectively, are added to the inertia matrix. These space rate equations contain linear functions of $\underline{\dot{x}}$ which appear in their expressions for the applied disturbance torques. These linear terms are transferred into their proper position in the inertia matrix, coupling the space rate equations to the hull equations. These disturbance torques are further described in Section 2.4.

The vertical acceleration equation $\ddot{Y}_H$, derived in Section 2.2, is completely uncoupled and therefore can be evaluated separately with no loss of accuracy. This allows the terms represented by the sixth column of the inertia matrix to be moved to the right hand side of the formula, yielding

$$\begin{bmatrix} 5 \times 5 \\ \text{Inertia Matrix} \end{bmatrix} \begin{bmatrix} \dot{\omega}_{hx} \\ \dot{\omega}_{hy} \\ \dot{\omega}_{hz} \\ \dot{SRTR} \\ \dot{SRE} \end{bmatrix} = \begin{bmatrix} \Sigma M_{sx} \\ \Sigma M_{sy} \\ \Sigma M_{sz} \\ \Sigma M_{tn} \\ \Sigma M_{gn} \end{bmatrix} - \begin{bmatrix} \text{NONLINEAR} \\ \text{TERMS} \end{bmatrix} - \begin{bmatrix} J_{16} \\ J_{26} \\ J_{36} \\ J_{46} \\ J_{56} \end{bmatrix} \ddot{Y}_H \tag{2.41}$$

The subscript n on the turret and gun external moments signify that the linear terms have been removed and placed in the inertia matrix.

Finally, the time derivatives of the five coupled state variables are evaluated simultaneously by premultiplying the right hand side of equation (2.41) by the inverse of the inertia matrix.

2.4 Turret and Gun Equations

The differential equations governing the turret traverse and gun elevation space rates are obtained by applying equation (2.2) to the turret and to the gun. As in the derivation of the hull equations, rotating reference frames attached to these bodies are employed. In each case equation (2.2) yields three equations governing the x, y, and z components of rigid body angular motion. Only one component, however, is needed to calculate $\frac{d}{dt}$ (SRTR) and $\frac{d}{dt}$ (SRE) - the y_B and z_C components of the turret and gun equations, respectively.

The derivation of the turret equation is simplified by considering the turret-gun system rather than the turret alone, because this system internalizes the dynamic reactions exerted by the gun at the trunnion and considerably simplifies the external moment calculation. The application of equation (2.2) to this two-body system then requires an approach similar to the derivation of the hull equations, and yields equations which couple the traverse and elevation space rates. This coupling is very weak in the turret equation, however, and

neglected in the present formulation. Therefore the turret space rate equation is derived as if the turret-gun system were a single body with mass center at point D and with variable moments of inertia that depend on the elevation angle. Changes in the position of point D due to variations in the elevation angle, E, are negligible because the gun c.g. lies only 3 mm away from the trunnion. The turret-gun system moments of inertia about axes attached at D are

$$J_{tx_D} = J_{tx_B} + m_t \bar{z}_1^2 + J_g \sin^2 E + m_g \bar{z}_2^2 \tag{2.42a}$$

$$J_{ty_D} = J_{ty_B} + m_t(\bar{x}_1^2+\bar{z}_1^2) + J_g \cos^2 E + m_g(\bar{x}_2^2+\bar{z}_2^2) \tag{2.42b}$$

$$J_{tz_D} = J_{tz_B} + m_t \bar{x}_1^2 + m_g \bar{x}_2^2 \tag{2.42c}$$

where $\bar{x}_1$, $\bar{x}_2$, $\bar{z}_1$ and $\bar{z}_2$ are defined in Fig. 2.3. The angular momentum of the turret about D is therefore,

$$(H_t)_D = \begin{bmatrix} J_{tx} & 0 & 0 \\ 0 & J_{ty} & 0 \\ 0 & 0 & J_{tz} \end{bmatrix} \begin{bmatrix} \omega_{tx} \\ \omega_{ty} \\ \omega_{tz} \end{bmatrix} \tag{2.43}$$

so that the y_D component of the results of equation (2.2) becomes

$$(\Sigma M_t)_D = J_{ty} \dot{\omega}_{ty} + (J_{tx} - J_{tz}) \omega_{tx} \omega_{tz} \tag{2.44}$$

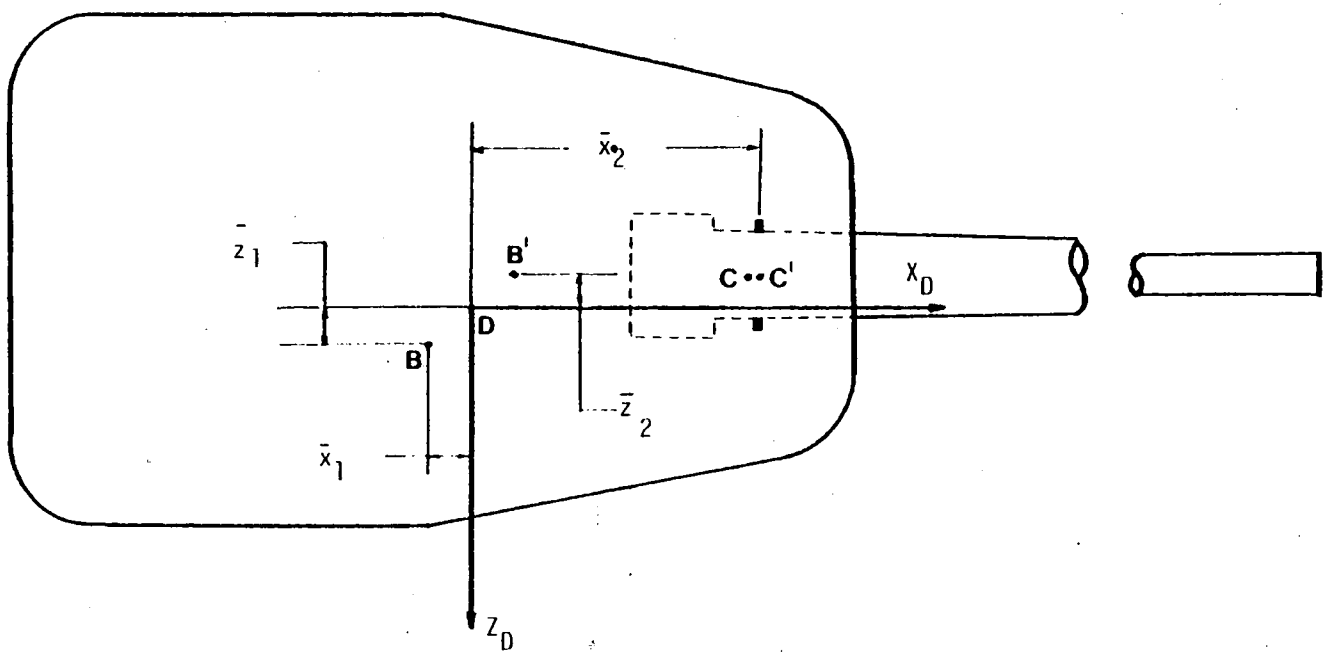

Fig. 2.3 Turret-Gun CG(D) and Turret CG(B) Positions

(The D subscript has been dropped in equations (2.43) and (2.44) for clarity). The turret angular velocities are expressed in terms of known state variables using the transformation

$$\omega_{tx} = \omega_{hx} \cos TR - \omega_{hz} \sin TR \tag{2.45a}$$

$$\omega_{ty} = SRTR \tag{2.45b}$$

$$\omega_{tz} = \omega_{hx} \sin TR + \omega_{hz} \cos TR \tag{2.45c}$$

Finally, the turret equation becomes

$$(\Sigma M_t)_D = J_{ty} \dot{SR}TR + (J_{tx}-J_{tz})[(\omega_{hx}^2-\omega_{hz}^2) \sin TR \cos TR + \omega_{hx} \omega_{hz} \cos 2TR] \tag{2.46}$$

The external moment about the y_D axis of the turret, ΣM_t, comprises a control torque, a friction torque, and a disturbance torque. Expressions for the control and friction torques are taken directly from the Kaminsky azimuth model [4]. This model does not include any hull rolling, pitching, or vertical motion, so a new disturbance torque expression which recognizes this motion is developed. This disturbance torque is caused by the resultant dynamic force, called F_B', exerted on the turret by the hull. Force F_B' is assumed to intersect the traverse axis at point B', thereby causing a moment about the turret-gun mass center at point D.[1] A summation of forces on the

[1] The traverse axis is defined as the axis of rotation of the turret with respect to the hull.

turret-gun consists of force F_B' and gravity:

$$\Sigma F_{x_D} = (F_B')_{x_D} - (m_t + m_g)\, g\, (V_{xy} \cos TR - V_{zy} \sin TR) \tag{2.47a}$$

$$\Sigma F_{z_D} = (F_B')_{z_D} - (m_t + m_g)\, g\, (V_{zy} \cos TR + V_{xy} \sin TR) \tag{2.47b}$$

The total acceleration of point D is known, and therefore ΣF is known by Newton's second law:

$$\Sigma F_{x_D} = (m_t + m_g)(\bar{a}_D)_{x_D} \tag{2.48a}$$

$$\Sigma F_{z_D} = (m_t + m_g)(\bar{a}_D)_{z_D} \tag{2.48b}$$

Combining equations (2.47a) through (2.48b) yields

$$(F_B')_{x_D} = (m_t+m_g)[(\bar{a}_D)_{x_D} + g(V_{xy} \cos TR - V_{zy} \sin TR)] \tag{2.49a}$$

$$(F_B')_{z_D} = (m_t+m_g)[(\bar{a}_D)_{z_D} + g(V_{zy} \cos TR + V_{xy} \sin TR)] \tag{2.49b}$$

Finally, the disturbance torque is calculated;

$$DSTQTR = r \times F_B' = \begin{vmatrix} \underline{i}_D & \underline{j}_D & \underline{k}_D \\ -d_{11} & 0 & -d_{12} \\ (F_B')_{x_D} & 0 & (F_B')_{z_D} \end{vmatrix}$$

$$= (F_B')_{z_D}\, d_{11} - (F_B')_{x_D}\, d_{12} \tag{2.50}$$

where d_{11} and d_{12} are the x_D and z_D distances from point B' to point D, respectively.

At this point equation (2.50) is substituted into the fourth row of the matrix formulation described in Section 2.3. This substitution requires the transferal of all linear terms into the inertia matrix and all nonlinear terms over to the right hand side of the equation. With the exception of J_{ty} $\dot{SRTR}$ of equation (2.46), all of these linear terms appear as angular accelerations contributing to the turret disturbance torque. These terms are therefore placed into the proper columns of the fourth row of the inertia matrix leaving only the nonlinear disturbance torque terms in the external moment summation.

The derivation of the gun equation is similar to that of the turret equation, but simpler because the gun is (1) a single rigid body, and (2) axisymmetric with a negligible x_C axis moment of inertia. The angular momentum of the gun about its mass center is,

$$(Hg)_C = J_g\ \omega_{gy_C}\ \underline{j}_C + J_g\ \omega_{gz_C}\ \underline{k}_C \qquad (2.51)$$

As before, equations (2.2) and (2.10) are used to derive the governing equation, which is

$$J_g\ \dot{SRE} = (\Sigma M_g)_{z_C} - J_g\ \omega_{gx_C}\ \omega_{gy_C} \qquad (2.52)$$

However, since

$$\omega_{gx_C} = (\omega_{hx} \cos TR - \omega_{hz} \sin TR) \cos E + SRTR \sin E \tag{2.53a}$$

$$\omega_{gy_C} = SRTR \cos E - (\omega_{hx} \cos TR - \omega_{hz} \sin TR) \sin E \tag{2.53b}$$

the gun equation becomes

$$J_g \dot{SRE} = (\Sigma M_g)_{z_C} - J_g \{[SRTR^2 - (\omega_{hx} \cos TR - \omega_{hz} \sin TR)^2]^{\frac{1}{2}} \sin 2E + (\omega_{hx} \cos TR - \omega_{hz} \sin TR) SRTR \cos 2E\} \tag{2.54}$$

where the summation of external moments again comprises a control torque, a friction torque, and a disturbance torque. Equation (2.54) becomes, after the proper placement of the linear and nonlinear terms, the fifth row of the matrix formulation.

2.5 Models of the Hydraulic Gun Drives

The hydraulic gun drives are modeled following Kaminsky [4], with certain simplifications. The Kaminsky model includes a number of elements which make it very sensitive to high frequency excitations of the turret and gun. The effect that some of these elements have on the simulated control system

performance is negligible, however. For example, the main gun first mode of bending vibration has very little effect on the system behavior. This was determined by examining the simulated results obtained by running the tank over a standard test bump using conventional controllers and a Kaminsky model which included and then omitted the gun bending; the results were indistinguishable [3]. This test sparked an examination of the remaining portions of the Kaminsky model that possessed high characteristic frequencies. On the basis of this examination, the following portions were omitted or replaced (by constants) in the nonlinear model described herein:

1)	Gun Bending	120 rad/sec.
2)	Rate Sensor Dynamics	157 rad/sec.
3)	Spring-Damper model between the turret and basket	~100 rad/sec.

In addition to the above, the hydraulic supply pump and relief valves also are omitted to further reduce the system order and to avoid the complicated but relatively unimportant transients that they produce throughout the simulations. For example, the hydraulic pump, which serves to fill an accumulator, switches on and off when the control system supply pressure reaches 960 and 1240 psi, respectively. Instead, the supply pressure was fixed at its mean value of 1100 psi. Further, the relief valve flow is set at zero and a flag is printed during

the simulations if the normal opening pressure is exceeded. These simplified elevation and traverse control systems are shown in Figs. 2.4 and 2.5.

2.51 Conventional Controllers

Transfer functions and block diagrams representing the conventional elevation and traverse hydraulic system controllers were supplied by Ref. [4]. This traverse controller and a modified version of the elevation controller were employed in this study. The original elevation controller contained a pair of complex conjugate poles and zeros specifically designed to produce a notch filter to suppress the excitation of the first mode of vibration of the gun. Since this mode of vibration was stricken from the model, the related poles and zeros were removed from the controller, resulting in the conventional elevation controller shown in Fig. 2.6.

The conventional traverse time optimal controller has not been altered and is shown in Fig. 2.7. This controller claims to be time optimal, implying that it will employ saturation control (see Chapter 3), however, it selects a control which is proportional in nature (see Fig. 4.4). Therefore, its claim of time optimality is questionable.

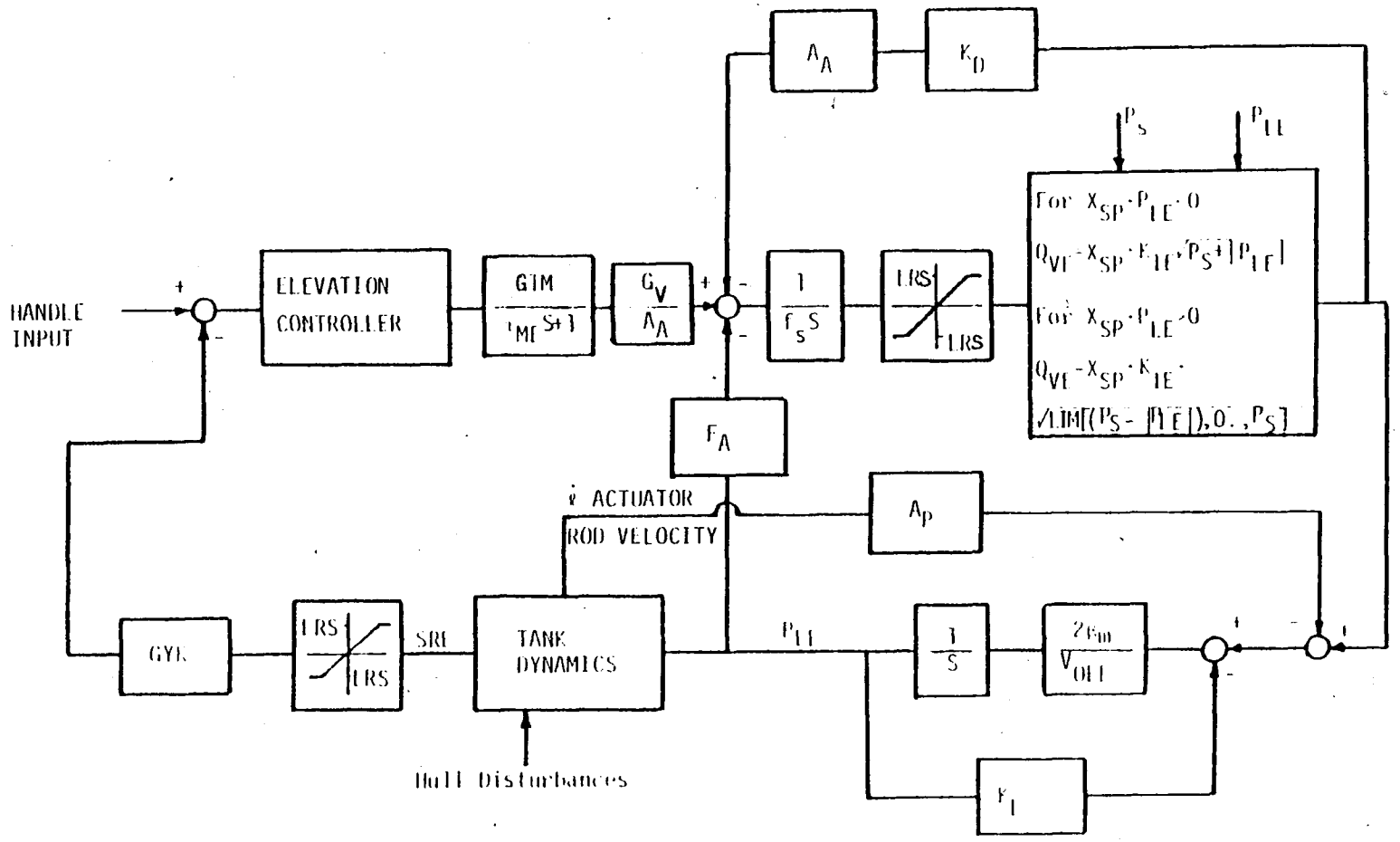

Fig. 2.4 Elevation Hydraulic Gun Drive System

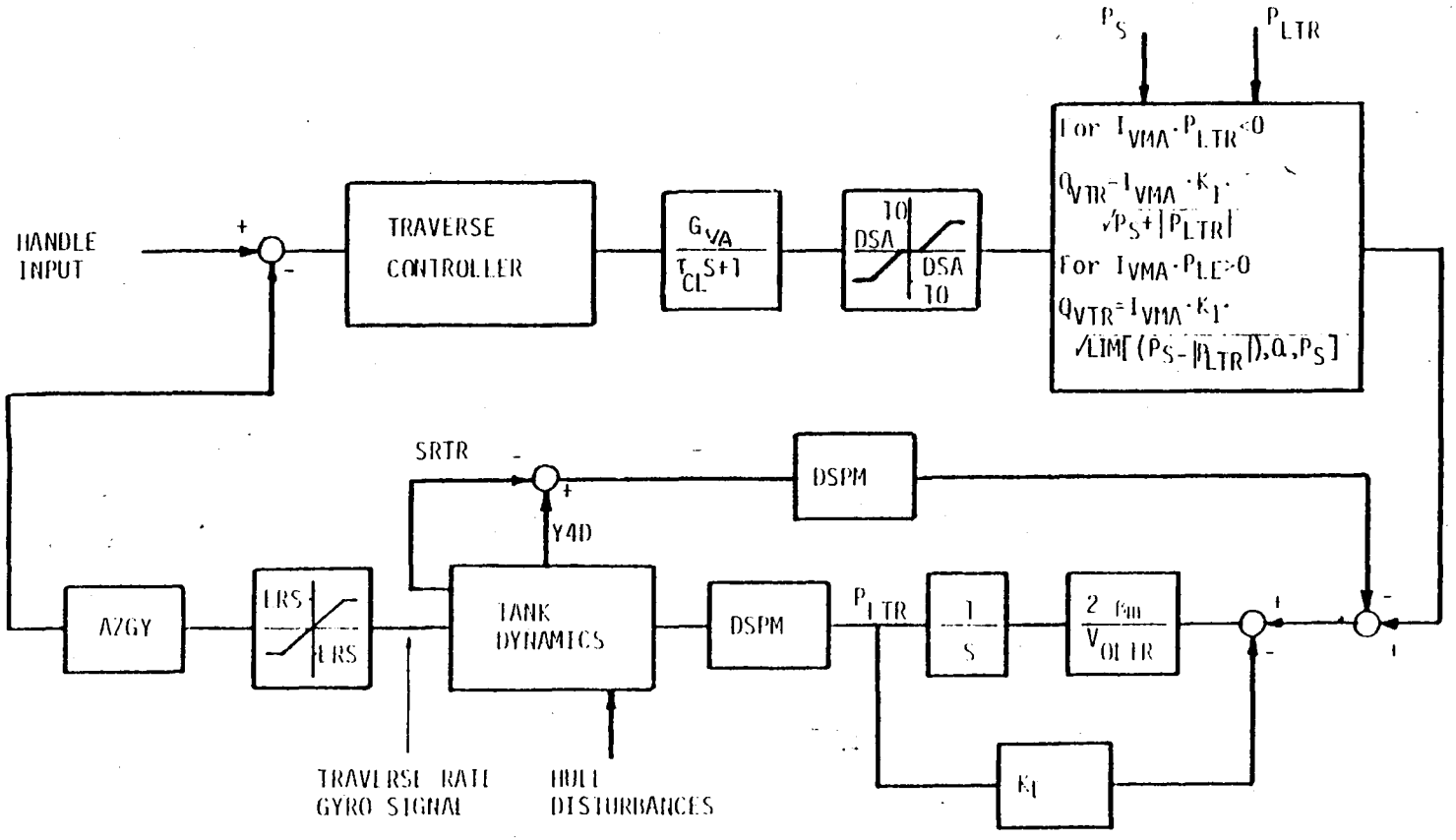

Fig. 2.5 Traverse Hydraulic Gun Drive System

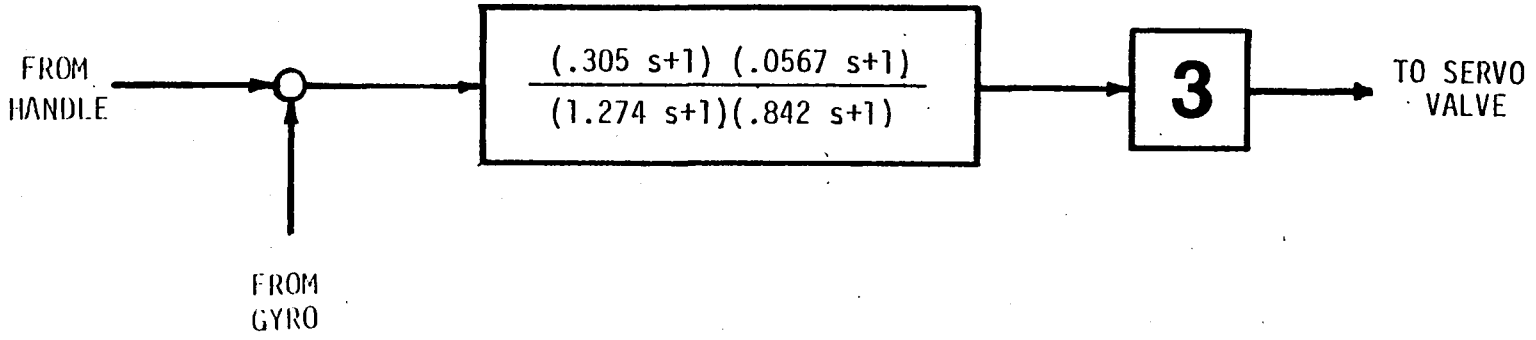

Fig. 2.6 Simplified Conventional Elevation Controller

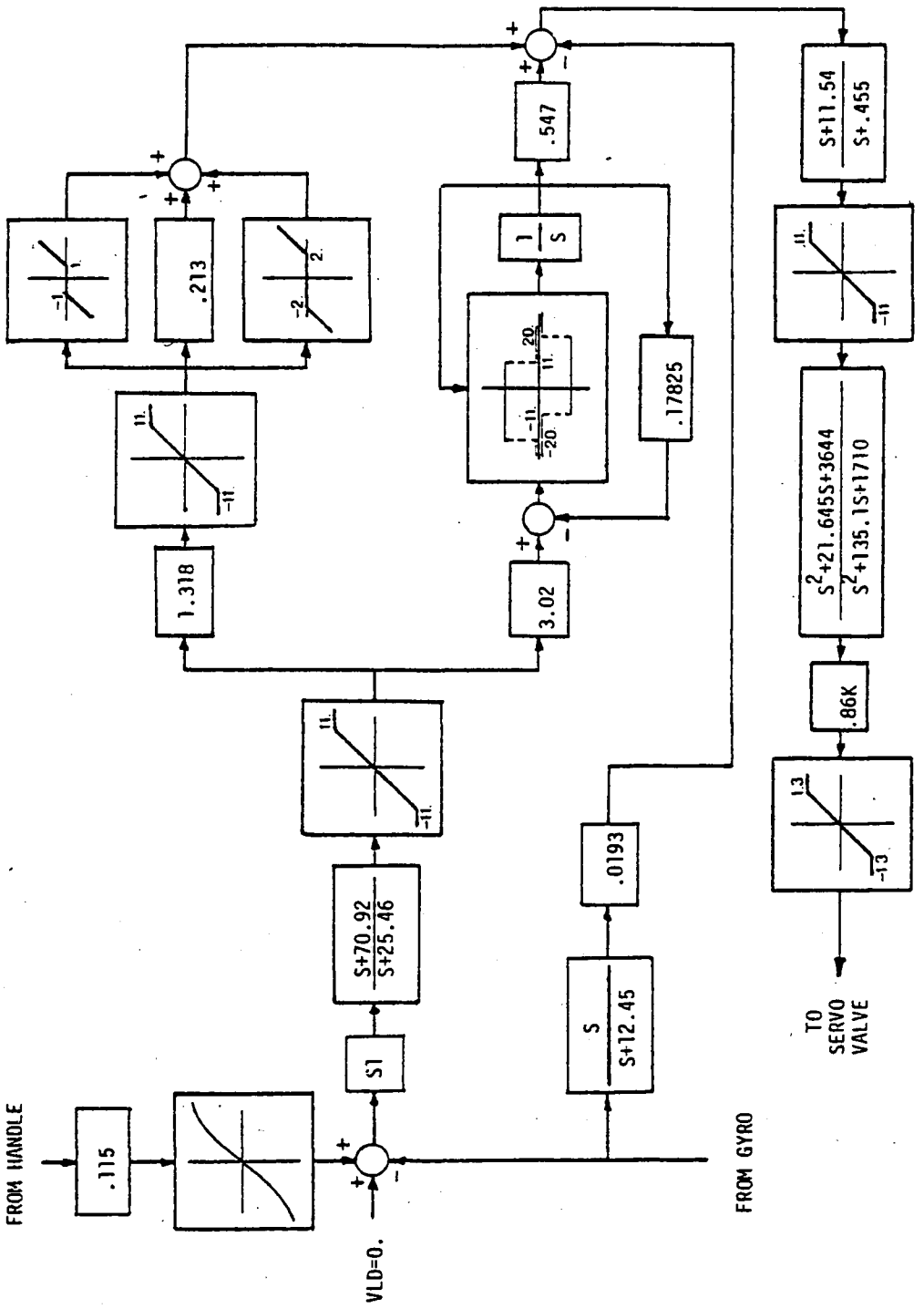

Fig. 2.7 Conventional Traverse Time Optimal Controller

2.6 Model Linearization

The time optimal controllers developed in Chapter 3 are based on simple linear models derived by linearizing small portions of the complete nonlinear model previously derived. These small portions are isolated by neglecting the elevation and traverse disturbance torques. Consequently, the turret and gun become completely uncoupled from the hull resulting in simple models comprising gun and gun drive dynamics only.

The elevation and traverse gun space rate equations are gyrationally coupled as shown by equation (2.54). This gyrational coupling is removed by linearization. The nonlinearities which remain occur in the gun drives. The electric gun drive models are non-dynamic and linear, as previously mentioned. As a consequence, the electric drive time optimal controllers are very simple and insensitive to modeling errors. The hydraulic drive models, on the other hand, are dynamic and nonlinear. Their linearization includes (1) the removal of all saturation limiters, (2) the replacement of the traverse servo valve deadband limiter by a constant gain of .985 arrived at by a describing function analysis, and (3) the modification of the servo valve flow equations. These servo valve equations are of the form:

$$Q_V = x \cdot k \cdot \sqrt{P_S + |P_L|} \qquad x \cdot P_L < 0 \qquad (2.55a)$$

$$= x \cdot k \cdot \sqrt{\text{Lim}\,(P_S - |P_L|), 0., P_S} \qquad x \cdot P_L > 0 \qquad (2.55b)$$

in which x is the input, k is the flow coefficient, P_s is the supply pressure, P_L is the differential pressure producing the control torque, and the Lim function is defined in Fig. 2.8a. The condition for equation (2.55a) applies only for very brief periods of time characterized by the lag in the pressure, P_L, with respect to the input, x, and therefore this equation is discarded in the linearization. Equation (2.55b) is linearized by removing the limiter and by selecting the proper square root argument. This linearized equation is

$$Q_v = x \cdot k \cdot \sqrt{P_s - P_{LMN}} \qquad (2.56)$$

where P_{LMN} represents the mean of $|P_L|$ which occurs during a simulation. The character of $|P_L|$ is suggested in Fig. 2.8b. The elevation and traverse mean pressure magnitudes are estimated using the results of the nonlinear conventionally controlled model simulation. They are

$$P_{LEMN} = 3.0 \times 10^5 \text{ Pa}$$

$$P_{LTRMN} = 25.0 \times 10^5 \text{ Pa}$$

This completes the linearization.

The linearized elevation gun drive system is further simplified by removing its very fast eigenvalues [2]. This is done by replacing the spool position and pressure differential

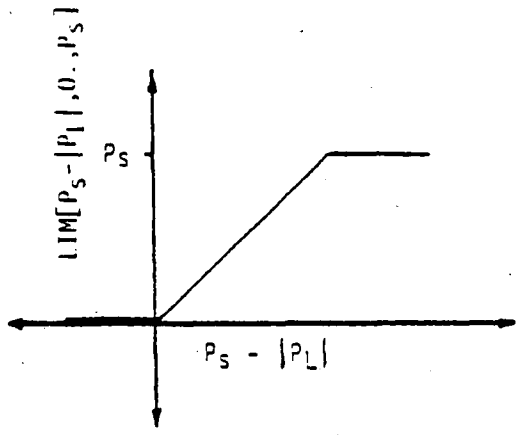

Fig. 2.8a Limit Function

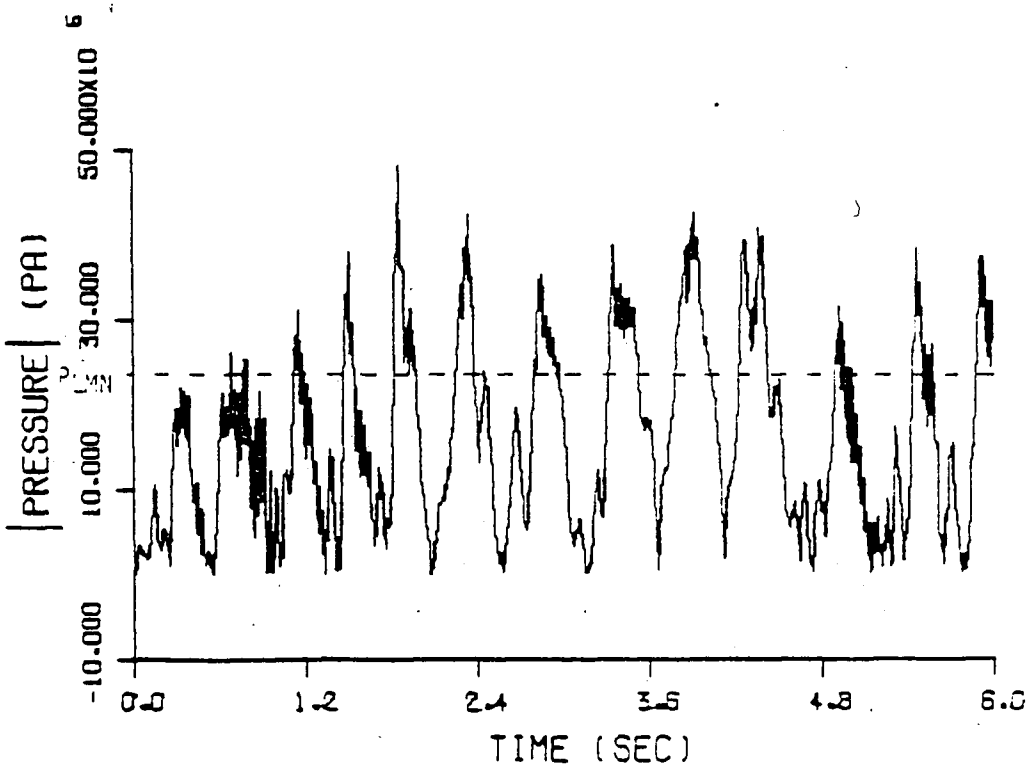

Fig. 2.8b Pressure Differential Magnitude, P_L, and P_{LMN}

loops (see Fig. 2.6) by constant gains that are calculated using simple block diagram reductions which assume that the particular time constants in question are negligible. A block diagram of the resulting elevation hydraulic gun drive system is shown in Fig. 2.9. This model and the linearized traverse gun drive model are employed in the development of the hydraulic system time optimal controllers of Section 3.2.

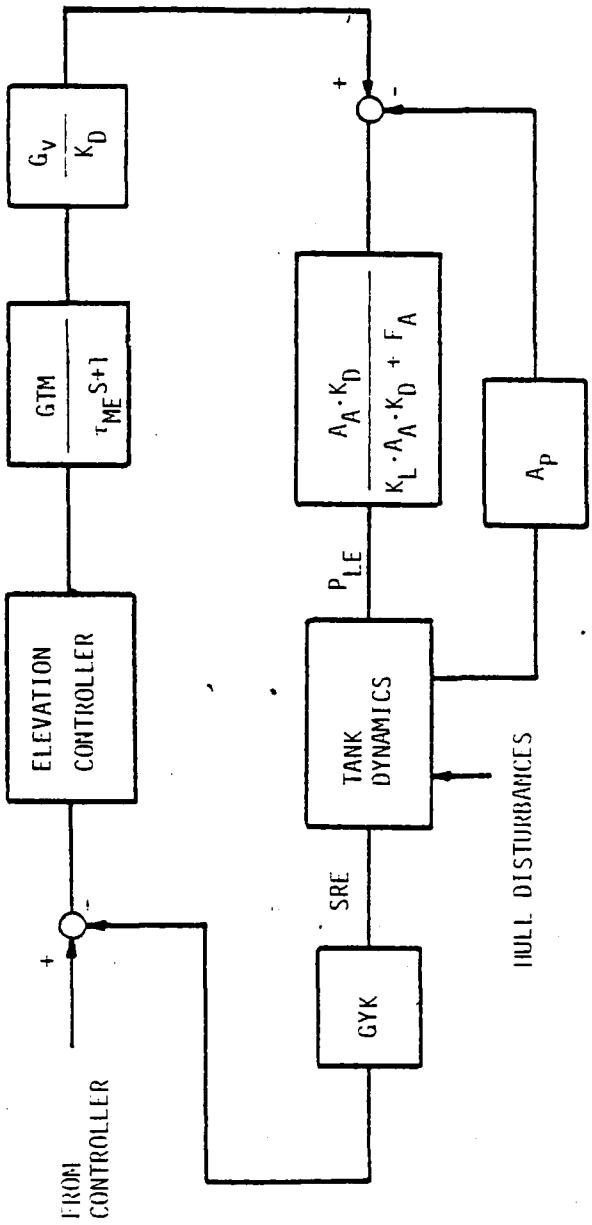

Fig. 2.9 Simplified Elevation Hydraulic Gun Drive System

3. TIME OPTIMAL CONTROL

Time optimal control theory is applied to the electric and hydraulic gun drive systems of the M60 tank. A preliminary study has been reported [1]. If perfect observation is assumed, the quality of the control theoretically increases without limit as the disturbances become smaller, unlike proportional control. This plus its simplicity and stability make it highly attractive. In practice, however, the quality of the control is limited by imperfect observation and by errors in the assumed model of the system and the controller at high frequencies. Also, the wear, noise, vibration, and quiescent power drain of the valve and actuator mitigates against its use. The study which follows is directed at actual control performance but not questions of life and power consumption. (These questions are discussed in Section 5.1, however.)

The performance index of the time optimal control problem is simply

$$J = \int_0^{t_f} dt \qquad (3.1)$$

which is obviously an extremal when the final time is minimized. Time optimal controllers inherently move the state point to the origin at the final time, so equation (3.1) contains no explicit weighted combination of the state that would tend to constrain

the angle errors.[1] The control levels, on the other hand, must be explicitly constrained by enforcing separate limits on their magnitudes. In this case, there are two inputs and two constraints:

$$|u_i| \leq (u_i)_{max} \quad , \; i = 1,2 \tag{3.2}$$

Equation (3.1) and (3.2) are employed to show that bang-bang (maximum effort) control is the operating mode indicated by the Pontriagin Maximum Principle for time optimal performance [5].

A bang-bang control function is characterized by instantaneous polarity switches which allow the control to remain on the boundaries of the limited control range, as shown in Fig. 3.1. The number and precise timing of the polarity switches can be selected to achieve time optimality. Bellman's n-interval theorem addresses this problem stating that the time optimal control of an n^{th} order system having only non-positive real poles and no zeros comprises n-1 polarity switches separating n intervals of constant full-positive and full-negative control [5]. The calculation of the precise timing of these switches and the initial control polarity is discussed in Section 3.1.

[1] Time optimal controllers can be designed to force the state onto a desired trajectory in minimum time, but only the regulator problem is of current interest.

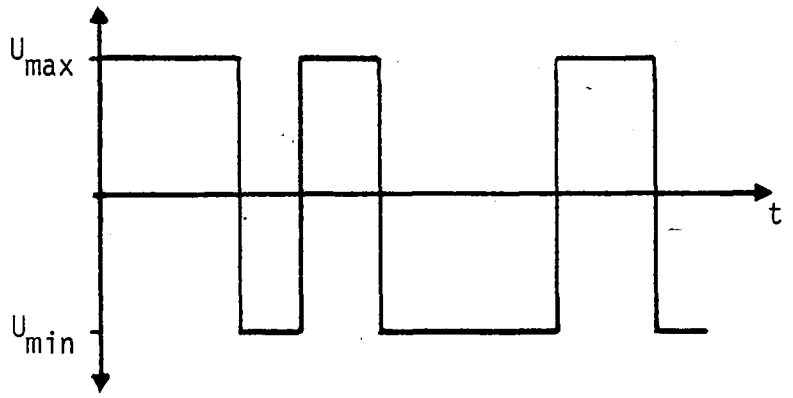

Fig. 3.1 Bang-bang Control

The implementation of time optimal control in a high order system such as a tank is impractical because the switching-time calculations tend to become very difficult. In practice, therefore, time optimal controllers are based on simple low order approximate models. Second order models lead to very simple time optimal controls, and are used to develop the elevation and traverse electric gun drive TOCS.[1] For example, suppose that a disk (a 2nd order system possibly representing a turret) must be rotated from -90 to 0 degrees with zero initial and final velocities in minimum time. Obviously, full-positive torque is initially applied followed by a switch to full-negative torque when the disk reaches -45 degrees. At the precise moment that the disk reaches 0 degrees the motion has stopped and the control is turned off. The point of control switching occurs when the state point $(\theta,\dot{\theta})$ reaches what is called the switching curve (see Fig. 3.2). The branches of this curve separate the state plane into two regions of opposite initial control polarity.

Third and fourth order models are used to develop the elevation and traverse hydraulic gun drive TOCS, respectively. Therefore, in the case of the elevation control, there are two switches. One switch occurs when the state point reaches the switching surface, which separates the three-dimensional state

[1] Time optimal controllers are sometimes referred to as TOCS.

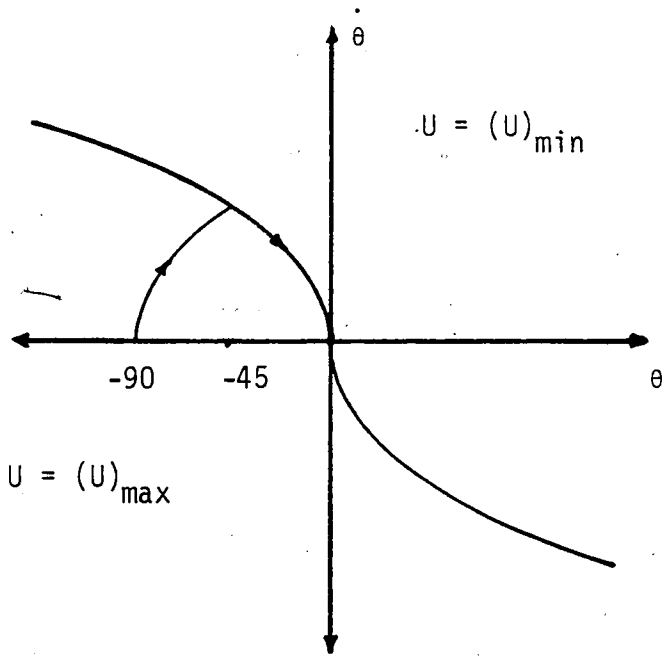

Fig. 3.2 Switching Curve

space into two regions of opposite initial control polarity. The second switch occurs when the state point reaches the switching curve, which is contained within the switching surface. Finally, the state point follows the switching curve to the origin (see Fig. 3.4). The behaviour of the fourth-order traverse time optimal control is similar except for an additional switch which occurs when the state lies in a particular four-dimensional sub-state-space.

3.1 The Switching-Time Method

The time optimal control of a dynamic system can be implemented in one of the following two ways: (1) by a continuous monitoring of the state point within the state space and execution of control polarity switches when the monitored point intersects a switching surface, or (2) by a calculation of the control polarity switching-times based on the initial state and the system model, assuming no further disturbance. The second case is employed in the tank because it distinguishes the processes of control calculation (performed by a microprocessor on board the tank) and control execution (the actual controller implementation of the previously calculated control). As mentioned above, time optimal controllers based their control selection on the present state. Microprocessors, however, require a finite time interval to perform the control

calculations, and during this time interval the state changes. Therefore, an extrapolation of the state is required in conjunction with a delay between control calculation and execution. This delay, although not recognized in the present study, is a natural extension of the second case.

The switching-time method is used to determine the control polarity switching-times for time optimal control [6]. To develop this method, the following Laplace Transformation theorem is employed:

> If the transformable and bounded function $x(t)$ is truncated, that is, if
>
> $$x(t) = \begin{cases} f(t) & t_0 < t < t_f \\ 0 & t < t_0,\ t > t_f \end{cases}$$
>
> then its Laplace transform, $X(s)$, is entire (i.e. analytic for all finite values of s).

In other words, if the state point $\underline{x}(t)$ is to move from its initial condition $\underline{x}(t_0)$ to the origin, $\underline{x}(t_f) = \{0\}$, within a finite interval of time (i.e. $\underline{x}(t)$ is truncated), then each component of $\underline{X}(s)$ is entire.

The Laplace transformation of a linear state equation,

$$\dot{\underline{x}} = \underline{A}\,\underline{x} + \underline{b}\,u,$$

is,

$$\underline{X}(s) = \underline{\Phi}(s)\underline{x}(0) + \underline{G}(s)U(s) \qquad (3.3)$$

where $\underline{\Phi}(s)$ is the resolvant matrix, $\underline{x}(0)$ is the initial state, $U(s)$ is the Laplace transform of the control u, and $\underline{G}(s)$ is a vector of transfer functions relating the control to the state. Since bang-bang control applies,

$$U(s) = \pm \frac{k}{s} [1 - 2e^{-T_1 s} + 2e^{-T_2 s} - \ldots + 2(-1)^{n-1} e^{-T_{n-1} s} + (-1)^n e^{-T_n s}] \tag{3.4}$$

where k is the control magnitude, T_i ($i = 1,2,\ldots,n-1$) are the unknown control switching-times, and T_n is the unknown control shut-off time. To satisfy Bellman's n-interval theorem, the index n is set equal to the system order. Since the elements of $\underline{G}(s)$ have n poles, n conditions can be imposed for the n unknown switching-times. Finally, the initial polarity of $U(s)$ is selected so that the switching-times which result are real and positive.

3.2 Application to the Hydraulic System

A precise application of time optimal control to the 17^{th} order hydraulic gun drive tank is highly impractical. Solving seventeen nonlinear switching-time equations in addition to somehow accommodating the effects of ground disturbances would be extremely complex. Instead, the elevation and traverse TOCS are based on crude third and fourth-order models,

respectively. These crude models assume that the turret and gun and their controlling hydraulic systems are autonomous. In other words, the disturbance torques caused by hull motion are neglected.

Time optimal control switching-time equations are derived for the elevation and traverse hydraulic systems in Sections 3.21 and 3.22, respectively. Attempts to solve the traverse switching-time equations failed, however, because of severe numerical convergence problems, so the development of the traverse TOC is as yet incomplete. The elevation switching-time equations, on the other hand, are easily solvable, giving the complete development of an elevation TOC. This controller is tested in conjunction with the Kalman filter type iterative observer of Ref. [2].

A measurement and control sequence consists of (1) an observer estimation of the present state, (2) solution of the switching-time equations which are functions of the state, and (3) the execution of the selected time optimal control. Time optimal control polarity switches are commonly executed during the time interval before the next observation, causing a problem in the Kalman filter observer which assumes constant control over the entire interval. This problem is remedied by giving the time-average control during the interval to the observer, while estimating the servo motor current with the

exact step-wise control and the linear lag model of the servo motor. The errors resulting from use of the time-averaged control in the remainder of the observer are not too large.

The use of the stochastic optimal Kalman filter observer with the elevation TOC is very inefficient. The Kalman filter estimates the entire seventeen element state vector in addition to estimating 51 ground contour states and six axle forces, but only three of these states are needed by the elevation TOC. Therefore, this observer can be replaced by the simpler nonlinear gun position observer of Section 3.3, which estimates the needed angle error. The second needed estimate is of the elevation space rate. This is measured directly, and we propose direct use of the measurement rather than a complicated but marginally improved Kalman filter version thereof. The third variable is the servo motor current, which is easily calculated. Thus, all the needed state variables are specified. This simpler observation scheme was developed after the testing of the elevation hydraulic system TOC, however, and is not examined further.

A final point to be made concerns the accuracy of the control polarity-switch timer. This timer receives the switching-times at the start of a time interval from the switching-time equation solver (microprocessor), and then proceeds to signal polarity switches when a switching-time is reached.

However, the timer cannot be expected to signal switches as precisely as the m digit accuracy of the on-board equation solver. Therefore, the switching-times are rounded to their nearest 0.001 seconds, which becomes the assumed timer accuracy and is one-tenth of the controller time interval. This rounding obviously introduces some suboptimality.

3.21 Elevation Hydraulic System Time Optimal Control

The elevation TOC is based on the elevation gun dynamics and simplified elevation hydraulic gun drive system shown in Figures 3.3 and 2.9, respectively.[1] The pertinent differential equations are

$$\frac{d}{dt} IIN = \frac{1}{\tau_{ME}} (GTM \cdot ELVV - IIN) \tag{3.5}$$

$$\frac{d}{dt} SRE = (TQEL - FTQEL + DSTQEL)/J_g \tag{3.6}$$

$$\frac{d}{dt} AE = SRE \tag{3.7}$$

These equations govern the elevation servo motor current, gun elevation space rate, and absolute elevation angle error, respectively. In addition, ELVV is the elevation controller

[1] System parameters are listed and defined in Appendix A.

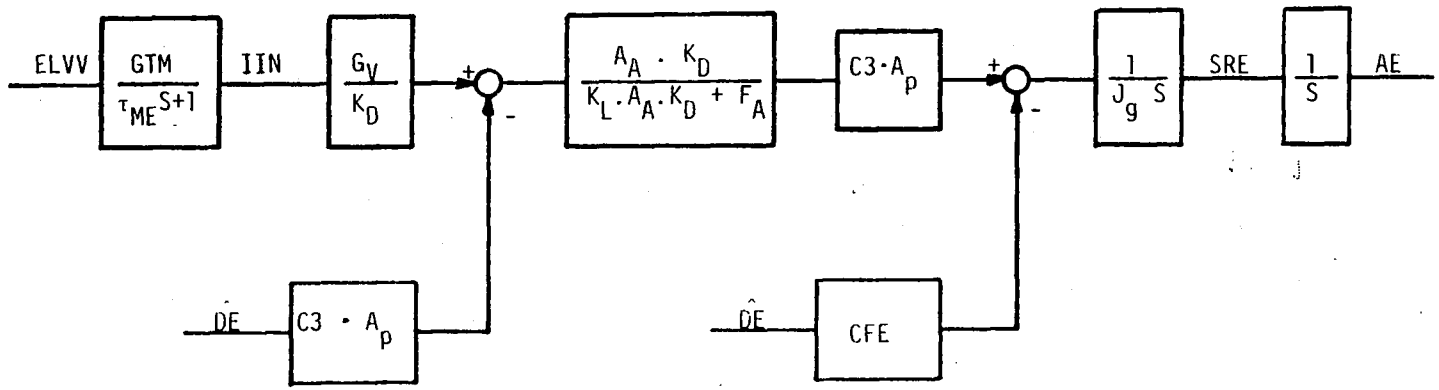

Fig. 3.3 Elevation Gun Dynamics - Hydraulic Drive

output voltage, TQEL and FTQEL are the control and friction torques, and DSTQEL is the neglected disturbance torque. All other terms are system parameters. Equation (3.6) is expanded by expressing TQEL and FTQEL in terms of system parameters and variables, yielding

$$\frac{d}{dt}\,SRE = \{(C3\cdot A_p\cdot CON\cdot\ G_V/K_D\ )IIN - (C3^2\cdot A_p{}^2/CON)DE - (CFE)DE\}/J_g \qquad (3.8)$$

In this expression, DE (the only new undefined variable) is the relative angular velocity between the gun and hull in elevation, and CON (an undefined system parameter) represents the term in the largest block of Fig. 3.3. Equations (3.5), (3.7), and (3.8), written in state space form, become

$$\begin{bmatrix}\dot{AE}\\ \dot{IIN}\\ \dot{SRE}\end{bmatrix} = \begin{bmatrix}0 & 0 & 1\\ 0 & A & 0\\ 0 & B & 0\end{bmatrix}\begin{bmatrix}AE\\ IIN\\ SRE\end{bmatrix} + \begin{bmatrix}0\\ 0\\ C\end{bmatrix}DE + \begin{bmatrix}0\\ D\\ 0\end{bmatrix}ELVV \qquad (3.9)$$

where A, B, C, and D represent groups of parameters.

The switching-time method is applied to equation (3.9) by forcing its Laplace transform, $\underline{X}(s)$, to be entire. This is accomplished fully by forcing $X_1(s)$, the first element, to be entire. This element is

$$X_1(s) = \frac{x_1(0)}{s} + \frac{B\ x_2(0)}{s^2(s-A)} + \frac{x_3(0)}{s^2} + \frac{C}{s}R(s) + \frac{BD}{s^2(s-A)}U(s) \qquad (3.10)$$

where $U(s) = L\{ELVV(t)\}$, $R(s) = L\{DE(t)\}$, $X_1(s) = L\{AE(t)\}$, and where $x_1(0)$, $x_2(0)$, and $x_3(0)$ are AE(0), IIN(0), and SRE(0), respectively. The control, ELVV(t), is to be time optimal. Therefore,

$$U(s) = \pm \frac{K}{s} [1 - 2e^{-T_1 s} + 2e^{-T_2 s} - e^{-T_3 s}] \qquad (3.11)$$

The remaining function, DE(t), is unknown, but its value is estimated by the observer. Using these estimates the average value of DE(t) over the next time interval is estimated. This average value, called DEH, is assumed to approximate DE(t) over the interval, so that

$$R(s) = \frac{DEH}{s} [1 - e^{-Ts}] \qquad (3.12)$$

Using these expressions for U(s) and R(s), equation (3.10) becomes

$$X_1(s) = \frac{\{x_1(0)s^2(s-A) + Bx_2(0)s + x_3(0)s(s-A) \pm B \cdot D \cdot K[1-2e^{-T_1 s}+2e^{-T_2 s}-e^{-T_3 s}]+C \cdot DEH(s-A)[1-e^{-Ts}]\}}{s^3(s-A)} \qquad (3.13)$$

Finally, the switching-time equations are derived by forcing $X_1(s)$ to be analytic at s=A and s=0. This is accomplished by setting the numerator equal to zero with s=A, and the first and second derivatives of the numerator with respect to s equal to zero with s=0. The equations are:

$$B \cdot A\, x_2(0) + B \cdot D \cdot K[1 - 2e^{-T_1 A} + 2e^{-T_2 A} - e^{-T_3 A}] = 0 \tag{3.14a}$$

$$B\, x_2(0) - A\, x_3(0) \pm B \cdot D \cdot K\, [2T_1 - 2T_2 + T_3] - C \cdot DEH \cdot A \cdot T = 0 \tag{3.14b}$$

$$-2A\, x_3(0) + 2\, x_2(0) \pm B \cdot D \cdot K\, [-2T_1^2 + 2T_2^2 - T_3^2] + C \cdot DEH\, [A\, T^2 + 2T] = 0 \tag{3.14c}$$

These equations must be solved for the switching-times. The last two equations were solved for T_2 and T_3 in terms of T_1 and inserted into the top equation yielding a single nonlinear equation of the form:

$$f(T_1) = 0 \tag{3.15}$$

This function is solved numerically for its only positive real root. The numerical approach employed consists of three parts: (1) a preliminary search routine to locate a region containing a root, (2) a complex-to-real switch routine to determine the value of $f(T_1)$ at the point that it initially becomes real, so that a real root is not missed, and (3) a Newton's method routine to quickly and precisely find the root after the preliminary search.[1] To determine the initial control polarity, the preliminary search routine executes a parallel evaluation

[1] The related computer coding will be given in "Modern Control Concepts Applied to Disturbance Accommodation of Tank Turrets-Phase III."

of $f(T_1)$ using both possible polarities, $f_1(T_1,+K)$ and $f_2(T_1,-K)$. The region containing the positive real root corresponds to one of these functions, and thereby determines the initial polarity.

Occasionally the switching-time equations become impossible to solve numerically because of catastrophic cancellation (a numerical problem characteristic of digital computation). Specifically, the preliminary search routine fails to locate a region containing a root. When this occurs, the three switching equations are abandoned in place of two switching-time equations based on a model which neglects the servo motor current lag. This problem occurs only about 0.5% of the time.

A time optimal control of the elevation system with hull disturbances omitted is shown in Figure 3.4. Since the elevation controller design arises from this third-order system, the time optimal control is exact and the state point reaches the origin precisely. The presence of hull disturbances would produce some error, however. Control switches occur at Q_1 and Q_2 when the state point reaches the switching surface and switching curve, respectively.

3.22 Traverse Time Optimal Control

The uncompleted development of the traverse time optimal controller is based on a fourth-order model comprising the

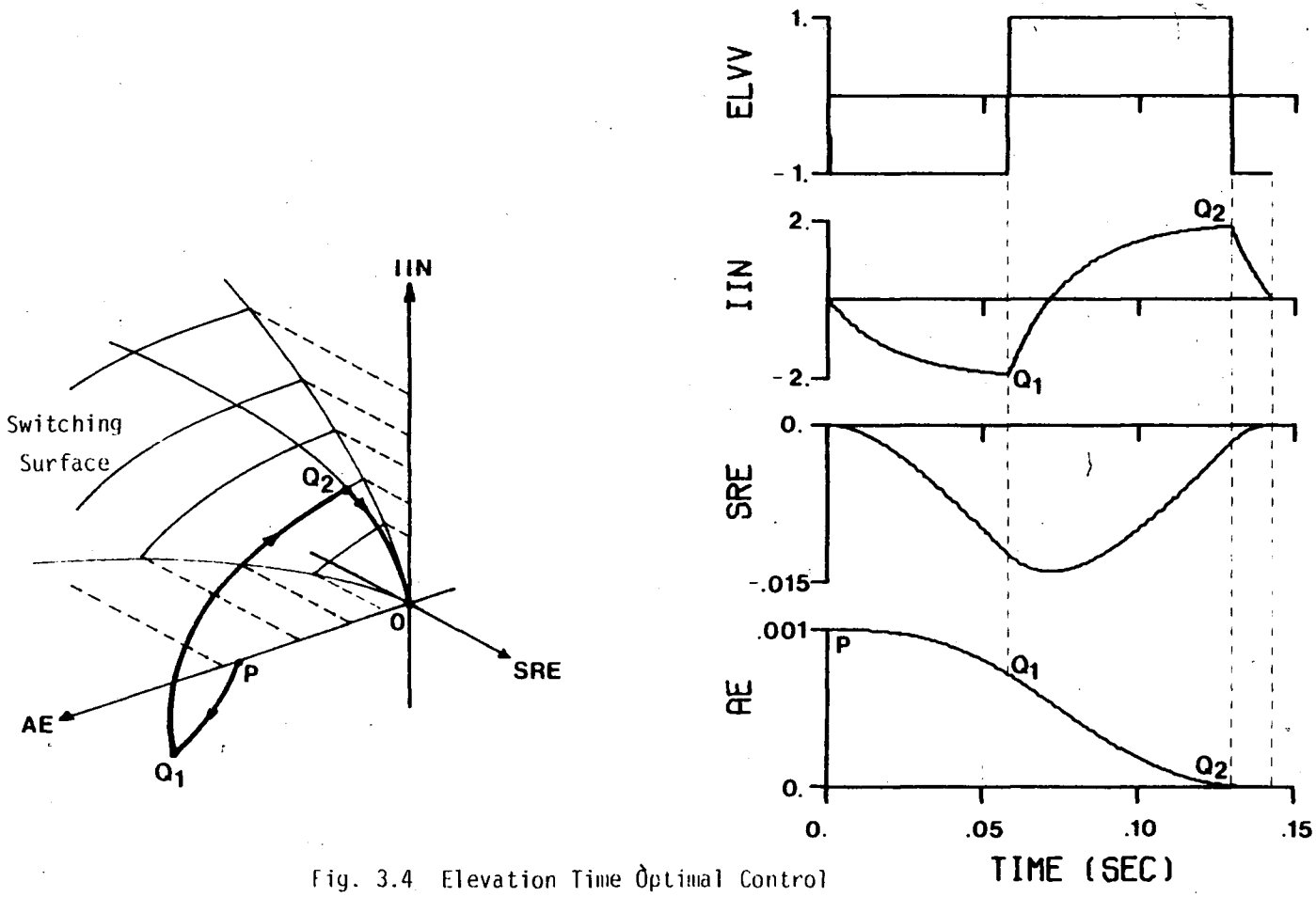

Fig. 3.4 Elevation Time Optimal Control

traverse hydraulic system and turret dynamics. This development parallels the approach leading to the elevation time optimal controller. However, two additional problems are encountered which greatly complicate the solution of the resulting switching-time equations. First, the traverse torque motor differential pressure responds more slowly than the elevation actuator differential pressure, and cannot be eliminated from the list of dynamic variables (i.e. replaced by a non-dynamic algebraic relation). Therefore, the traverse model is fourth-order rather than third. Second, a strong oscillatory coupling exists between the torque motor differential pressure and the traverse space rate, introducing a pair of lightly damped complex conjugate poles. Because of these poles, Bellman's n-interval theorem does not strictly apply. However, it has been shown that the switching-time method (which incorporates Bellman's n-interval theorem) yields optimal switching-times if the damping ratio of the complex poles exceeds 0.1 [7]. Unfortunately, the damping ratio of the traverse system complex poles is 0.07. This low damping ratio and the high system order mentioned above drastically reduced the odds of developing a successful traverse time optimal controller. An attempt which failed is described below.

The pertinent traverse system equations are:

$$\frac{d}{dt}\,IVMA = \frac{1}{\tau_{CL}}\,(G_{VA}\cdot VIN - IVMA) \qquad (3.16)$$

$$\frac{d}{dt} PLTR = \{(K_1 \cdot .985\sqrt{P_s - PLTRMN})IVMA - K_L \cdot PLTR + DSPM(GR12 + 1)SRTR\}2\beta_m V_{OLTR} \quad (3.17)$$

$$\frac{d}{dt} SRTR = (TQTR - FTQTR + DSTQTR)/J_{ty} \quad (3.18)$$

$$\frac{d}{dt} AT = SRTR \quad (3.19)^1$$

These equations govern the traverse servo motor current, torque motor differential pressure, space rate, and gun angle error. In addition, VIN is the traverse controller output voltage, TQTR and FTQTR are the control and friction torques, and DSTQTR is the neglected disturbance torque. When expressed in terms of system parameters and variables, equation (3.18) becomes

$$\frac{d}{dt} SRTR = \{-(GR12 \cdot DSPM)PLTR - DHT \cdot DTR - SIGN\ (CFT,DTR)\}/J_{ty} \quad (3.20)$$

This new variable, DTR, is the relative velocity between the turret and hull, and is related as shown to the viscous and coulomb friction torques. The characteristic roots of equations (3.16), (3.17), (3.19) and (3.20) are 0, 125, and -1.70 $\pm$ 23.7. These roots are calculated by setting DTR = 0, since

[1] This equation is modified in Section 3.4.

the related friction torques were to be added as a constant bias over the interval like friction torques in the elevation system.

At this point the switching-time method is applied yielding four complex nonlinear switching-time equations. Two of the switching-times can be eliminated leaving two equations of the form

$$f_1(T_1, T_2) = 0 \qquad (3.22a)$$

$$f_2(T_1, T_2) = 0 \qquad (3.22b)$$

These equations reflect the light damping of the system, making them very difficult to solve. Initially, Newton's method was applied without success (Newton's method only works for well-behaved functions). Secondly, the method of steepest descent was applied also without success. The presence of the lightly dampled complex poles allows several solutions to exist and makes the selection of the non-extraneous solution very difficult. A second approach which may relieve these numerical problems is discussed in Chapter 5.

3.3 A Nonlinear Gun Position Observer

A time optimal controller bases its control selection on the present condition of the entire state vector. In the current applications, however, the time optimal controllers

are based on simple second or third-order models and require only two or three state variables. Therefore, only a few elements of the tank system state vector are required; the rest of the states estimated by the Kalman filter observer of Ref. [2] are not used, representing unnecessary computation time and observer complexity. To simplify the system, an observer is devised which estimates only the gun position errors. This observer bases its observation only on gun angular rotation rates. As a result, a very simple and yet versatile gun position observer is developed.

Equations for the gun elevation and traverse position errors, AE and AT, depend on the gun direction cosines as shown here.

$$AE = SIN^{-1}\ (GCY) - AEO \tag{3.23}$$

$$AT = TAN^{-1}\ (-\frac{GCZ}{GCX}) - ATO \tag{3.24}$$

GCX, GCY, and GCZ are the x, y, and z gun direction cosines with respect to a non-rotating reference frame herein called OXYZ, and where AEO and ATO are the desired elevation and traverse gun angles also in frame OXYZ. These gun direction cosines are unknown , but their time derivatives are known and governed by the relationships derived below. This derivation requires the definition of a rotating frame, $Ox_gy_gz_g$, which is attached to the gun as shown in Fig. 3.5. Note that GC,

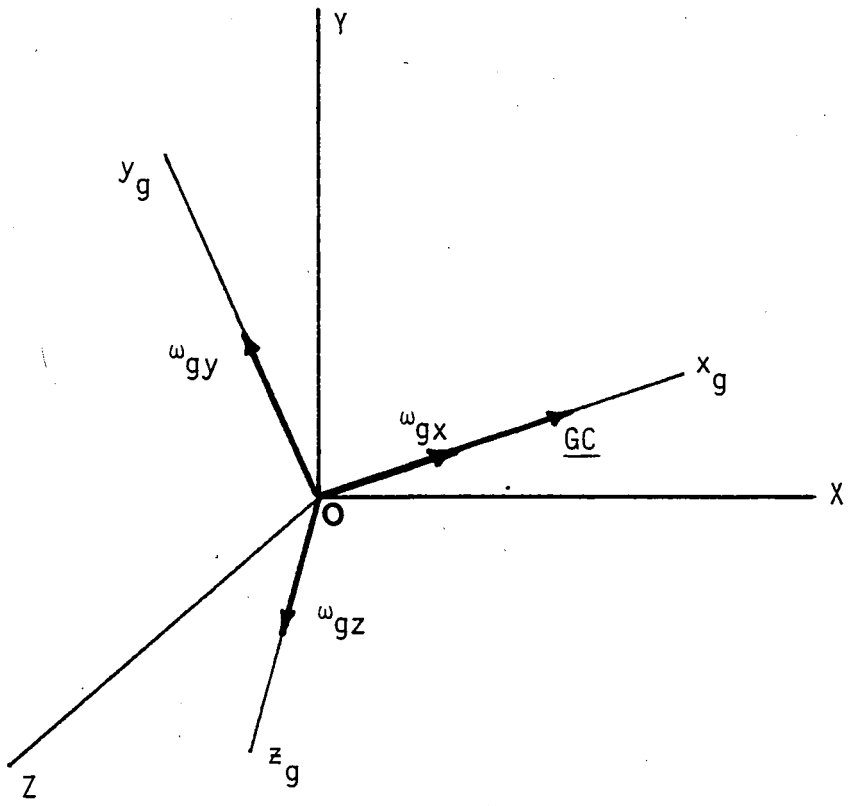

Fig. 3.5 Nonlinear Observer References Frames

the gun direction, is a unit vector along the axis of the gun and represents the vector sum of the gun direction cosines. The time derivative of $\underline{GC}$ with respect to the fixed frame equals the time derivative of $\underline{GC}$ with respect to the rotating frame plus $\underline{\Omega} \times \underline{GC}$, where $\underline{\Omega}$ is the angular velocity of the rotating frame. That is,

$$(\dot{\underline{GC}})_{OXYZ} = (\dot{\underline{GC}})_{Ox_gy_gz_g} + \underline{\Omega} \times \underline{GC} \tag{3.25}$$

Since the rotating frame is attached to the gun, $(\dot{\underline{GC}})_{Ox_gy_gz_g} = \{0\}$, and $\underline{\Omega}$ is the angular velocity of the gun, therefore

$$(\dot{\underline{GC}})_{OXYZ} = \omega_{gz}\, \underline{i}_g - \omega_{gy}\, \underline{k}_g \tag{3.26}$$

(Notice that ω_{gz} and ω_{gy} are the elevation and traverse rate gyro measurements.) Equation (3.26) is useless in its present form because the directions of $\underline{j}_g$ and $\underline{k}_g$ are unknown. Therefore, a coordinate transformation is performed using the $\underline{C}$ matrix shown below, which relates the rotating reference frame, $Ox_gy_gz_g$, to the fixed frame, OXYZ.[1]

$$\begin{bmatrix} GCX \\ GCY \\ GCZ \end{bmatrix} = \begin{bmatrix} C_{xx} & C_{xy} & C_{xz} \\ C_{yx} & C_{yy} & C_{yz} \\ C_{zx} & C_{zy} & C_{zz} \end{bmatrix} \begin{bmatrix} 0 \\ \omega_{gz} \\ -\omega_{gy} \end{bmatrix} \tag{3.27}$$

[1] Pars, A Treatise on Analytical Dynamics, pg. 104.

Where

$$\begin{bmatrix} C_{xx} & C_{xy} & C_{xz} \\ C_{yx} & C_{yy} & C_{yz} \\ C_{zx} & C_{zy} & C_{zz} \end{bmatrix} = \begin{bmatrix} \cos Pg \cos Yg - \sin Pg \sin Rg \sin Yg & -\sin Pg \cos Rg & \cos Rg \sin Yg + \sin Pg \sin Rg \cos Yg \\ \sin Pg \cos Yg + \cos Pg \sin Rg \sin Yg & \cos Pg \cos Rg & \sin Pg \sin Yg - \cos Pg \sin Rg \cos Yg \\ -\cos Rg \sin Yg & \sin Rg & \cos Rg \cos Yg \end{bmatrix}$$

(3.28)

The sin-cosine arguments are the roll, yaw and pitch angles of the gun with respect to frame OXYZ. But like the gun direction cosines, these angles are unknown . Instead, their time derivatives are known, and related to the gun angular velocities by equation (3.29).[1]

$$\begin{bmatrix} \dot{Rg} \\ \dot{Yg} \\ \dot{Pg} \end{bmatrix} = \begin{bmatrix} \cos Yg & 0 & \sin Yg \\ \frac{\sin Rg \sin Yg}{\cos Rg} & 1 & -\frac{\sin Rg \cos Yg}{\cos Rg} \\ -\frac{\sin Yg}{\cos Rg} & 0 & \frac{\cos Yg}{\cos Rg} \end{bmatrix} \begin{bmatrix} \omega_{gx} \\ \omega_{gy} \\ \omega_{gz} \end{bmatrix}$$

(3.29)

[1] ibid, pg. 106-107.

Unfortunately, equation (3.29) employs ω_{gx}, which is the gun spin rate about its axis of symmetry. Consequently, the nonlinear observation scheme will require a third rate gyro in addition to the two already employed for conventional control. Transducer requirements are compared and discussed in Chapter 5.

Finally, the derivatives of the gun angles and direction cosines can be integrated simultaneously, yielding the three direction cosines needed to solve for the gun pointing errors. The nonlinear gun position observer based on the above derivation is pictured in Figure 3.6. Relations R1 and R2 represent equations (3.29) and (3.27) respectively. In addition, the six 1/D terms represent six continuous time integrations which can be performed digitally or using analog equipment.

When the nonlinear observer is switched on, the non-rotating frame is fixed in its present position, which at that instant coincides with the rotating frame. This yields the following initial conditions:

Pg = 0.	Yg = 0.	Rg = 0.
GCX = 1.	GCY = 0.	GCZ = 0.

Until the observer is restarted, the absolute gun position errors are defined with respect to this fixed frame. Defining the errors in this manner produces some inconsistency, however. For example, suppose that the main gun is pointing straight

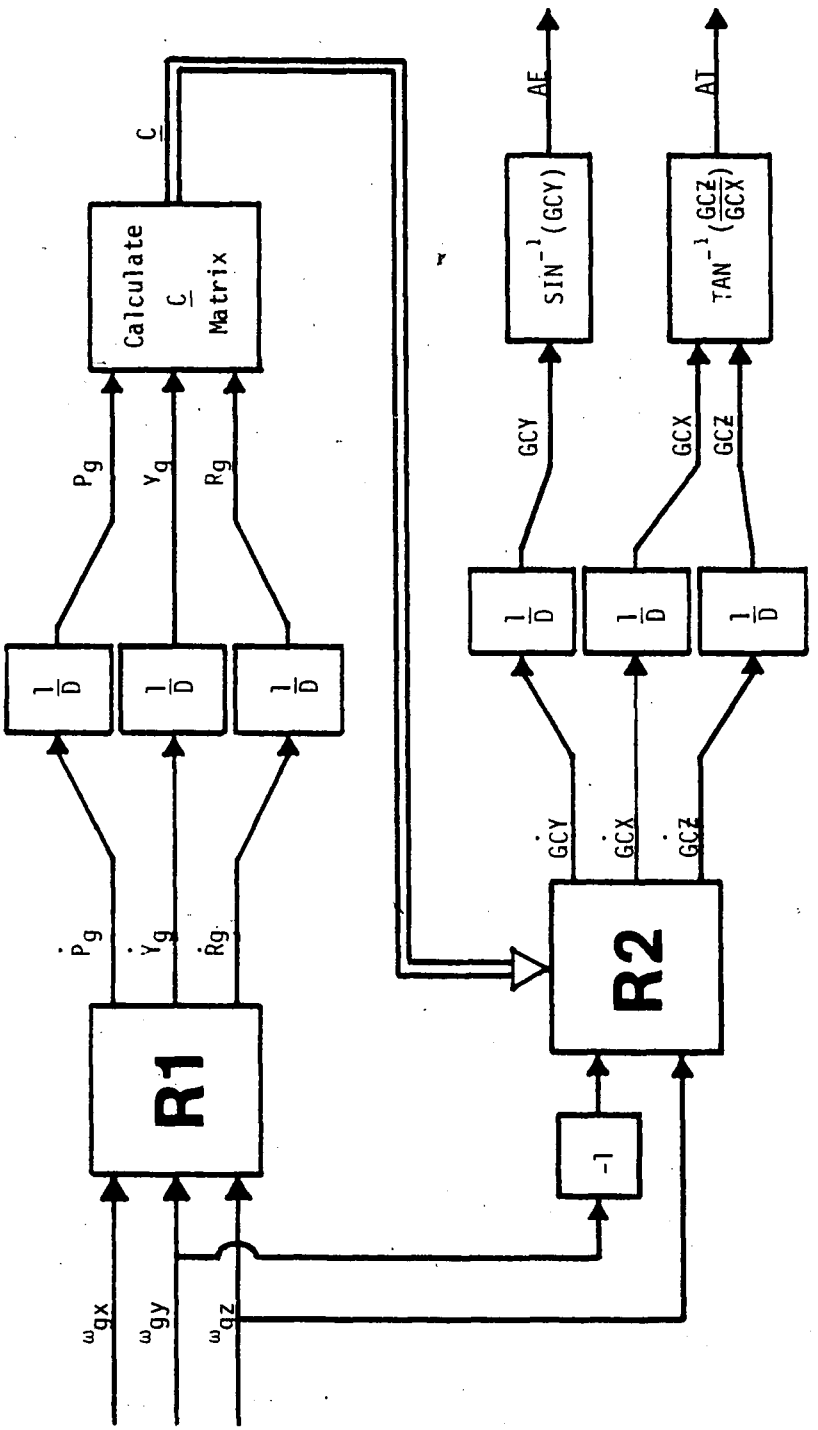

Fig. 3.6 Nonlinear Gun Position Observer

ahead and the tank is moving horizontally along a hillside sloping 45 degrees to the right when the observer is switched on. And as the tank proceeds the hillside levels out followed by a hillside sloping 45 degrees to the left. At this time the observer signals a traverse position error of +0.001 radians. This error is defined with respect to the frame tilting 45 degrees to the right and therefore can be presently corrected by a -0.001 radian change in gun elevation. To accommodate this effect and remove the inconsistency, the absolute position errors of the fixed frame are resolved onto the rotating frame using the $\underline{C}$ coordinate transformation matrix as shown here.[1]

$$\{\text{Abs Err}\}_{0_{x_g y_g z_g}} = [\underline{C}]^T \{\text{Abs Err}\}_{0XYZ} \qquad (3.30)$$

This is possible because the two position errors define a three-dimensional vector in space.

The beauty of the nonlinear gun position observer lies in its versatility. Since it is not based on a linearized model it works for any gun position, and since it is not directly affected by hull motion it works at any tank speed, while changing speed, or even while changing direction. Its performance is limited only by the accuracy of the rate gyros.

[1] $\underline{C}$ is an orthonormal matrix, therefore $\underline{C}^{-1} = \underline{C}^T$

One disadvantage, therefore, is its inability to filter out measurement noise. The possible development of an unconventional filtering algorithm has not been examined, but the effects of measurement noise are discussed in Chapter 5.

3.4 Applications to the Electric System

A precise application of time optimal control to the 12th order electric drive tank is impractical for the same reasons noted for the hydraulic drive tank. Instead, crude low order models are employed. The electric drive system is much simpler than the hydraulic drive system, because the electric controllers exert control torques directly on the gun, unlike the hydraulic controllers. Therefore, both elevation and traverse TOCS are based on simple 2nd order models.

The electric drive TOCS described herein employ the nonlinear gun position observer for state variable estimation. The Kalman filter observer of Ref. [2] could have been used, however, only four of the twelve estimated state variables are needed, so the nonlinear observer received precedence. As before, a control polarity-switch timer with a 0.001 second resolution time is assumed.

The elevation and traverse electric drive TOCS are almost identical, and therefore are discussed in parallel. Their pertinent equations in state space form are

$$\begin{bmatrix} \dot{x}_1 \\ \dot{x}_2 \end{bmatrix} = \begin{bmatrix} 0 & 1 \\ 0 & 0 \end{bmatrix} \begin{bmatrix} x_1 \\ x_2 \end{bmatrix} + \begin{bmatrix} 0 \\ 1/J \end{bmatrix} u + \begin{bmatrix} 0 \\ 1/J \end{bmatrix} T_q \qquad (3.31)$$

where x_1 is a position error (AE or AT), x_2 is a space rate (SRE or SRTR), u is a control torque, T_q is any additional torque (Coulomb friction, disturbance torque, etc.), and J is an inertia (gun elevation inertia or turret traverse inertia). Since u(t) is a time optimal bang-bang control,

$$U(s) = \pm \frac{T_m}{s} [1 - 2e^{-T_1 s} + e^{-T_2 s}] \qquad (3.32)$$

where $U(s) = L\{u(t)\}$, and T_m is the saturation control torque. The remaining unknown, $T_q(t)$, is the sum of a disturbance torque, gun drive coulomb friction, and, in elevation, a clockspring torque. The disturbance torque is neglected, however, allowing T_q to be represented as

$$TQ(s) = \frac{T_f}{s} [1 - e^{-Ts}] \qquad (3.33)$$

where $TQ(s) = L\{T_q(t)\}$. That is, the controller assumes that $T_q(t)$ is constant over the time interval of T seconds. This approximation is appropriate because a coulomb friction by definition remains constant except for changes in polarity. Tachometers which measure the elevation and traverse rates relative to the hull are employed to determine the coulomb friction torques; the clockspring torque is a simple function

of the relative elevation angle which can be estimated by a gunner or monitored by direct integration of the elevation tachometer signal. Therefore, the average additional torque over the next time interval, T_f, is easily estimated by extrapolating the monitored coulomb or coulomb-clockspring torques to the midpoint of the next time interval. Finally, the following two equations result from the application of the switching-time method:

$$x_2(0) \pm \frac{T_m}{J}[2T_1 - T_2] + \frac{T_f T}{J} = 0 \tag{3.34}$$

$$2x_1(0) \pm \frac{T_m}{J}[-2T_1^2 + T_2^2] - \frac{T_f T}{J} = 0 \tag{3.35}$$

Solving these equations for T_1 and T_2 yields

$$T_{1_{(1,2)}} = f_1(x_1(0),\ x_2(0),\ \pm T_m,\ T_f,\ J) \tag{3.36}$$

$$T_2 = f_2(x_1(0),\ x_2(0),\ \pm T_m,\ T_f,\ J) \tag{3.37}$$

where $T_{1_{(1,2)}}$ represents the two roots of a quadratic, such that $T_{1(1)} = A + \sqrt{B}$ and $T_{1(2)} = A - \sqrt{B}$. It turns out, however, that $T_{1(2)}$ is always extraneous, and can be eliminated from the TOC calculations. The resulting switching-time equations are

$$T_1 = \frac{1}{2}\left\{\mp \frac{2Z_2 J}{T_m} + \sqrt{2\left(\frac{Z_2 J}{T_m}\right)^2 \mp \frac{4Z_1 J}{T_m}}\right\} \tag{3.38}$$

$$T_2 = 2T_1 \pm \frac{Z_2 J}{T_m} \tag{3.39}$$

where

$$Z_1 = x_1(0) - \frac{1}{2}\frac{T_f T^2}{J}\ , \tag{3.40}$$

and

$$Z_2 = x_2(0) + \frac{T_f T}{J} \tag{3.41}$$

Equations (3.38) through (3.41) represent the entire elevation and traverse electric drive TOCS. The initial control polarity is determined by requiring that the switching-times are real and positive.

The state space representation shown as equation (3.31) assumes that $\dot{x}_1 = x_2$ (i.e. the time derivative of the angle error equals the space rate). However, this is strictly true only in elevation. To show this, derivatives of the angle errors are evaluated (see equations (3.23) and (3.24)):

$$\frac{d}{dt}\,AE = \frac{1}{\sqrt{1-(GCY)^2}}\ \dot{GCY} \tag{3.42}$$

$$\frac{d}{dt}\,AT = -\frac{1}{1+(\frac{GCZ}{GCX})^2}\ \frac{GCX\cdot\dot{GCZ}-GCZ\cdot\dot{GCX}}{(GCX)^2} \tag{3.43}$$

Since the nonlinear gun position observer resolves the angle errors onto the current rotating reference frame, their derivatives are evaluated with respect to the fixed frame

coinciding with the rotating frame at the beginning of the time interval. In this frame, GCX ≃ 1, and GCY ≃ GCZ ≃ 0. Also, equation (3.26) indicates that $\dot{GCX} \simeq 0$, $\dot{GCY} \simeq \omega_{gz}$, and $\dot{GCZ} \simeq -\omega_{gy}$. (Approximate signs are used because the two frames coincide only at the start of each interval.) Therefore equations (3.42) and (3.43) become

$$\frac{d}{dt} AE = \omega_{gz} \qquad (3.44a)$$

$$\frac{d}{dt} AT = \omega_{gy} \qquad (3.45a)$$

or equivalently

$$\frac{d}{dt} AE = SRE \qquad (3.44b)$$

$$\frac{d}{dt} AT = SRTR \cos E - (\omega_{hx} \cos TR - \omega_{hz} \sin TR)\sin E \qquad (3.45b)$$

Equation (3.44b) indicates that the elevation switching-time equations are correct as derived. On the other hand, equation (3.45b) reveals that the traverse switching-time equations must be modified. That is, SRTR must be replaced by ω_{gy} in equation (3.41), yielding $Z_2 = \omega_{gy} + T_f T/J$. This causes the traverse TOC to reduce AT and ω_{gy} to zero rather than AT and SRTR. Block diagrams of the elevation and traverse gun position dynamics as assumed by the time optimal controllers are shown in Figures 3.7 and 3.8 .

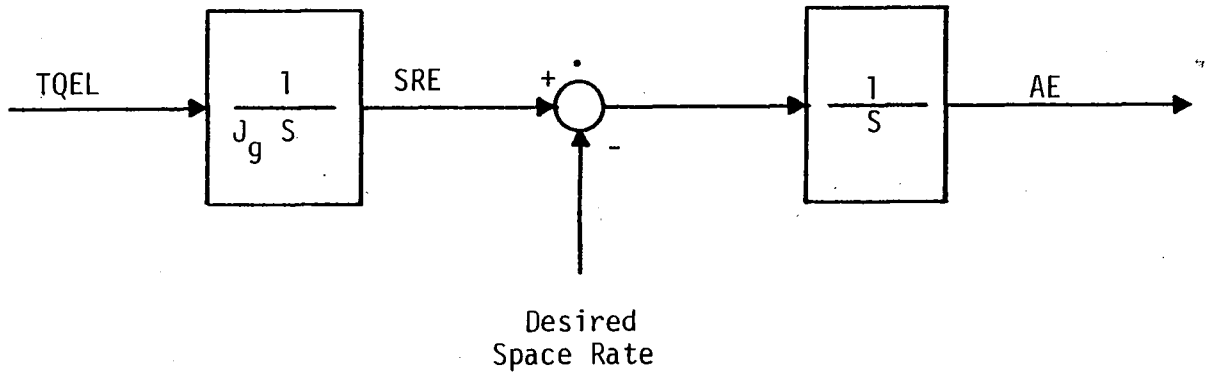

Fig. 3.7 Elevation Gun Dynamics - Electric Drive

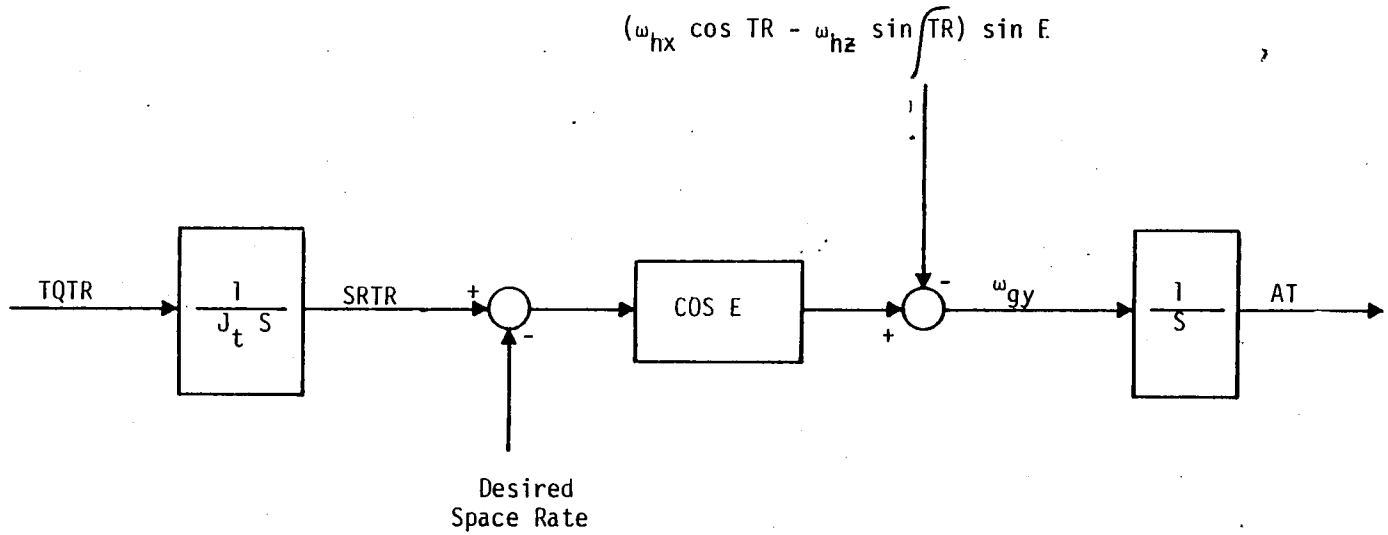

Fig. 3.8 Traverse Gun Dynamics - Electric Drive

3.41 Incorporation of Measurement Noise

The nonlinear gun position observer and time optimal controllers use variables which are directly measured; there is no (optimal) filtering performed to reduce the adverse effects of measurement noise. Fortunately, the nonlinear observer integrates these measurements, tending to smooth out the noise and lessen its ill effects. To assess the degredation in control system performance, gaussian white noise sequences are added to the measurements during a test simulation.

The five measurements employed by the electric drive time optimal control system comprise three rate gyro measurements and two tachometer measurements, such that

$$\begin{aligned} Y_1 &= \omega_{gx} + Yn_1 \\ Y_2 &= \omega_{gy} + Yn_2 \\ Y_3 &= \omega_{gz} + Yn_3 \\ Y_4 &= \dot{E} + Yn_4 \\ Y_5 &= \dot{TR} + Yn_5 \end{aligned} \tag{3.47}$$

where Y_i are the measured signals and Yn_i are the measurement noises. The representation of these continuous white noise signals within a digital computer is impossible, however. Therefore, they are each approximated by a multistage random sequence which produces an equivalent covariance matrix, $\underline{R}(t)$,

where $\underline{R}(t) = E\{\underline{x}(t) - \underline{x}(t)\}\{\underline{x}(t) - \underline{x}(t)\}^T$. This equivalence is satisfied when

$$\underline{Q}(t) = \underline{X}(k)\Delta t \qquad (3.48)^1$$

where $\underline{Q}(t) = E\{\underline{\omega}(t) - \bar{\underline{\omega}}(t)\}\{\underline{\omega}(t) - \bar{\underline{\omega}}(t)\}^T$, $\underline{X}(k) = E\{\underline{\omega}(k) - \bar{\underline{\omega}}(k)\}\{\underline{\omega}(k) - \bar{\underline{\omega}}(k)\}^T$, $\underline{\omega}(t)$ and $\underline{\omega}(k)$ are the continuous and multistage noise processes respectively, and Δt is the time interval of the sequence. In general, $\underline{Q}(t)$ and $\underline{X}(k)$ are diagonal matrices containing only noise variances.

The pertinent noise sequence variances used in the design of the stochastic optimal control system of Ref. [2] are listed in Table 1 and used to determine the equivalent variances for the time optimal control simulation. Since equal noise levels are assumed for both control schemes

$$\underline{X}_{SO}\Delta t_{SO} = \underline{X}_{TO}\Delta t_{TO} \qquad (3.49)$$

where $\Delta t_{SO} = 0.01$, the time interval of the stochastic optimal controller, and $\Delta t_{TO} = 0.0005$, the step size of the integration algorithm used to simulate the time optimal control systems. Therefore, $\underline{X}_{TO} = 20\ \underline{X}_{SO}$, as reflected in Table 1.

Five separate zero mean gaussian sequences having the variances listed in column 2 of Table 1 are added to $\underline{\omega}_g$,

[1] Bryson, Ho, Applied Optimal Control, pg. 343, 344.

$\dot{TR}$, and $\dot{E}$ during a time optimal control system simulation. The results are presented in Section 3.4.

TABLE 1

Measurement-Noise-Sequence Variances

Transducer	Variance	
	Stochastic Optimal Control	Time Optimal Simulation
Elevation Rate Gyro	1.79×10^{-7}	3.57×10^{-6}
Traverse Rate Gyro	6.01×10^{-9}	1.20×10^{-7}
Axial Spin Rate Gyro	N/A	3.57×10^{-6}
Elevation Tachometer	4.93×10^{-6}	9.86×10^{-5}
Traverse Tachometer	N/A	9.86×10^{-5}

4. RESULTS

The control systems discussed herein are evaluated in terms of the design objective of minimum gun pointing errors. Three control schemes are discussed in this section (the conventional and time optimal hydraulic system control and time optimal electric system control). A total of six control schemes are compared, however (the conventional, stochastic optimal, and time optimal control of both electric and hydraulic systems)[1]. Two methods of comparison are employed: (1) the graphical comparison of systems excited by the same random ground input, and (2) the comparison of performance indices.

The common right side ground input is shown in Figure 4.1; the left side is not excited, as mentioned previously. Unfortunately, however, the conventional control electric system simulation employed a different right side ground input. Nevertheless, a comparison is valid because both ground inputs possess equal statistical properties.

The results are condensed and compared in Table 2 using two performance indices: (1) the standard deviations of the gun pointing errors (σ), and (2) the average fractions of saturation control (w).

[1] The results for the stochastic optimal hydraulic system plus the conventional and stochastic optimal electric systems are taken from Ref. [2].

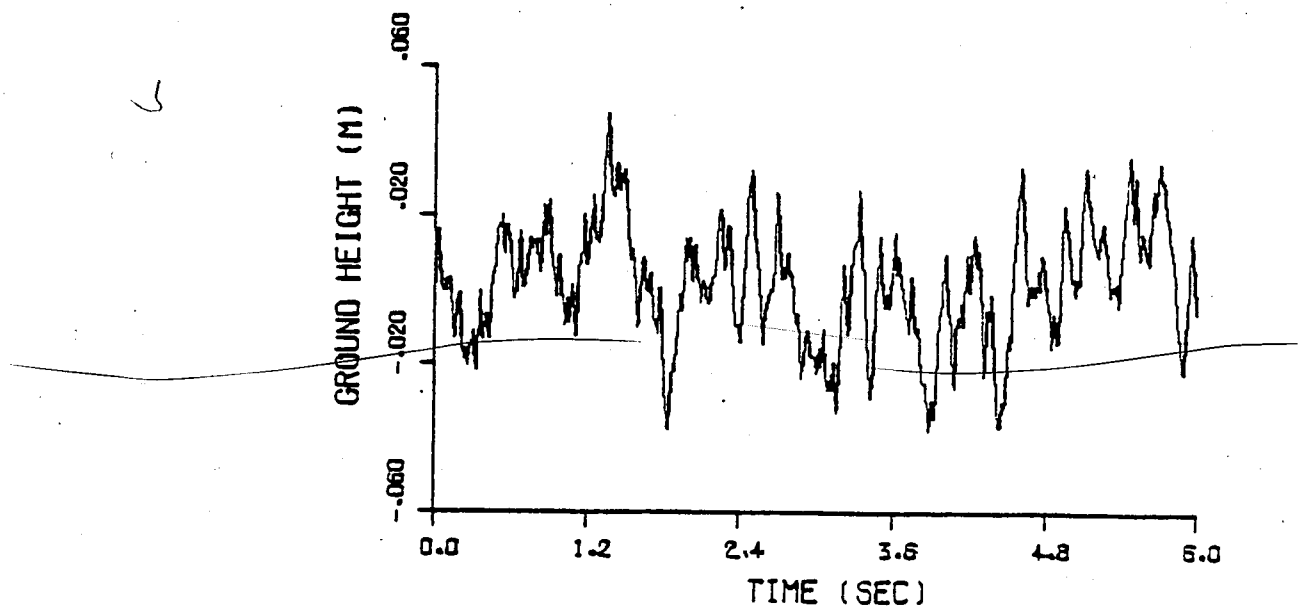

Fig. 4.1 Right-Side Ground Input

The standard deviations are computed in the normal fashion,

$$\sigma = \frac{1}{n} \sum_{i=1}^{n} e_i^2 \qquad (4.1)$$

using the n computer outputted angle errors called e. The average fractions of saturation control, on the other hand, are defined by

$$w = \frac{\frac{1}{n} \sum_{i=1}^{n} |u_i|}{(u)_{max}} \qquad (4.2)$$

Equation 4.2 employs the n outputted control magnitudes, $|u_i|$, and the saturation control, $(u)_{max}$. The results in Table 2 are discussed in Chapter 5.

4.1 Hydraulic System with Conventional Control

The nonlinear and linearized conventionally controlled hydraulic system models are graphically compared in Figures 4.2 and 4.3. The intrinsic dissimilarities between the two models become apparent in their behavioral differences, suggesting one possible source of error in the stochastic optimal control system which is based on the linear model. The time optimal controllers, however, incorporate only the model prelinearizations described in Section 2.6, and neglects hull disturbances. Therefore, these hull motion linear model errors have no effect on their performance.

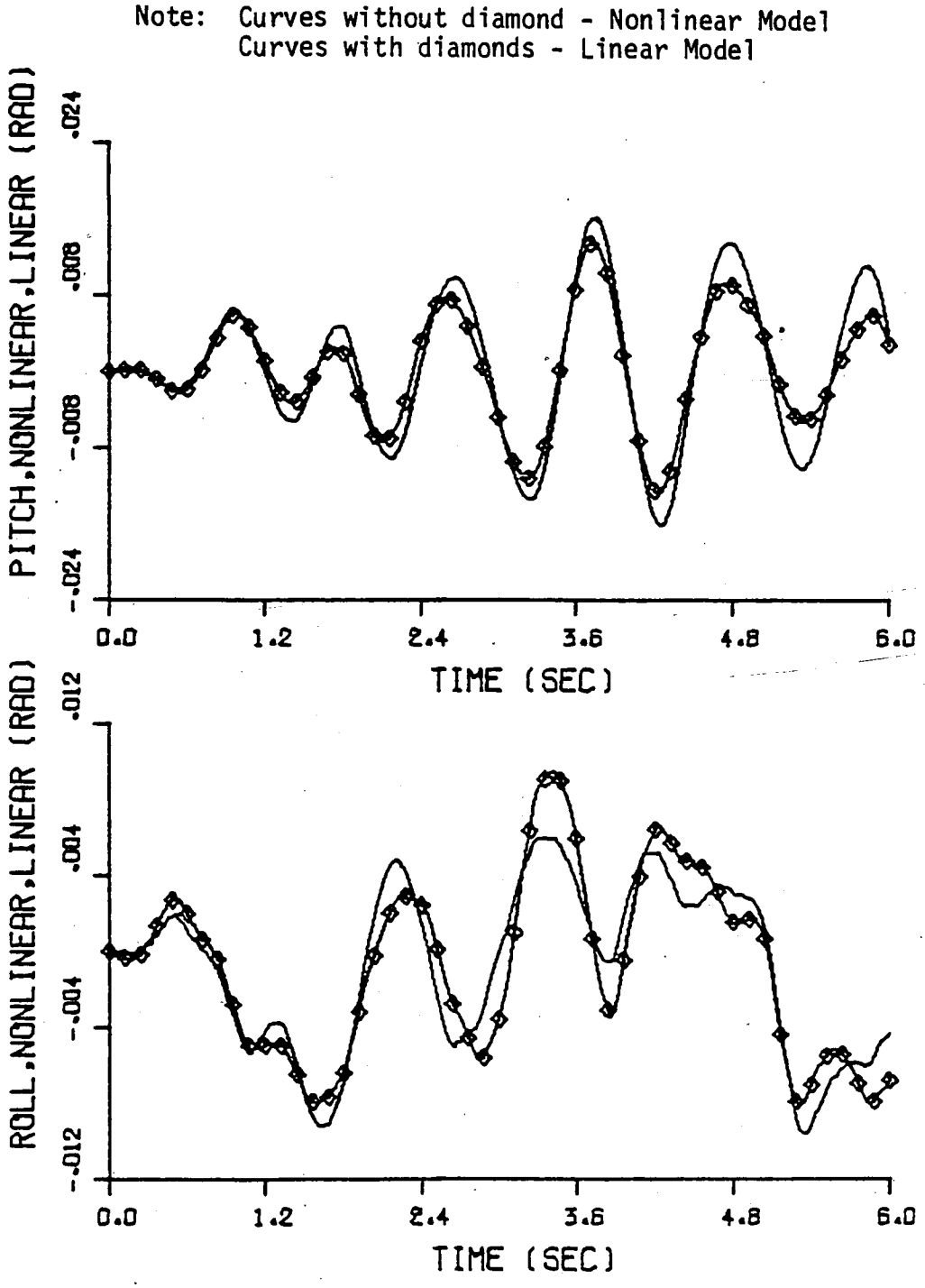

Fig. 4.2 Hull Pitch and Roll Angles, Conventional Control, Linear and Nonlinear Models, Hydraulic Gun Drives.

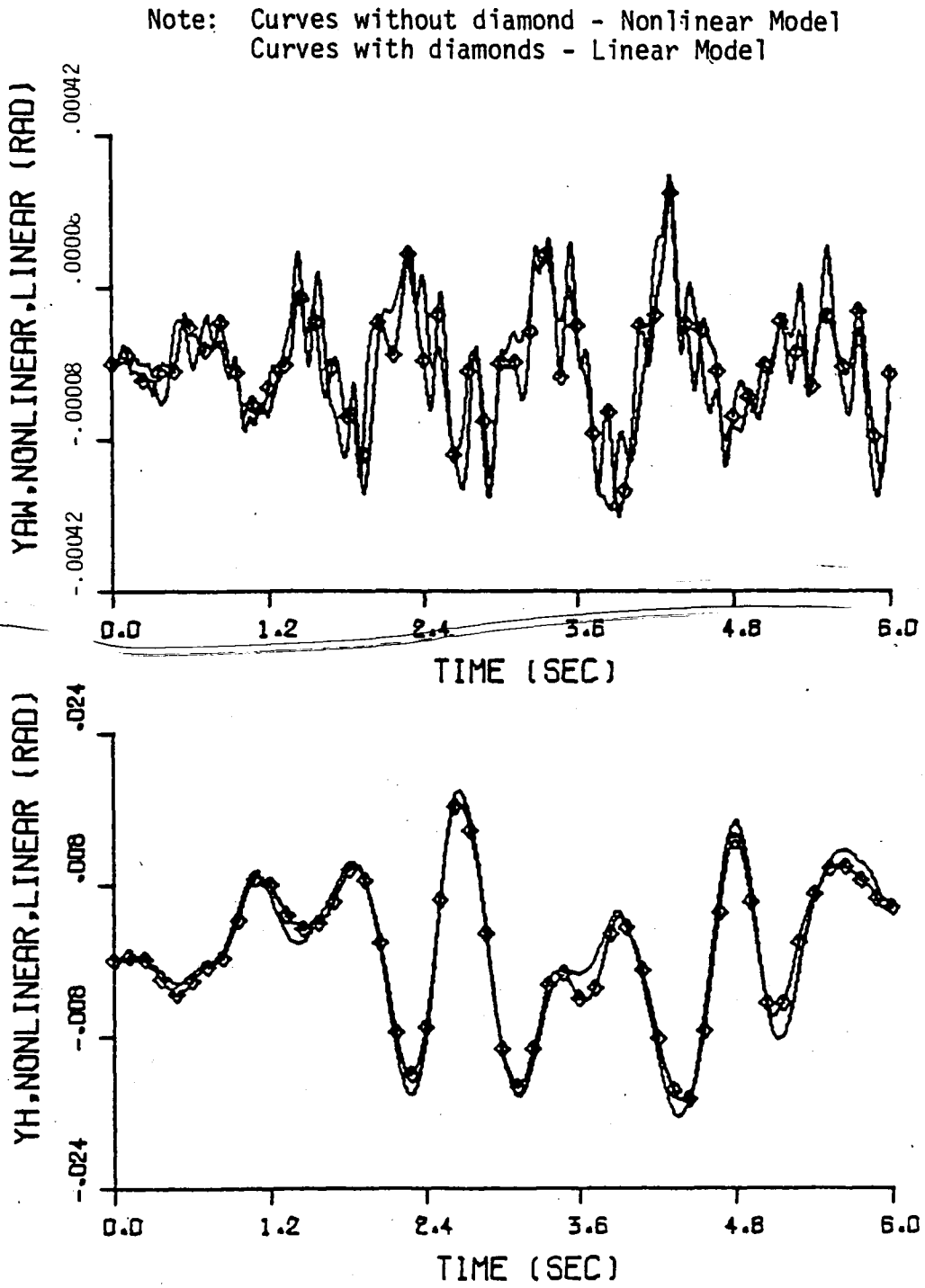

Fig. 4.3 Hull Yaw Angle and Verticle Position, Conventional Control, Linear and Nonlinear Models, Hydraulic Gun Drives.

Time histories of the traverse and elevation controller outputs and angle errors are shown in Figures 4.4 and 4.5, respectively. The bandwidths of the controller outputs are obviously narrow and situated in the lower frequency range, especially in elevation. Therefore, the angle errors wander in patterns having similar bandwidths and large amplitudes. A considerable tightening of the motion by controller output bandwidth widening occurs with the time optimal control schemes examined in the following sections.

4.2 Hydraulic System with Time Optimal Control

The time optimally controlled hydraulic drive tank employs the time optimal controller of Section 3.21 in elevation and the stochastic optimal controller of Ref. [2] in traverse. In addition, both use the Kalman filter observer of Ref. [2] for state variable estimation.

The traverse stochastic optimal controller output is virtually unaffected by the change from stochastic optimal to time optimal elevation control. Figure B1 of Appendix B is therefore not repeated. The elevation time optimal controller output, however, is shown in Figure 4.6. The uppermost plot of this figure represents the time history of the initial control voltages (i.e., the control at the start of each time interval); the three lower plots comprise the three

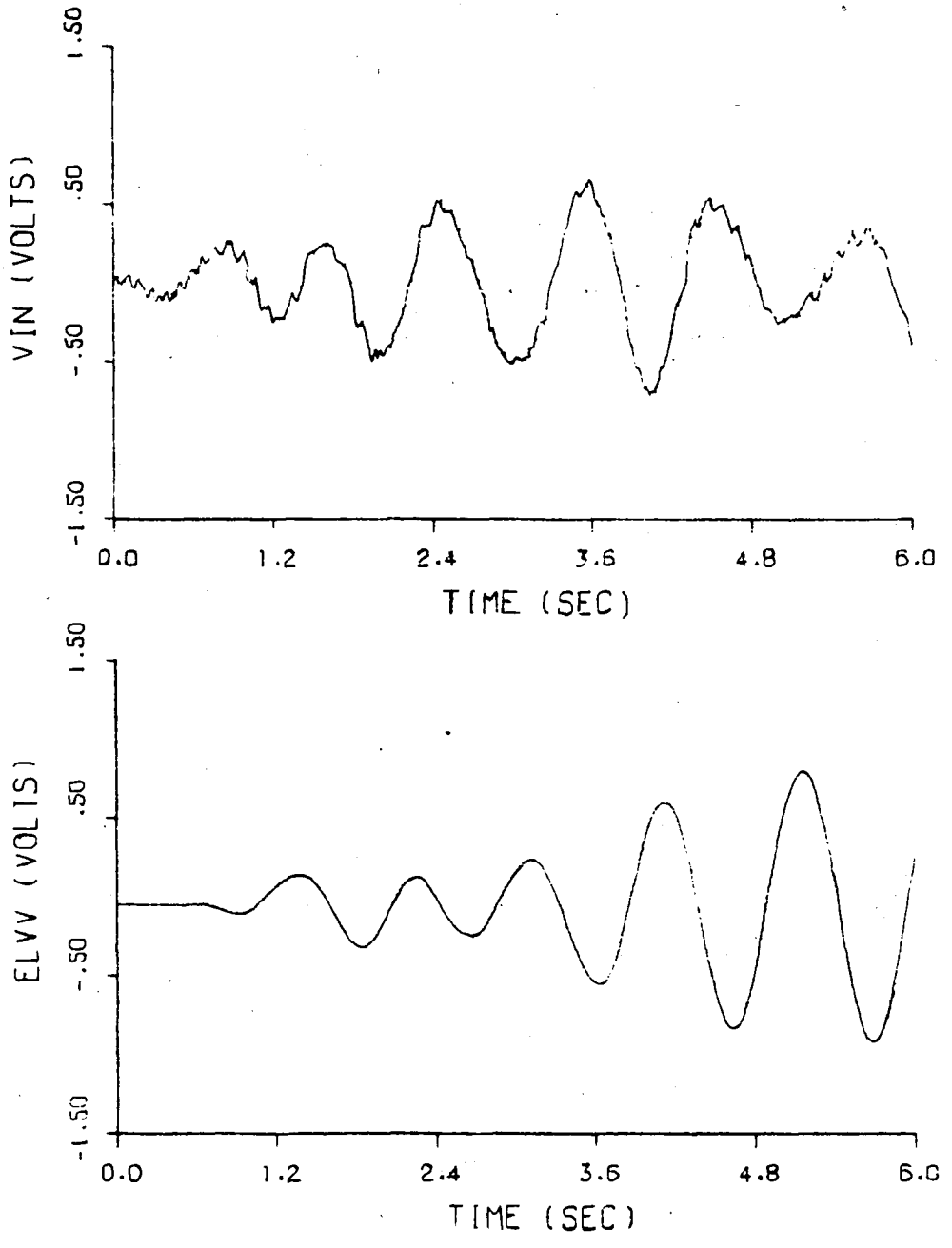

Fig. 4.4 Traverse (VIN) and Elevation (ELVV) Controller Outputs, Conventional Control, Nonlinear Model, Hydraulic Gun Drives.

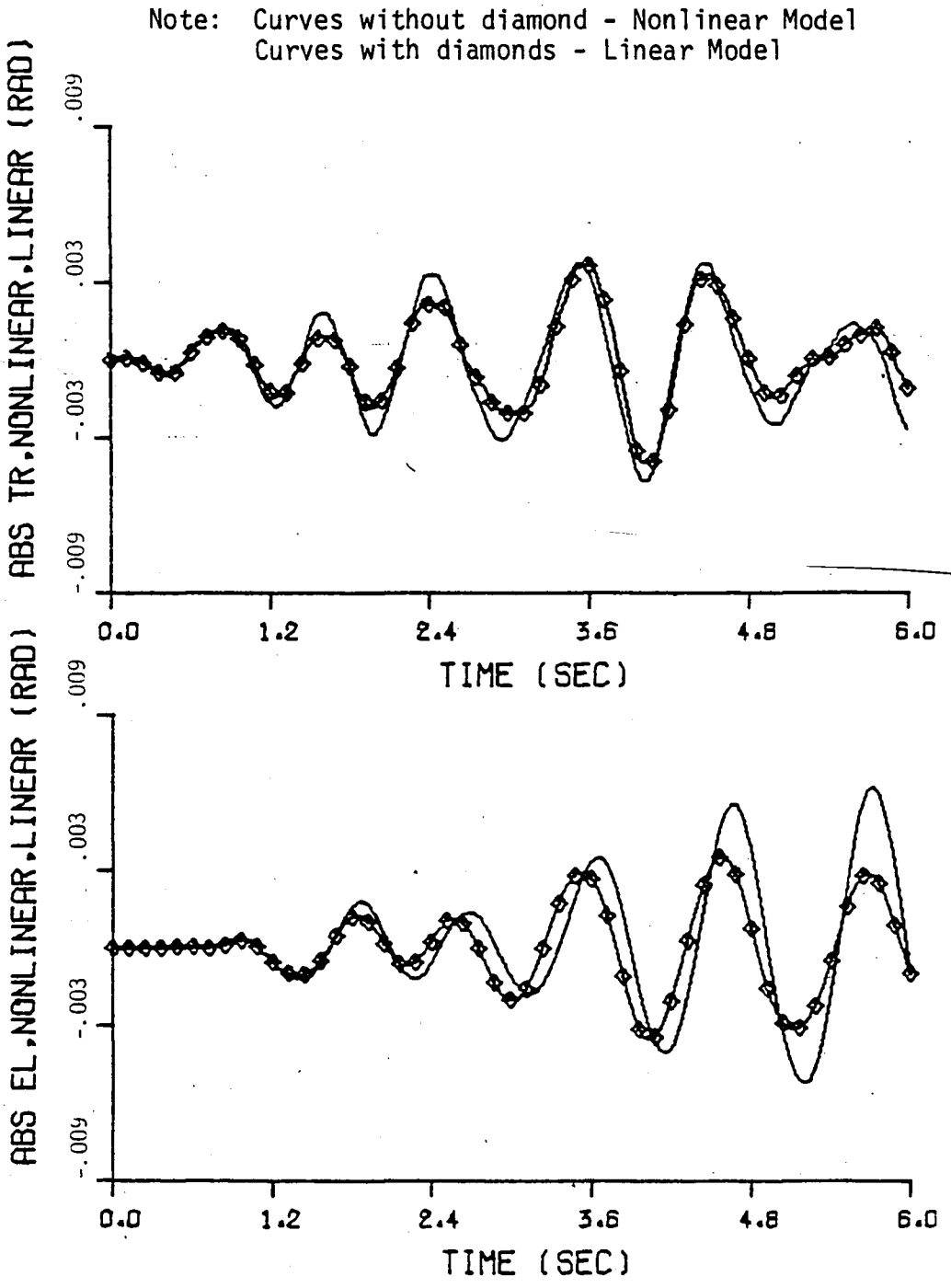

Fig. 4.5 Absolute Traverse and Elevation Pointing Errors, Conventional Control, Linear and Nonlinear Models, Hydraulic Gun Drives.

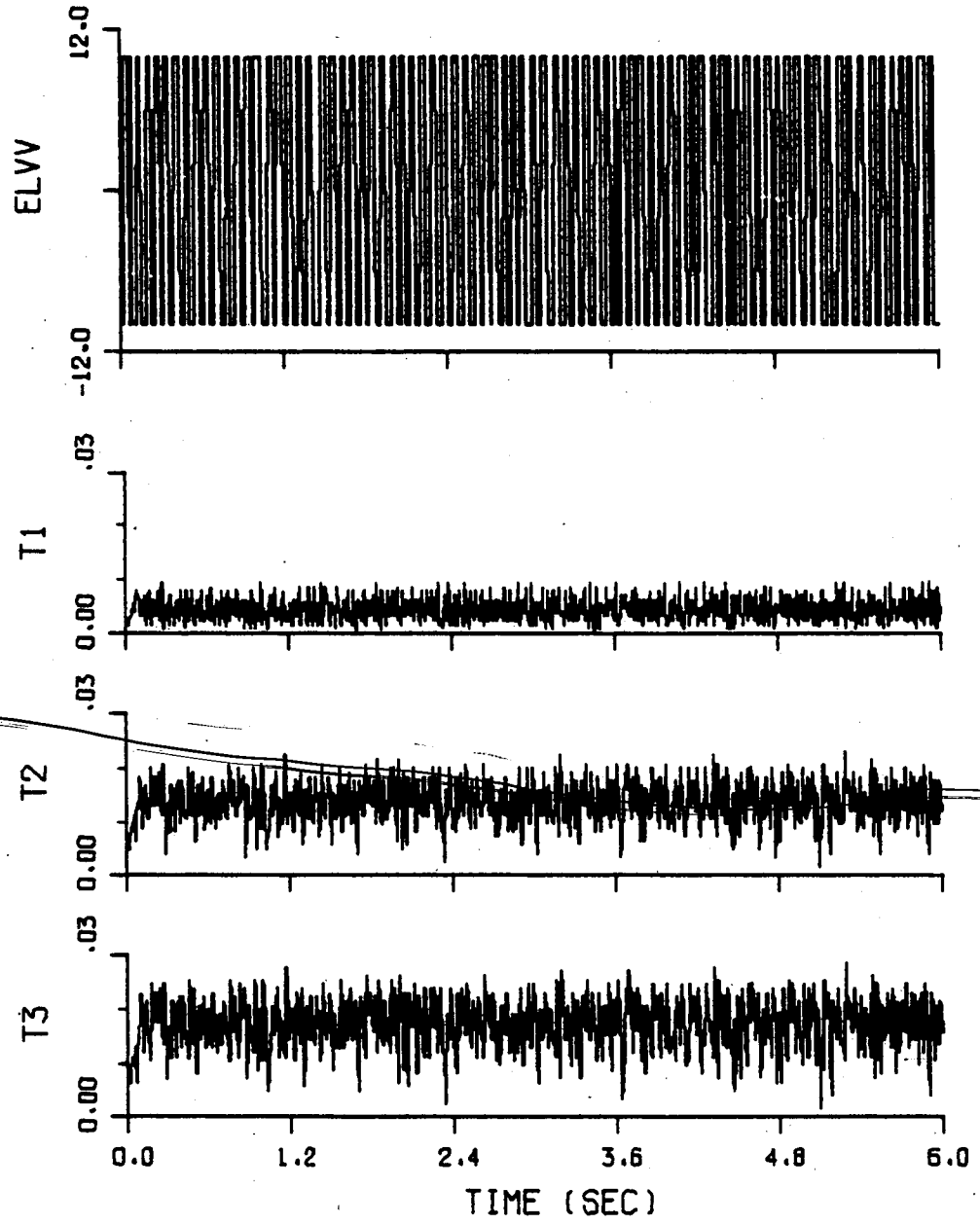

Fig. 4.6 Elevation Controller Output, Time Optimal Elevation Control, 10V Saturation Voltage, Hydraulic Gun Drives.

control switching-times. These four plots fully define the continuous elevation bang-bang control signal which would resemble a solid black rectangle if plotted on this time scale. In this case, the elevation saturation control magnitude is 10 volts.

The switching-time plots reveal that, in general, only the first control switch is executed within the .01 second time interval. The remaining control switches are outside the time interval and therefore never reached, indicating that the elevation controller time interval possibly could be increased without significant adverse effect.

The traverse and elevation gun angle errors are shown in Figure 4.7. The elevation errors are approximately 66% of those in the conventional case, and twice those in the stochastic optimal case. The traverse errors are also twice those of the stochastic optimal case even though the same stochastic optimal traverse controller is employed. This increase is attributed to the observation errors resulting from the elevation control averaging assumed by the observer (see Sec. 3.2).

Simulation results corresponding to a 1 volt elevation saturation control magnitude are shown in Figure 4.8. All three of the switching-times (not shown) increase due to the decrease in control magnitude. In general, the first switching-

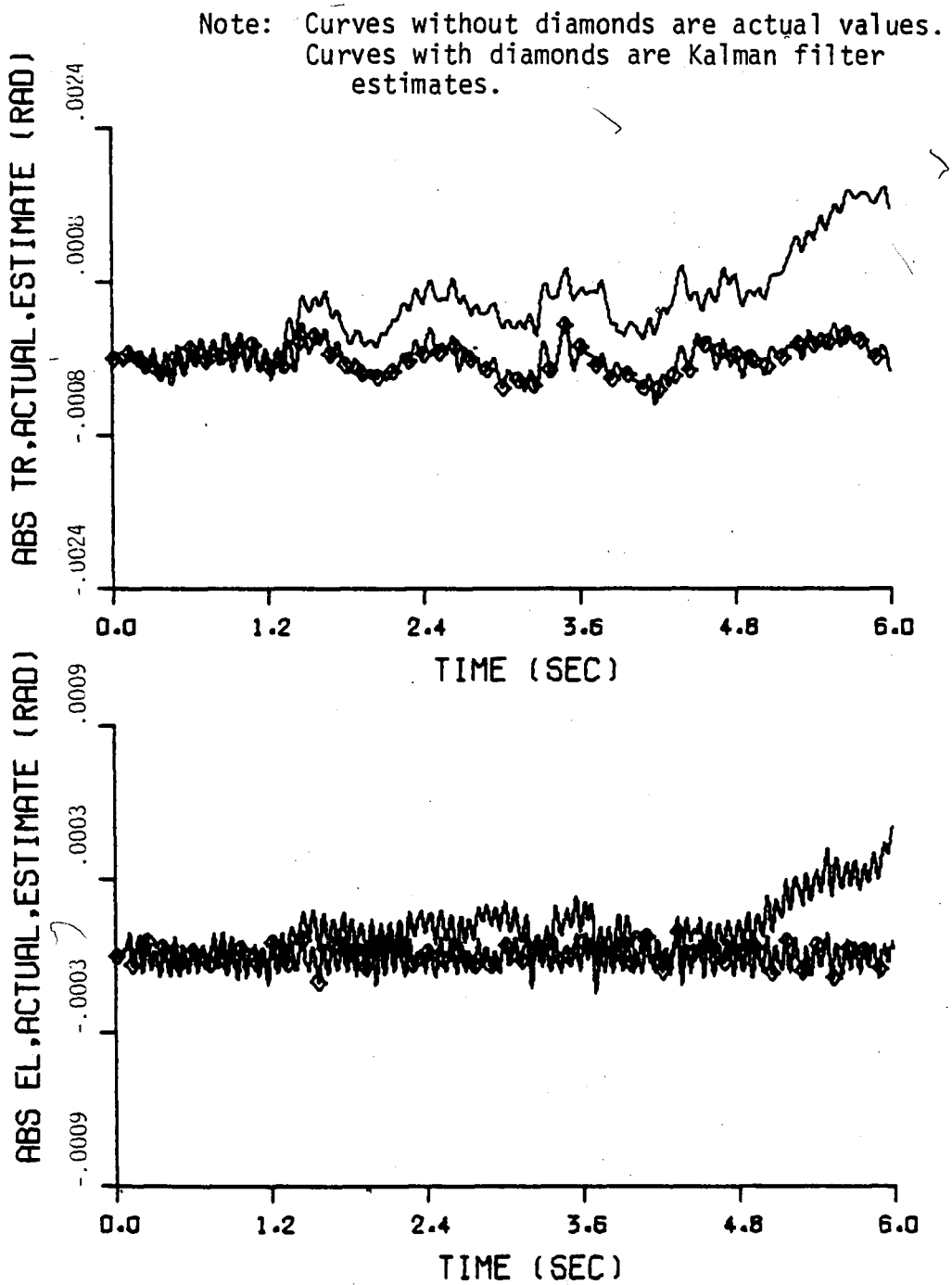

Fig. 4.7 Absolute Traverse and Elevation Pointing Errors, Time Optimal Elevation Control, 10V Saturation Voltage, Hydraulic Gun Drives.

Note: Curves without diamonds are actual values.
Curves with diamonds are Kalman filter estimates.

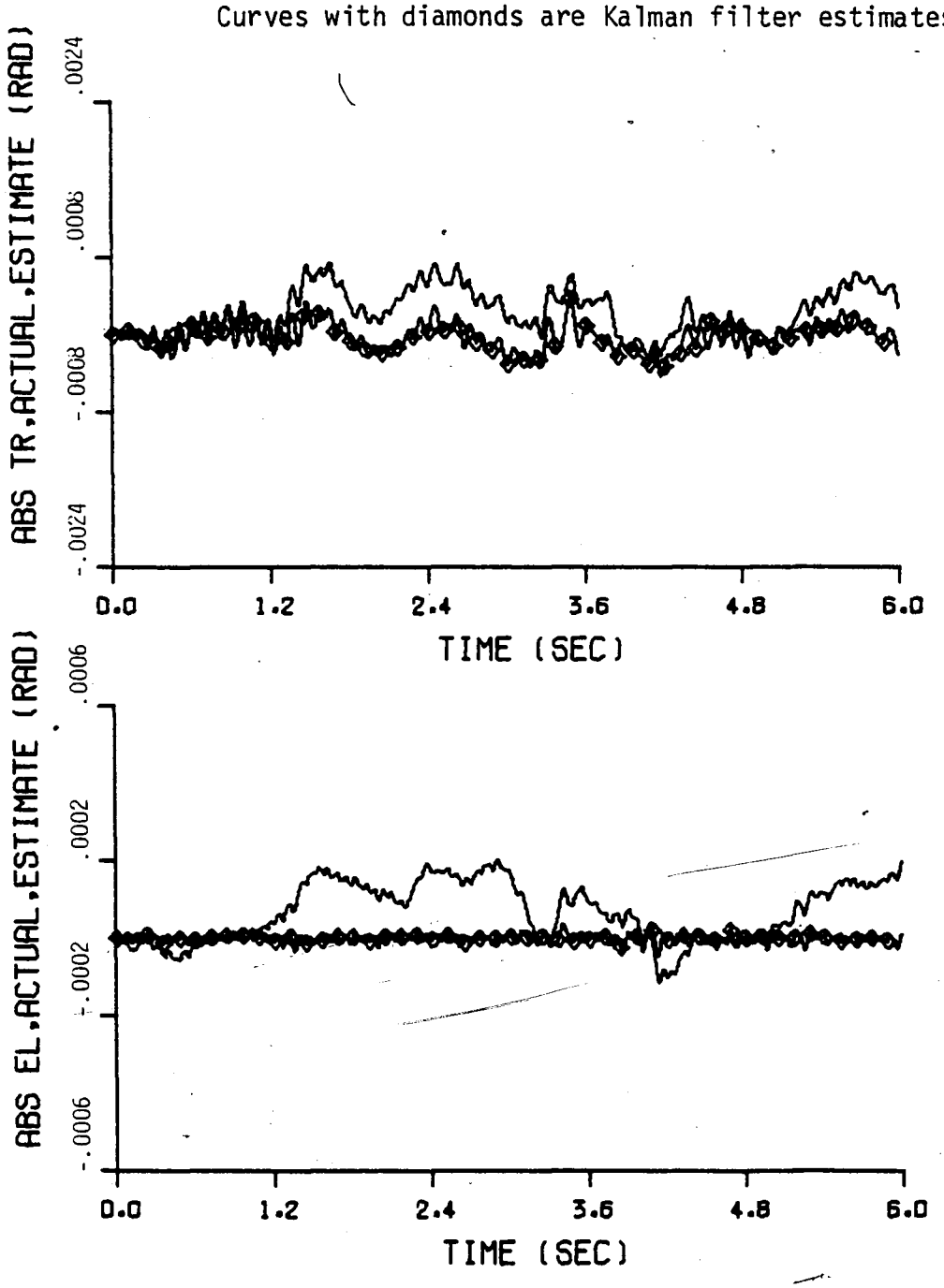

Fig. 4.8 Absolute Traverse and Elevation Pointing Errors, Time Optimal Elevation Control, 1 V. Saturation Voltage, Hydraulic Gun Drives.

time, T_1, exceeds the .01 second time interval. Therefore, the average elevation control over the interval equals the actual control and the additional traverse angle error is eliminated. The elevation angle errors, on the other hand, are of about the same magnitude as the 10 volt case.

Any increase in the elevation errors due to the control magnitude decrease are insignificant in comparison to the errors in the Kalman filter estimates. The elevation time optimal controller (like the stochastic optimal controller) is obviously drastically limited by the Kalman filter observer performance.

The hull motion is hardly changed from the conventional case so no new plots are given. Any significant dependence of the hull motion on the controller output should appear in comparisons of these extreme cases - conventional and bang-bang control. Evidently, only the ground disturbance inputs significantly affect the hull motion of the hydraulic gun drive tank.

4.3 Electric System with Time Optimal Control

Simulated results of the electric gun drive tank employing time optimal controllers and the nonlinear gun position observer are presented in this section. Two cases, with and without measurement noise, are examined. In both cases, the elevation

and traverse bang-bang control magnitudes are set at the saturation levels of their respective motors:

TQEL = 6997 N-m

TQTR = 15877 N-m

The elevation and traverse controller outputs corresponding to the noise-free case are shown in Figures 4.9 and 4.10. As before, the uppermost plots represent the initial control inputs at the start of each time interval, and the lower plots represent the switching-times selected for execution during the time interval. Two features concerning the switching-times are evident. First, both sets of switching-time plots (especially in Fig. 4.9) display the coarseness resulting from the control polarity-switch timer, which collocates the controller selected switching-times at increments of .001 seconds, the switch-timer resolution time. Second, the traverse switching-times are about twice the elevation switching-times on the average, reflecting the greater power-to-load ratio in elevation. In fact, the average elevation switch-off time, T_2, is about 0.005 seconds, or one-half the controller time interval. During the time remaining between T_2 and the start of the next interval, the gun drifts under no elevation control. Therefore, the elevation control magnitude probably could be decreased, to save power and spread the control

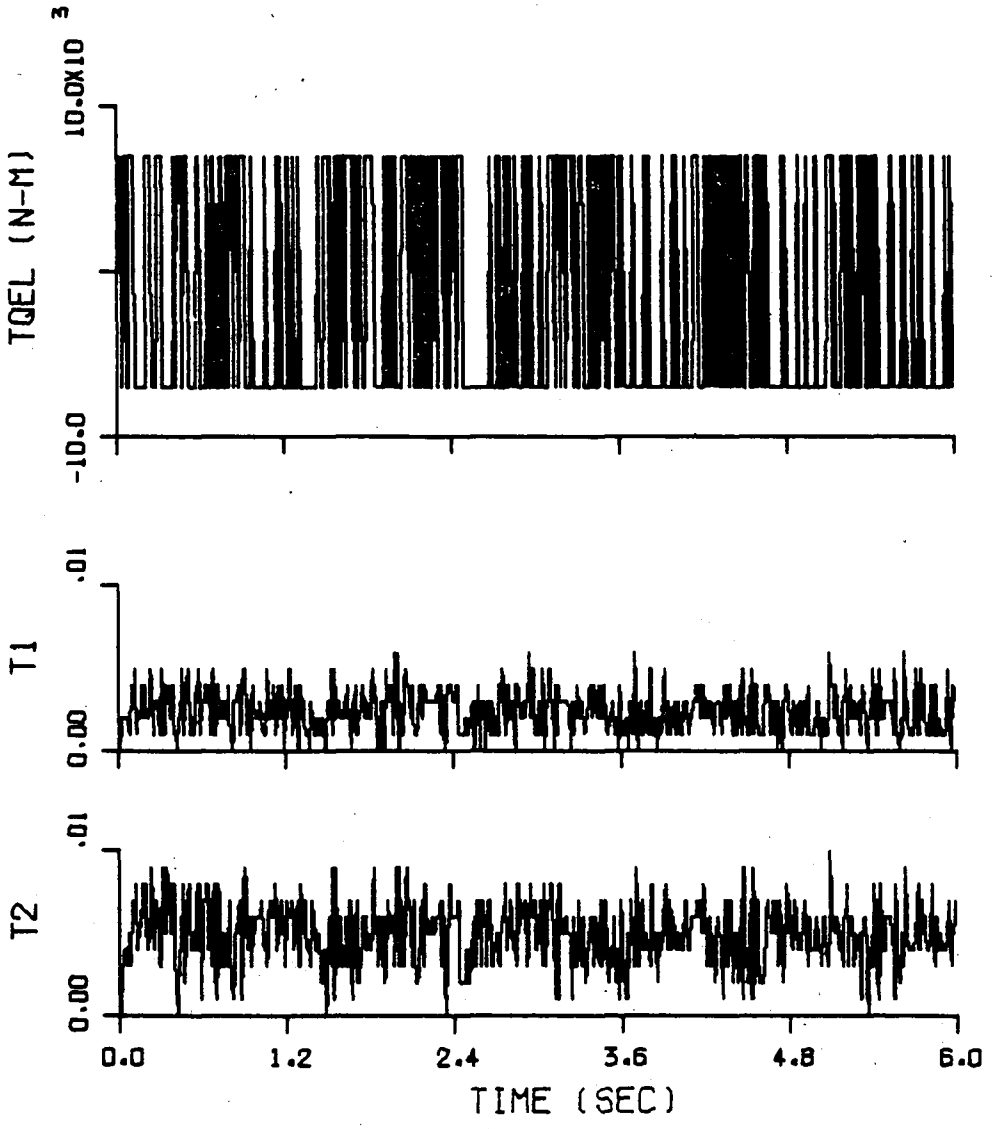

Fig. 4.9 Elevation Controller Output, Time Optimal Control, Noise-free Case, Electric Gun Drives.

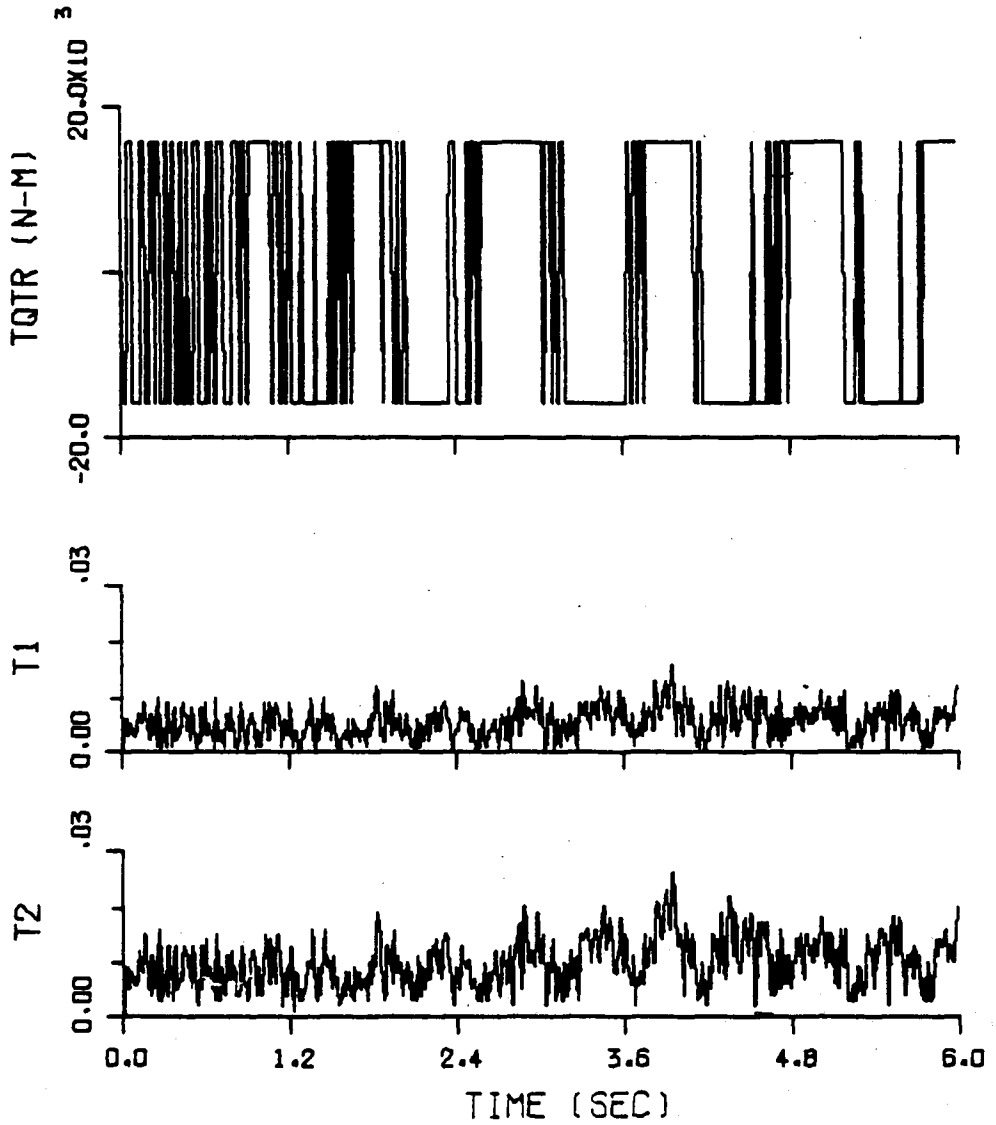

Fig. 4.10 Traverse Controller Output, Time Optimal Control, Noise-free Case, Electric Gun Drives.

over the entire interval, without much degredation in performance. The average traverse switch-off time, on the other hand, is approximately 0.01 seconds, indicating that the traverse control magnitude of 15877 N-m appropriately accommodates the ground input disturbances employed during this simulation.

The elevation and traverse actual and estimated angle errors are shown in Figure 4.11. These results are compared to the stochastic optimal and conventional results which also assumed no measurement noise (see Appendices B and C). The elevation and traverse errors are about 25% and 2% of those in the conventional case, and about 35% and 40% of those in the stochastic optimal case, respectively.

In the noise-free case being considered, the nonlinear gun position observer identifies the angle errors precisely. Therefore, the actual and estimated error curves appear as a single curve in both plots. Consequently, the case of noise-free measurements with the nonlinear observer is consumate to having deterministic angle errors. The consequence is excellent performance by the time optimal controllers. This is an ideal case, however, because measurement noise is sure to exist.

Time histories of the elevation and traverse rate gyro measurements are shown in Figure 4.12. The integral relationships derived in Section 3.4 between these measured angular

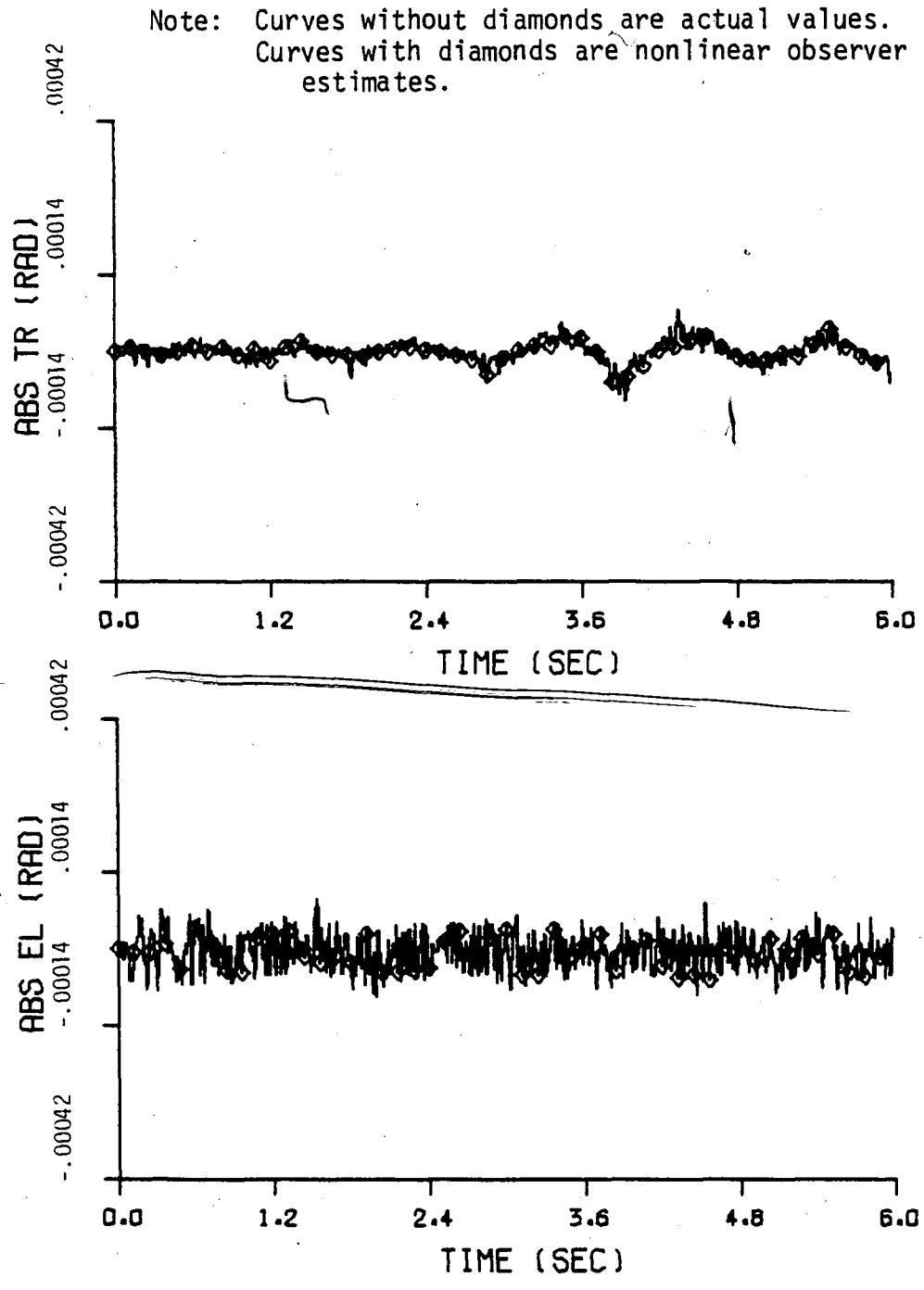

Fig. 4.11 Absolute Traverse and Elevation Pointing Errors, Time Optimal Control, Noise-free Case, Electric Gun Drives.

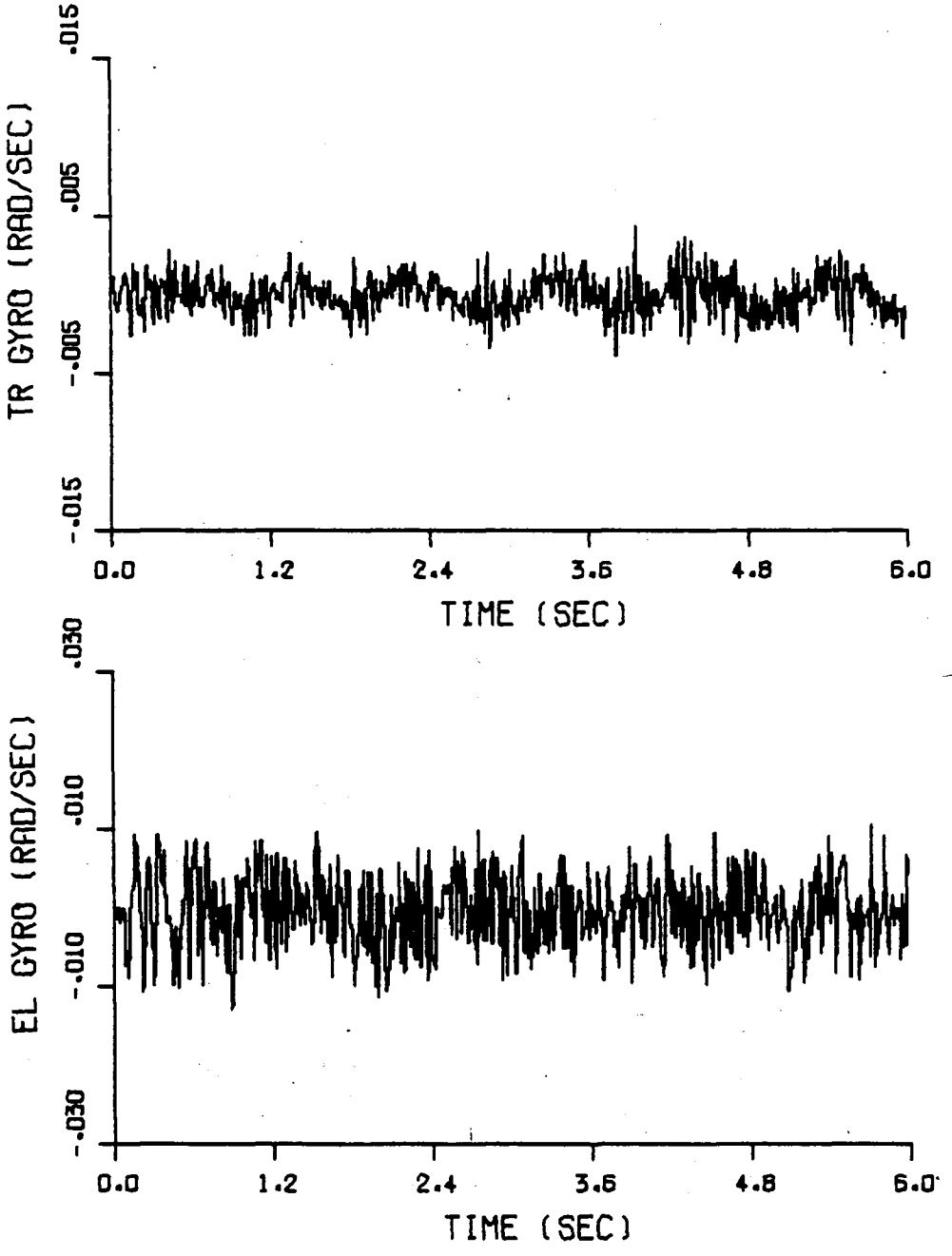

Fig. 4.12 Traverse and Elevation Rate Gyro Measurements, Time Optimal Control, Noise-free Case, Electric Gun Drives.

rates and the angle errors of Figure 4.11 are illustrated by the common trends shared by the corresponding curves.

Changes in hull motion due to the application of bang-bang control are evident in Figures 4.13 and 4.14 when compared to Figures D1 and D2 of the stochastic optimal case (see Appd. D). The large differences occur primarily in the roll and yaw motions and are caused by the traverse motor saturation control torques exerted early in the simulation, when the linear quadratic stochastic optimal control torques are still rather small.

Figures 4.15 to 4.18 comprise the simulated results corresponding to the case with measurement noise. These results differ from those of the noise-free case in two respects: (1) the elevation and traverse switching-times are slightly longer due to larger angle errors, and (2) the nonlinear gun position observer estimates are not exact, allowing the gun to drift. The results are still very good, however.

The noisy rate gyro measurements are shown in Figure 4.18. These plots display only part of the noisy measurement signals, however. Unfortunately, the descrete point plotter used to create these plots eliminates a major portion of the noise. The actual signals occurring in the simulation are much denser with measurement noise than the signals shown.

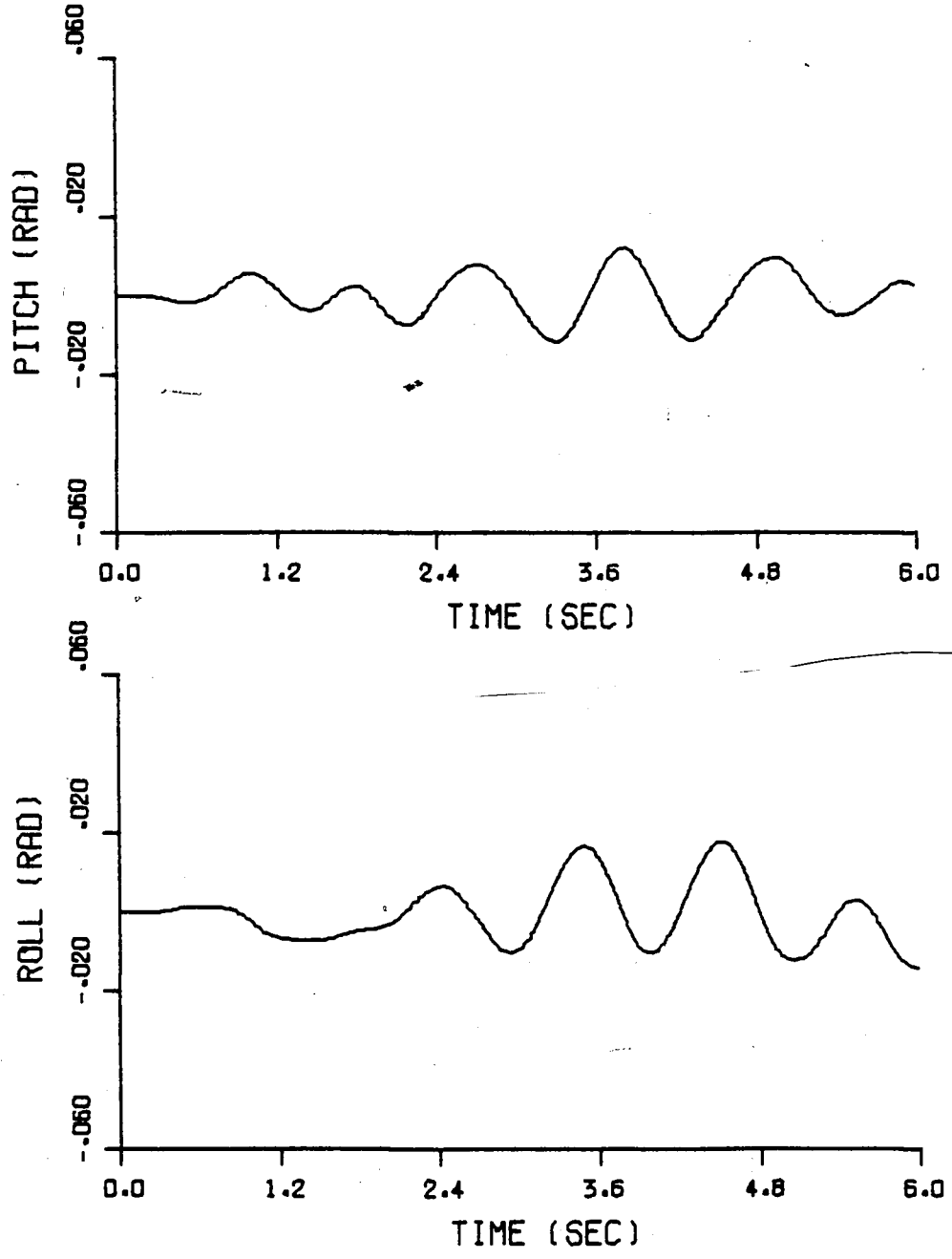

Fig. 4.13 Hull Pitch and Roll Angles, Time Optimal Control, Electric Gun Drives.

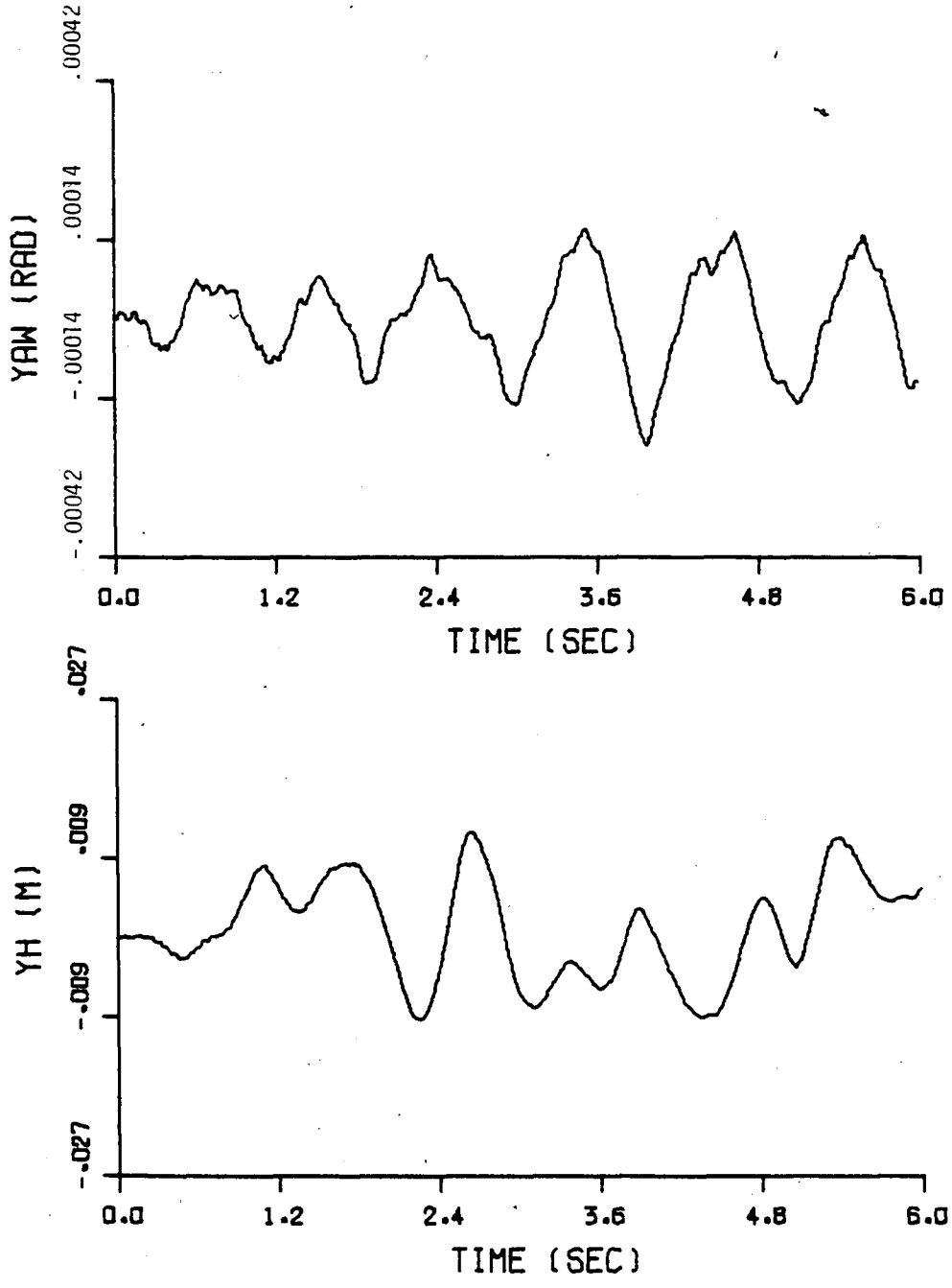

Fig. 4.14 Hull Yaw Angle and Vertical Position, Time Optimal Control, Electric Gun Drives.

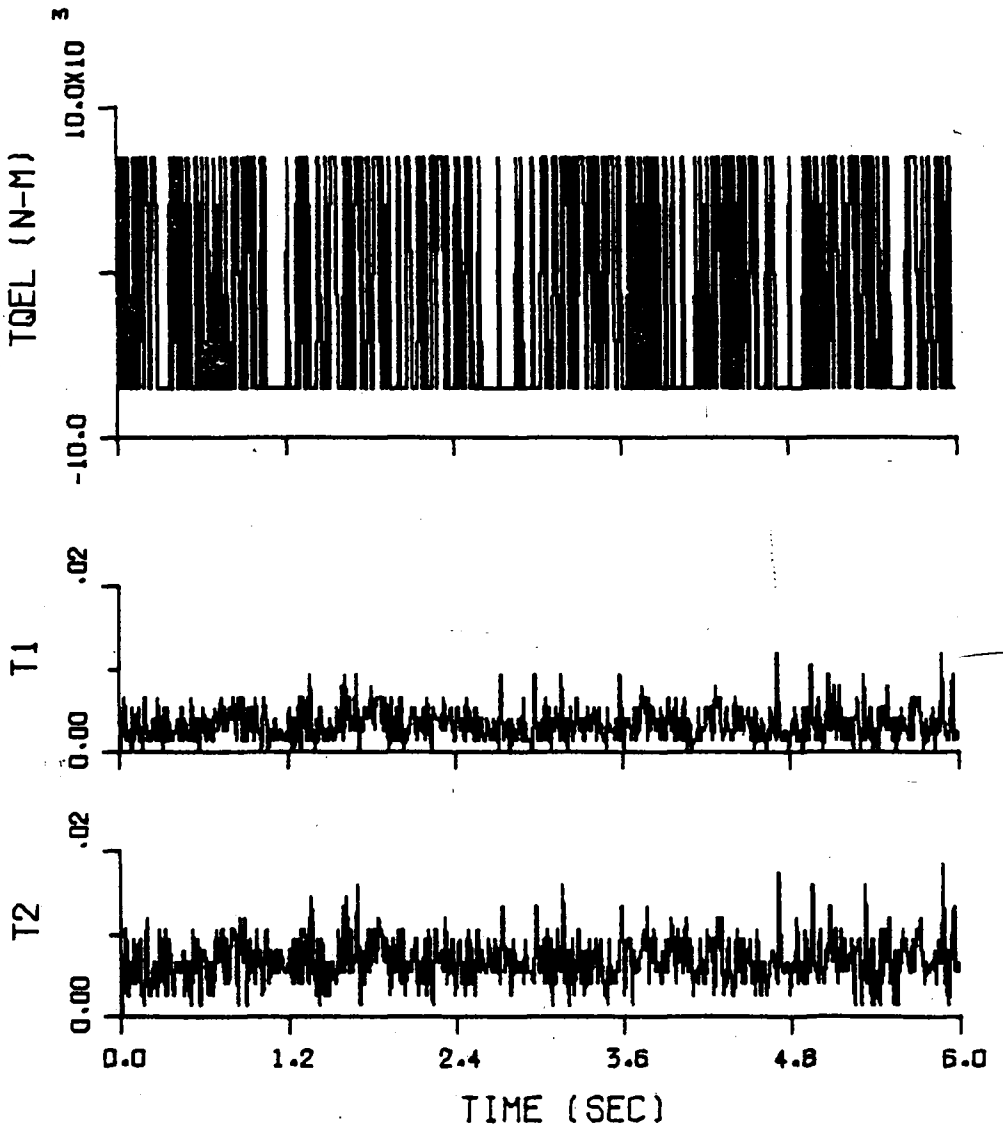

Fig. 4.15 Elevation Controller Output, Time Optimal Control, Noise-added Case, Electric Gun Drives.

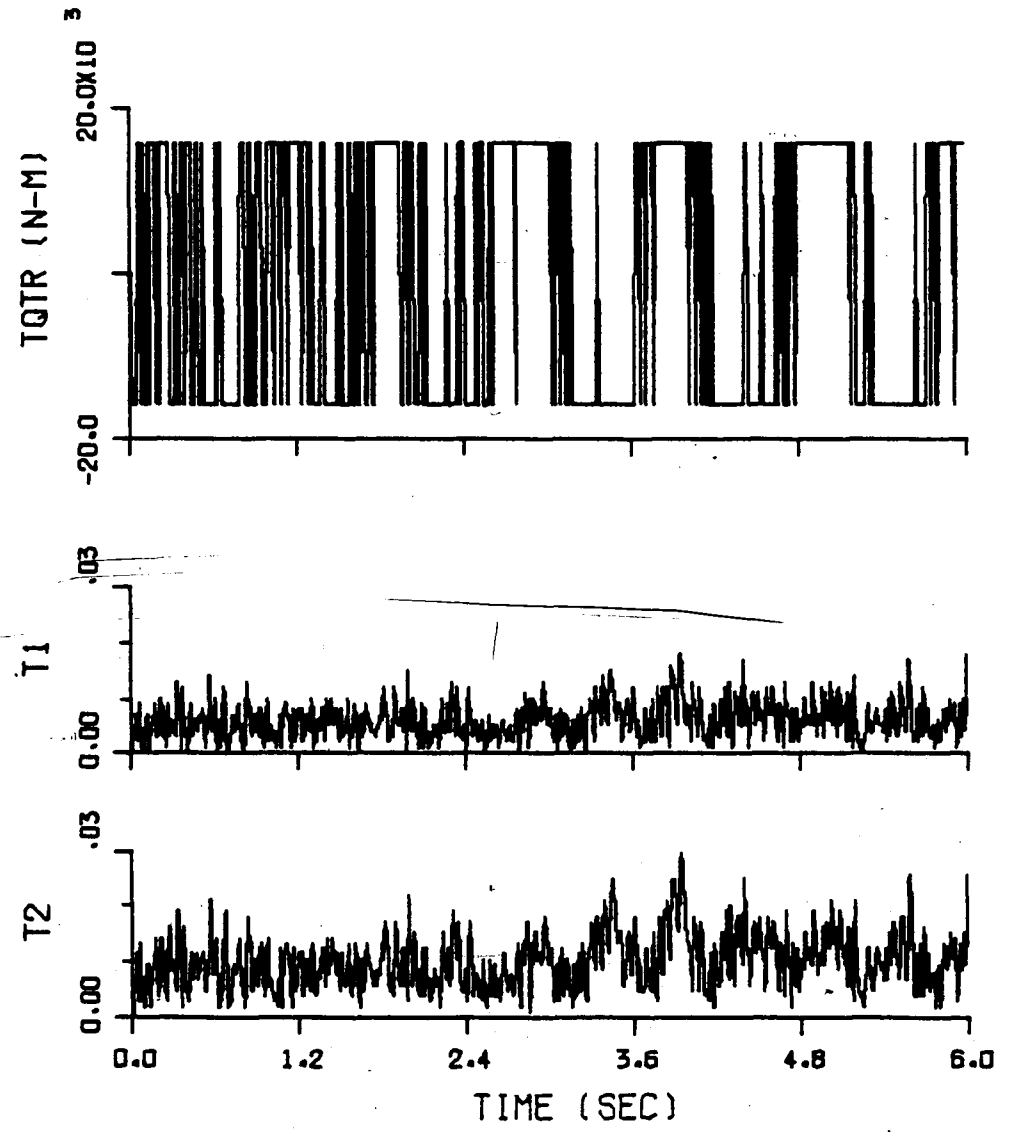

Fig. 4.16 Traverse Controller Output, Time Optimal Control, Noise-added Case, Electric Gun Drives.

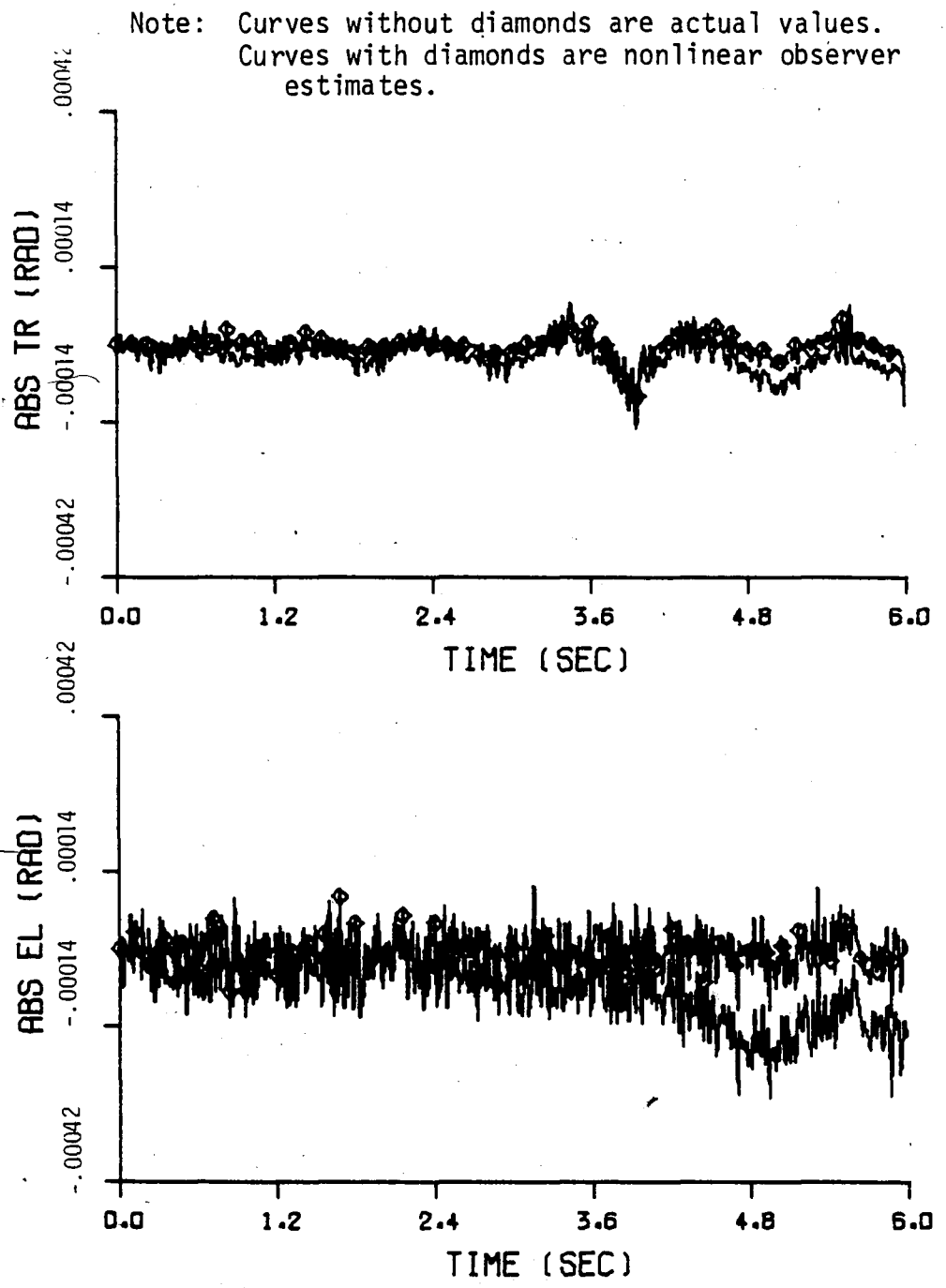

Fig. 4.17 Absolute Traverse and Elevation Pointing Errors, Time Optimal Control, Noise-added Case, Electric Gun Drives.

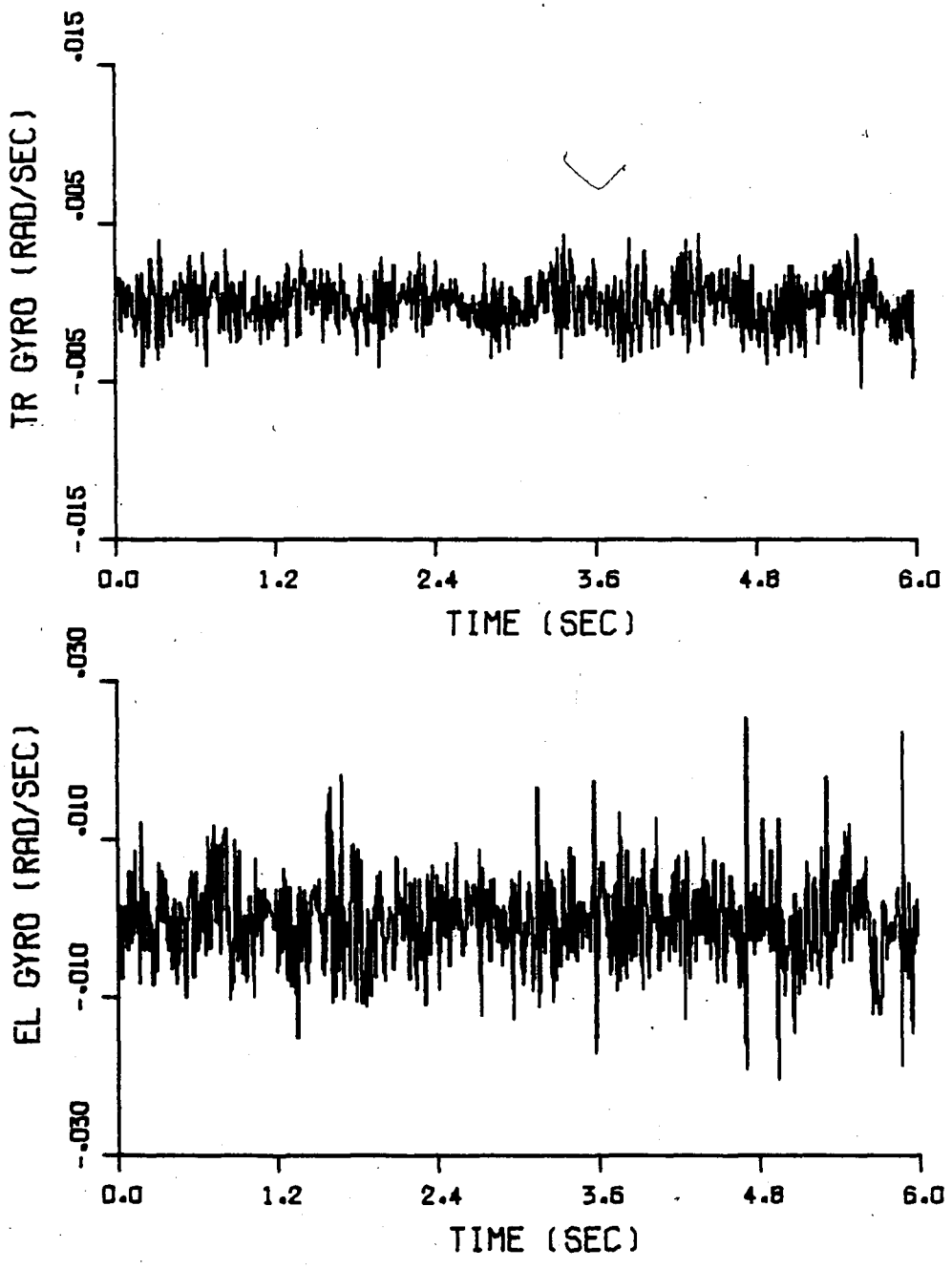

Fig. 4.18 Traverse and Elevation Rate Gyro Measurements, Time Optimal Control, Noise-added Case, Electric Gun Drives.

TABLE 2 SUMMARY COMPARISON OF CONTROL SYSTEMS

Gun Drive System	Type of Control System	Pointing Error Std. Deviation Elevation	Traverse	Avg. Fraction of Sat. Control Elevation	Traverse
Hydraulic	Conventional	2.43×10^{-3}	1.93×10^{-3}	.027	.025
	Stochastic Optimal	1.27×10^{-4}	3.88×10^{-4}	.013	.032
	Time Optimal [1] (elevation only)	1.55×10^{-4}	7.26×10^{-4}	.990	.032
Electric	Conventional [2]	1.4×10^{-4}	1.6×10^{-3}	.069	.190
	Stochastic Optimal [2]	6.55×10^{-5}	8.64×10^{-5}	.091	.255
	Time Optimal (noise-free case)	3.27×10^{-5}	1.95×10^{-5}	.540	.910
	Time Optimal (noise-added case)	9.54×10^{-5}	3.45×10^{-5}	.840	.930

[1] The stochastic optimal controller was used in traverse.

[2] These results are taken from Ref. [2].

5. DISCUSSION

Three basic accomplishments have been made. First, an improved mathematical model of the tank was established which includes all important nonlinearities and cross couplings. Second, a set of near-time-optimal controllers were developed for the hydraulic and electric gun drive systems. And third, a nonlinear gun position observer was derived to estimate the gun pointing errors based on continuous measurements of the gun angular rates. The time optimal controllers and nonlinear observer compose an entire control scheme which is therefore compared to the stochastic optimal control scheme of Ref. [2]. The conventional control is employed as a basis of comparison.

The optimal control schemes being examined employ a fixed time interval of 0.01 seconds. Control actions are selected based on feedback information at the start of each interval, and executed in an open loop fashion during the interval. The near-time-optimal scheme neglects hull disturbances which occur during the interval, so it would not be truly time optimal unless time interval became infinitesimal. Sufficient time must be allowed for microprocessor control computations, however. The designation near-time-optimal results from the use of a small but finite time interval.

Although the control action is computed only once for each 0.01 second time interval , the action is based on an assumed instantaneous processing of the most recent measurements from the feedback instruments. The same is true of the previous studies [2]. In practice a short delay between measurement and control decision would be necessary. This is not a particularly difficult change to implement, but a small deterioration of performance is inevitable.

Standard deviations for the gun pointing errors corresponding to conventional, stochastic optimal, and time optimal control are listed in Table 2, as mentioned previously. In all cases, the pointing error minimization performance of the electric system exceeds that of the hydraulic system by nearly half an order of magnitude. Evidently, the lag between controller input and control torque execution present in the hydraulic system severely hinders gun drive effectiveness. As a result, fire-on-the-move ability will be more readily achieved with the electric gun drives.

The stochastic optimal and time optimal control schemes being compared consist of two fundamental parts: an observer and controller. Previous studies of the stochastic optimal scheme [2] reveal that controller performance is limited by errors in the Kalman filter observer estimates (i.e. deviations

between the actual and estimated states), which result primarily from modeling errors unavoidably incorporated in the pseudo-linear model built into the observer. Quasi-optimal estimates are attained, nevertheless, by summing the model predicted state and the Kalman correction term, which is based on differences between transducer measured and model predicted output variables and known measurement noise levels. Eight transducers are employed: three rate gyros measuring the absolute elevation and traverse rates and the absolute hull rate about a horizontal axis perpendicular to the gun, one tachometer measuring the elevation rate relative to the hull, and two position and velocity sensors measuring the front wheel motion relative to the hull. A pseudo-linear model is employed because practical observation schemes do not exist for nonlinear systems of high order. Linearization forces the observer to assume one particular nominal gun angle. Therefore, a realizable observer would be expanded to incorporate a step-wise linearization which allows its coefficients to be modulated by gun position. In addition, the stochastic optimal observer presently can accommodate one tank speed and single-side ground excitation; the observer coefficient matrices are speed dependent and unrealizably large if both-side excitation is accommodated. These restrictions make the stochastic optimal observer

impractical; their removal is a topic of ongoing study.

The nonlinear gun position observer used in the near-time-optimal control system eliminates these restrictions by avoiding the use of the usual dynamical model. Instead, it employs exact kinematical expressions (derived in Sec. 3.3) which relate the absolute pointing errors to the gun angular rates. Three rate gyros are employed to continuously measure the gun elevation, traverse, and axial spin rates. The consequent observer is very simple and versatile (unrestricted), making it very attractive in comparison to the stochastic optimal observer; however, without the embodiment of a dynamical model of some sort, it defies most applications of typical filtering algorithms. Consequently, direct measurements are employed resulting in observation error. The actual and estimated gun pointing errors diverge, as shown in Fig. 4.17, and the gun slowly drifts off target. The purpose of the control, however, is to relieve the gunner of the need to compensate for rapid changes in gun angle. Instead, the gunner must compensate for a very gradual drift.

The observer counterparts, called controllers, employ the observer estimates. Fortunately, both the stochastic and time optimal controllers are very simple, requiring only a matrix-vector multiplication in the stochastic case, and the solution of switching-time equations in the time optimal case[1]. Both

[1] see Ref. [1], pg. 63.

operations employ less than ten lines of computer code[1]. The stochastic optimal controller, however, has two notable advantages: linearity and sophistication. A portion of the stochastic control action is based on 51 state variables representing the ground contour under the tread. The controller, therefore, anticipates the effect of propagating ground disturbances, giving it a preview feature [2]. Linearity, on the other hand, implies proportional control, or small control action for small disturbances. This matches the need well and saves power. Unfortunately, however, the controller, like the observer, assumes one particular nominal gun angle, the tank speed, and single-side excitation. The necessary overcoming of these limitations will substantially increase complexity.

The time-optimal controller, on the other hand, is versatile, nonlinear, and unsophisticated. Speed and gun angle restrictions are nonexistent because the hull motion and ground disturbances are neglected in the controller formulation. A very simple controller which is insensitive to modeling errors results. In essence, the sophistication and power efficiency of preview control are exchanged for the simplicity, muscle and relative

[1]This applies to the electric system only. The solution of the hydraulic switching-time equations is more extensive in elevation and thus far is unaccomplished in traverse.

inefficiency of nonlinear bang-bang control. A total of five transducers are employed (instead of the eight for the sophisticated system): three rate gyros attached to the gun and two tachometers measuring the elevation and traverse rates relative to the hull.

The time optimal controllers recognize all friction torques as external forces which modify the switching curve. Coulomb friction torques are included in this manner, since to leave them in the models on which the controllers are based would ruin the necessary linearization. The viscous friction torques present in the hydraulic system model were also removed, for convenience, and their estimates added to those of the coulomb frictions. Friction torque magnitudes are estimated by extrapolating the tachometer measurements to the midpoint of the next time interval. The controller assumes that these torques are constant over the interval with these extrapolated values. This assumption is appropriate because the angular velocities of the gun relative to the hull are strongly dependent on the hull motion which usually is not significantly altered during one time interval even with bang-bang control.

The development of the traverse hydraulic system time optimal controller is unfinished. Two conditions were imposed in the derivation of the related switching-time equations:

(1) that there is n-1 control switches, and (2) that the state is transferred to the origin. This does not produce a unique solution because of the strong oscillatory behavior of the lightly-damped traverse model. The damping was made small, however, by removing the coulomb and viscous friction torques from the model, as mentioned previously. Hopefully, reinsertion of the viscous frictions would increase the damping in the switching-time equations sufficiently to eliminate or at least reduce the number of extraneous solutions, and to simplify associated convergence problems. Even if some ambiguity remains, time optimality would be assured by selecting the solution possessing the smallest non-negative control switch-off time. It seems likely these modifications will succeed.

Both the time optimal and stochastic optimal hydraulic system elevation controllers can employ the Kalman filter observer, while the nonlinear gun position observer can be used only in the time optimal case. Equal observation errors unfairly hinder the time optimal controller, which probably would do better with the nonlinear observer. These controllers, therefore, are not compared in isolation from the observers. The entire time optimal control scheme including the nonlinear observer was tested with the electric gun drive tank. The corresponding performance indices listed in Table 2 reveal that the time

optimal scheme is (1) high performance, performing slightly better than the stochastic scheme in the noise-free case, (2) relatively noise sensitive, shown by the performance deterioration in the case with noise, and (3) power inefficient, employing control magnitudes several times larger than those in the stochastic case to achieve comparable results. The average fractions of saturation time optimal control are not identically one because some control switch-off times occurred before the end of the time interval, producing regions of zero control rather than saturation control. This result is discussed further in the next section.

5.1 Conclusions and Recommendations

The time optimal control scheme which was investigated has two salient features: simplicity and versatility. This versatility implies that the performance is unaffected by changes in the nominal gun angle, tank speed, or other operator selected parameters. Simplicity implies that practical implementation using a digital microprocessor is possible. An undesirable feature, on the other hand, is the inappropriate matching of large control action to small disturbances. This is unnecessarily inefficient and may cause undesirable vibration and shorten life. As disturbances become smaller, the time

optimal switching-times become shorter, producing regions of zero control, as previously mentioned. These regions could be eliminated by shortening the time interval and consequently tightening the control as the disturbances become small, however, this would not provide the finite time required for control calculations. Alternately, the control magnitude could be decreased to increase the switching-times, spreading the control over the entire fixed interval, saving power, reducing vibration and extending life. The following procedure is suggested to implement this idea: (1) calculate the average switch-off time using the switching-times of the last m time intervals, and (2) adjust the control magnitude so the average switch-off time tends to equal one time interval in length. The value of m should be chosen large enough so control magnitudes do not oscillate, yet small enough so that changes in the disturbance magnitudes are rapidly compensated. The lag between disturbance change and control magnitude adjustment might still be excessive. If so, it could be avoided altogether by appropriately varying the current control magnitude and iteratively calculating the switching-times until a satisfactory switch-off time is reached. Or, if the simple electric drive TOCS are employed, the control magnitude can be directly calculated by setting the switch-off time equal to the time interval in the switching-time equations.

This calculated magnitude would apply only if it is less than the control saturation levels, of course. In any case, the time optimal control could adapt itself to various terrain configurations and use full saturation control only when strictly needed.

The strengths and weaknesses of the time optimal and stochastic optimal controls are rather different. The time optimal scheme is simple and versatile but power inefficient; the stochastic optimal scheme is sophisticated and therefore power efficient, but restricted and sensitive to modeling errors. A scheme which combines time optimal and stochastic optimal control may result in a superior design, blending reasonable simplicity, insensitivity and efficiency with high performance and versatility. Since the time optimal schemes work well alone, the complexity of the stochastic control scheme could be substantially reduced. A hybrid control scheme has been proposed which combines the time optimal scheme in its present form with a modified stochastic optimal scheme which eliminates the gun angle change and tank speed change problems. A portion of the overall control action is allotted to each scheme: the time optimal control acts on the gun pointing errors measured by the nonlinear observer; the stochastic optimal control accommodates the disturbance torques excited by the ground roughness.

This differs from previous stochastic control [2] which also acted on the gun pointing errors.

The ground contour representation and preview feature will be retained in the modified stochastic scheme to increase the power efficiency of the hybrid scheme. A simplified model of the tank which lumps the turret, hull, and gun into one rigid body will be assumed by the stochastic optimal observer. Observer estimates of the hull vertical velocity, angular rates and the axle forces, in addition to tachometer measurements of the relative turret and gun rates can then be employed to calculate and accommodate the disturbance torques which are and will be exerted on the gun. Consequently, the portion of the control action governed by the time optimal scheme may be reduced, lessening the adverse effects which accompany bang-bang control.

Alternate methods for the design of optimal controllers with preview action for combination with the time optimal scheme may follow from Ref. [10]. A preliminary study of hybrid control is given in Ref. [1], and current research on this topic may be reported in the Phase III portion of "Modern Control Concepts Applied to Disturbance Accommodation of Tank Turrets."[1]

[1]The final of a series of three reports presently comprising references [1] and [2].

Recommendations for further work include, in light of the above:

(1) Development of an algorithm which would vary the time optimal control magnitude levels, giving the time optimal scheme an adaptive feature.

(2) Development of a measurement noise filtering scheme for the nonlinear gun position observer (this may be unnecessary if low noise is anticipated).

(3) Simulation studies of a modified time optimal control scheme which accounts for the delay between observation and control.

(4) Development of a numerical approach for solution of the traverse hydraulic drive switching-time equations which explicitly include the viscous friction torques.

(5) Development of time-optimal controllers for the electric drives with motor lags included. Preliminary studies neglected these lags, which have 0.004 second time constants, because of their negligible effect on the conventional control [1]. Their incorporation in the design of the faster time optimal controllers is imperative, however. The new controllers would be third order, having a structure identical to that of the elevation hydraulic drive time optimal controller.

(6) Simulations studies of the time optimal control scheme including rate gyro dynamics. These dynamics were removed because they had no effect on the measurements occurring during conventional control (see Sec. 2.5). Measurement signal bandwidth is increased by time optimal control, however, so these gyro dynamics may be significant.

(7) Development and evaluation of the hybrid time-optimal stochastic-optimal controller as described above.

References

1. Brown, F.T., Johnson, S.H. and Barr, M.C., "Modern Control Concepts Applied to Disturbance Accommodation of Tank Turrets", report to the U.S. Army Armament R&D Command, Dover, NJ, by Department of Mechanical Engineering and Mechanics, Lehigh University, Bethlehem, PA 18015, Nov. 1978, under contract DAAK 10-78-C-0002.

2. Brown, F.T., and Haessig, D.A., "Modern Control Concepts Applied to Disturbance Accommodation of Tank Turrets - Phase II", ibid, June 1980, under contract DAAK 10-78-C-0368.

3. Johnson, S.H., and Haessig, D.A., "The Implementation of a Computer Model for the M60 Tank Stabilization System", ibid, 20 Nov. 1979, under contract DAAK 10-79-M-4447.

4. Kaminsky, A.P., "A Mathematical Representation of the M60A1 Azimuth and Elevation Control and Add-On Stabilization System", report to the U.S. Army Material Command by Defence Engineering Division, Chrysler Corporation, 2 Nov. 1971, under contract DAAF 03-70-C-0075.

5. Bellman, R., Glicksberg, I., and Gross, O., "On the Bang-bang Control Problem", Quart. Appl. Math., 14, 1959, pp. 11-18.

6. Csaki, F., Modern Control Theories, Akademiai Kiado, Budapest, 1972.

7. Schmidt, S.F., "The Analysis and Design of Continuous and Sample Data Feedback Control Systems with Saturation Type Nonlinearity", NASA TN D-20, Aug. 1959.

8. Pars, L.A., A Treatise on Analytical Dynamics, John Wiley and Sons, New York, 1965.

9. Bryson, A.E., and Ho, Y.C., Applied Optimal Control, John Wiley and Sons, New York, 1975.

10. Tomizuka, M., and Rosenthal, D.E., "On the Optimal Digital State Feedback Controller with Integral and Preview Action", ASME Transactions, Journal of Dynamic Systems, Measurement and Control, Vol. 101, No. 2, June 1979, pp. 172-178.

APPENDIX A - Symbol List and Parameter Values for the Hydraulic Gun Drive Tank

State Variables

SYMBOL	DESCRIPTION	UNIT	DERIVATIVE SYMBOL
Y_H	Vertical displacement of vehicle CG	m	$\dot{Y}_H$
R	Hull roll angle	rad	$\dot{R}$
P	Hull pitch angle	rad	$\dot{P}$
TR	Turret traverse angle relative to hull	rad	$\dot{TR}$
E	Gun elevation angle relative to hull	rad	$\dot{E}$
$\dot{Y}_H$	Vertical velocity of vehicle CG	m/sec	$\ddot{Y}_H$
ω_{hx}	Hull roll rate[1]	rad/sec	$\dot{\omega}_{hx}$
ω_{hz}	Hull pitch rate[1]	rad/sec	$\dot{\omega}_{hz}$
ω_{hy}	Hull yaw rate[1]	rad/sec	$\dot{\omega}_{hy}$
SRTR	Turret traverse space rate	rad/sec	$\dot{SRTR}$

[1] with respect to frame $Gx_hy_hz_h$

SYMBOL	DESCRIPTION	UNIT	DERIVATIVE SYMBOL
SRE	Gun elevation space rate	rad/sec	$\dot{SRE}$
Y	Hull yaw angle	rad	$\dot{Y}$
Y4D	Hydraulic motor velocity	rad/sec	$\dot{Y4D}$
Y4	Hydraulic motor position	rad	$\dot{Y4}$
PLTR	Pressure differential - traverse hydraulic motor	Pa	$\dot{PLTR}$
IIN	Elevation servo valve current	ma	$\dot{IIN}$
IVMA	Traverse servo valve current	ma	$\dot{IVMA}$
PLE	Pressure differential - Elevation	Pa	$\dot{PLE}$
XSP	Elevation spool valve position	m	$\dot{XSP}$

ADDITIONAL VARIABLES

SYMBOL	DESCRIPTION	UNIT
AE	Absolute elevation pointing error	rad
AT	Absolute traverse pointing error	rad
r_T	Vertical displacement of point T	m
ω_{tx}	Turret roll rate[1]	rad/sec
ω_{ty}	Turret yaw rate[1]	rad/sec
ω_{tz}	Turret pitch rate[1]	rad/sec
ω_{gx}	Gun axial-spin (roll) rate[2]	rad/sec
ω_{gy}	Gun traverse (yaw) rate[2]	rad/sec
ω_{gz}	Gun elevation (pitch) rate[2]	rad/sec
DE	Gun elevation rate relative to hull	rad/sec

[1]with respect to frame $Bx_By_Bz_B$

[2]with respect to frame $Cx_Cy_Cz_C$

SYMBOL	DESCRIPTION	UNIT
DTR	Turret traverse rate relative to hull	rad/sec
ELVV	Elevation control voltage	volts
VIN	Traverse control voltage	volts
ΣM_t	Sum of turret external moments	N-m
TQTR	Turret control torque	N-m
FTQTR	Sum of turret friction torques	N-m
DSTQTR	Turret disturbance torque	N-m
ΣM_g	Sum of gun external moments	N-m
TQEL	Elevation control torque	N-m
FTQEL	Sum of gun friction torques	N-m
DSTQEL	Gun disturbance torque	N-m
ΣF_s	Total vertical suspension force	N

SYMBOL	DESCRIPTION	UNIT
ΣM_{sx}	Suspension moment about x_h axis	N-m
ΣM_{sz}	Suspension moment about z_h axis	N-m
ΣM_{sy}	Suspension moment about y_h axis	N-m
Pg	Gun pitch angle	rad
Rg	Gun roll angle	rad
Yg	Gun yaw angle	rad
C3	Actuator moment arm	m

PARAMETERS

SYMBOLS	DESCRIPTION	UNIT	VALUE	SOURCE
m_v	Total vehicle mass.	Kg	47695	C
m_h	Hull mass	Kg	35158	C
m_t	Turret mass	Kg	9225	C
m_g	Gun mass	Kg	3311.9	A
d_1	x_h- Distance, vehicle CG to hull CG	m	-.11	C
d_2	y_h- Distance, vehicle CG to hull CG	m	.74	C
d_3	z_h- Distance, vehicle CG to hull CG	m	0.	C
d_{11}	x_B- Distance, TR-axis to turret-gun CG	m	-.0022	C
d_{12}	y_B- Distance, TR-axis to turret-gun CG	m	.054	C
J_{hx}	Hull x_A- axis inertia	kg-m^2	58970.	C
J_{hy}	Hull y_A- axis inertia	kg-m^2	90370.	C
J_{hz}	Hull z_A- axis inertia	kg-m^2	187750	C
J_{tx}	Turret x_B- axis inertia	kg-m^2	2775.5	C

SYMBOLS	DESCRIPTION	UNIT	VALUE	SOURCE
J_{ty}	Turret y_B- axis inertia	kg-m^2	22670	C
J_{tz}	Turret z_B- axis inertia	kg-m^2	12352	C
J_g	Gun inertia	kg-m^2	5169.8	A
Y_{CG}	y_h- Distance, point T to vehicle CG	m	.98	C
DHT	Turret-hull viscous damping coefficient	N-m-s	75.936	A
CFE	Viscous damping coef. at trunnion	N-m-s	1627.2	A
CFT	Traverse coulomb friction coefficient		1600.	A
R43	Gear ratio	-	21.428	A
R12	Gear ratio	-	.02331	A
GR12	Gear ratio[1]	-	919.3	A
G_{VA}	TR- servo valve torque motor gain	ma/volt	2.	A
DSA	TR- servo valve dead band	ma	.0262	A

[1]GR12 = R43/R12

SYMBOLS	DESCRIPTION	UNIT	VALUE	SOURCE
K_1	TR- Servo valve flow coefficient	$\frac{m^4}{N^{\frac{1}{2}}\text{-ma-s}}$	$3.158\text{x}10^{-8}$	A
τ_{CV}	TR- Servo valve torque motor time constant	sec	.008	A
DSPM	Hydraulic motor displacement	m^3/rad	$2.098\text{x}10^{-6}$	A
β_m	Bulk modulus of hydraulic fluid	N/m^2	$1.293\text{x}10^{-9}$	A
V_{OLTR}	TR- entrained volume	m^3	$4.916\text{x}10^{-4}$	A
K_L	Hydraulic motor leakage coefficient	$m^3\text{-Pa/s}$	$6.417\text{x}10^{-13}$	A
GTM	EL- servo valve torque motor gain	ma/volt	2.	A
G_V	EL- servo valve 1st stage gain	Pa/ma	537810.	A
A_A	El- servo valve amplifier area	m^2	$2.303\text{x}10^{-5}$	A
F_A	El- servo valve feedback area	m^2	$1.123\text{x}10^{-5}$	A
K_D	El- servo valve droop constant	$Pa\text{-s}/m^3$	$4.675\text{x}10^{9}$	A
f_s	El- servo valve spool friction coef.	N-s/m	35.02	A
L_s	El- servo valve spool limit	m	$2.794\text{x}10^{-4}$	A
A_P	Actuator piston area	m^2	$3.045\text{x}10^{-3}$	A
V_{OLE}	El- entrained volume	m^3	$8.948\text{x}10^{-4}$	A

SYMBOLS	DESCRIPTION	UNIT	VALUE	SOURCE
K_L	El- leakage flow coefficient	m^3-Pa/s	1.188×10^{-12}	A
τ_{ME}	El- servo valve torque motor time constant	sec	.02	A
K_{1E}	El- servo valve flow coefficient	$\frac{m^3}{N^{\frac{1}{2}}\text{-s}}$	7.304×10^{-4}	A
AZGY	TR- rate gyro gain	Volts-s/rad	150.	A
GYK	El- rate gyro gain	Volts-s/rad	150	A
LRS	Rate sensor limits	rad/sec	.175	A
P_S	Hydraulic supply pressure	Pa	1100	A
g	Gravity	m/s^2	9.81	
T	Control time interval	sec	0.01	D

Source code for values:

A. Ref. [4] Systems Analysis Report, A.P. Kaminsky

B. Hitpro run supplied by Dr. Coleman of Picatinny Arsenal

C. Values calculated by author using source B. The changes are due to the replacement of the small gun (electric drive) by the large gun (hydraulic drive).

D. Value assumed by author.

APPENDIX B: Hydraulic System with Stochastic Optimal Control

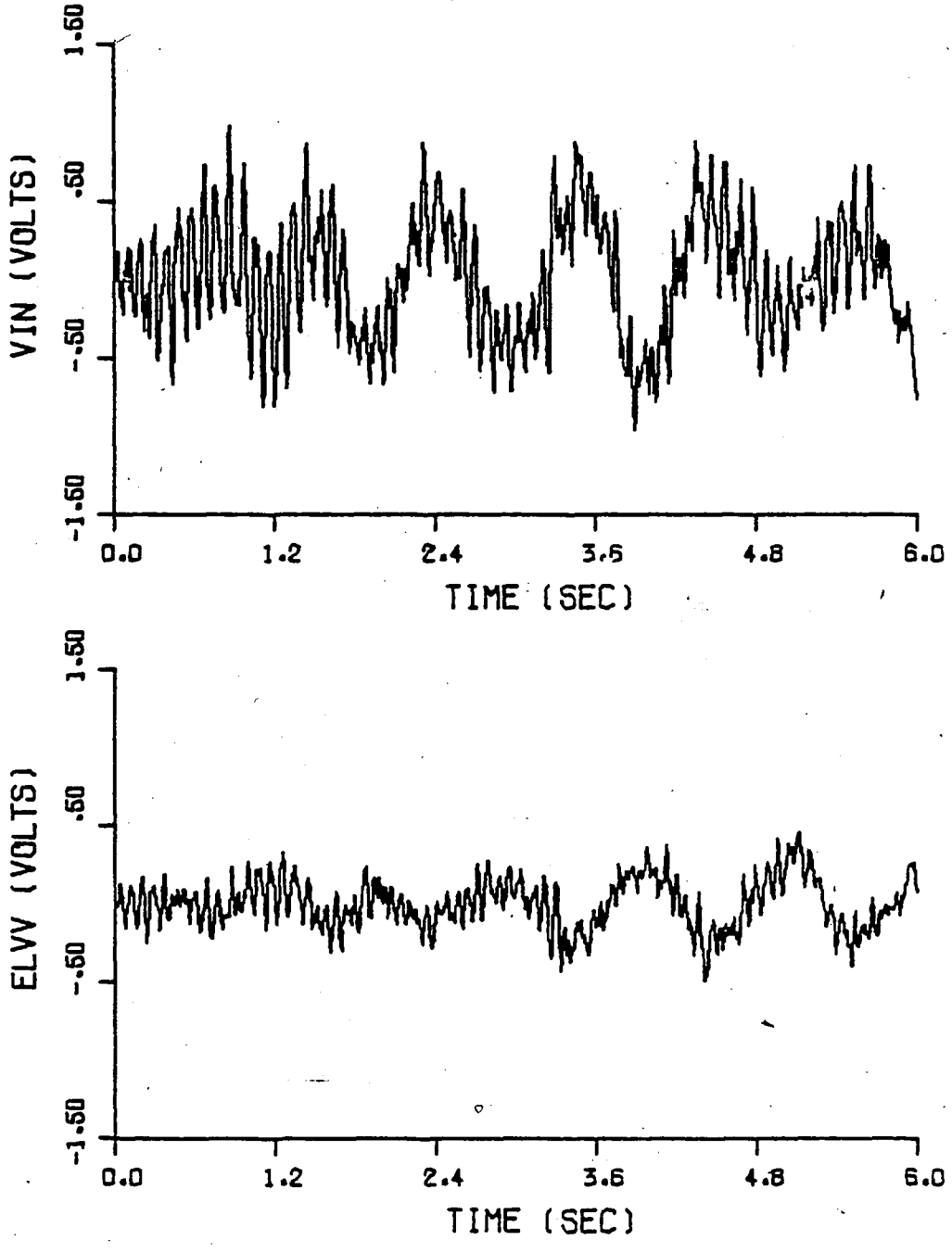

Fig. B1 Traverse (VIN) and Elevation (ELVV) Controller Outputs, Stochastic Optimal Control, Hydraulic Gun Drives.

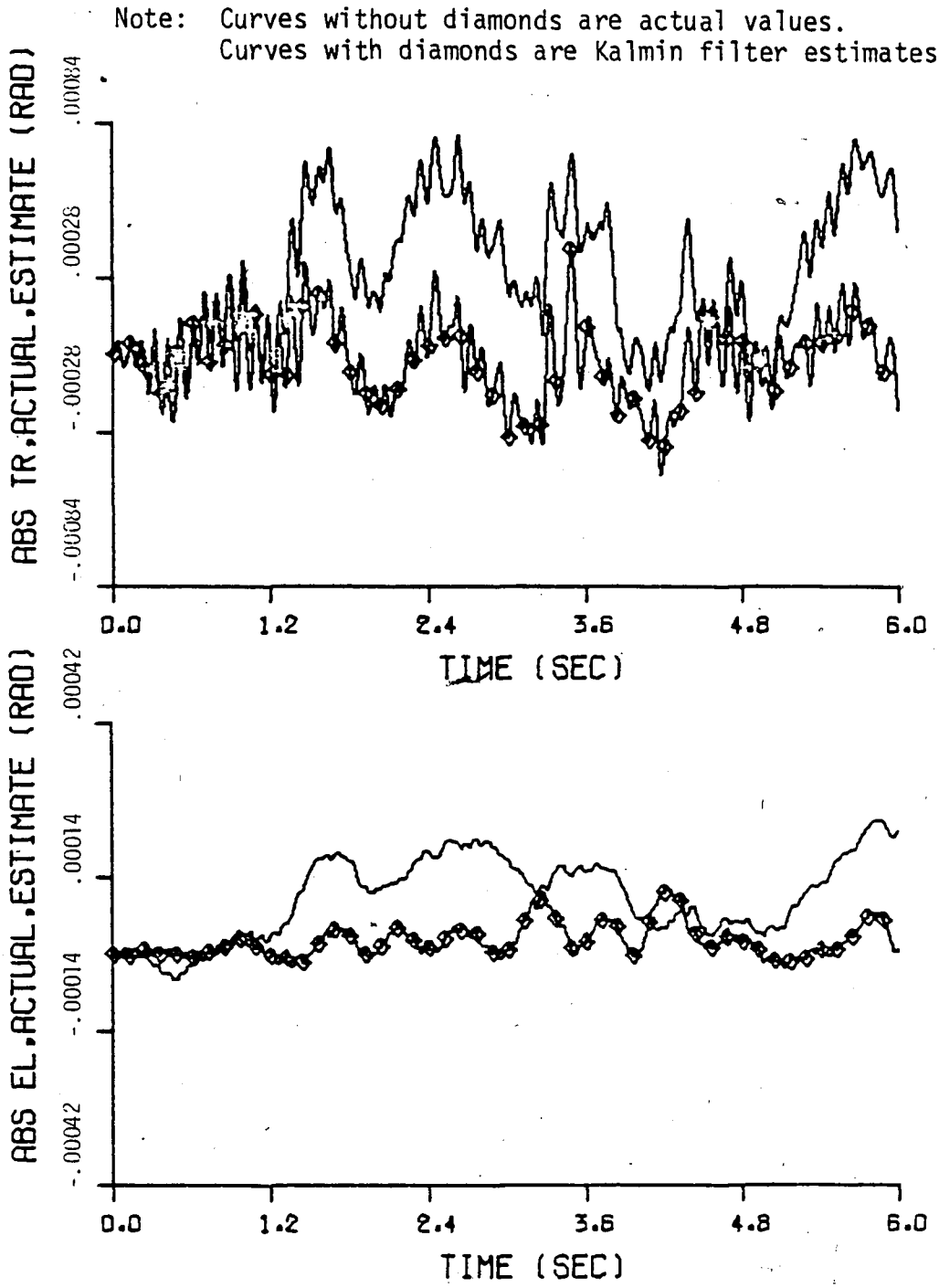

Fig. B2 Absolute Traverse and Elevation Pointing Errors, Stochastic Optimal Control, Hydraulic Gun Drives.

APPENDIX C: Electric System with Conventional Control

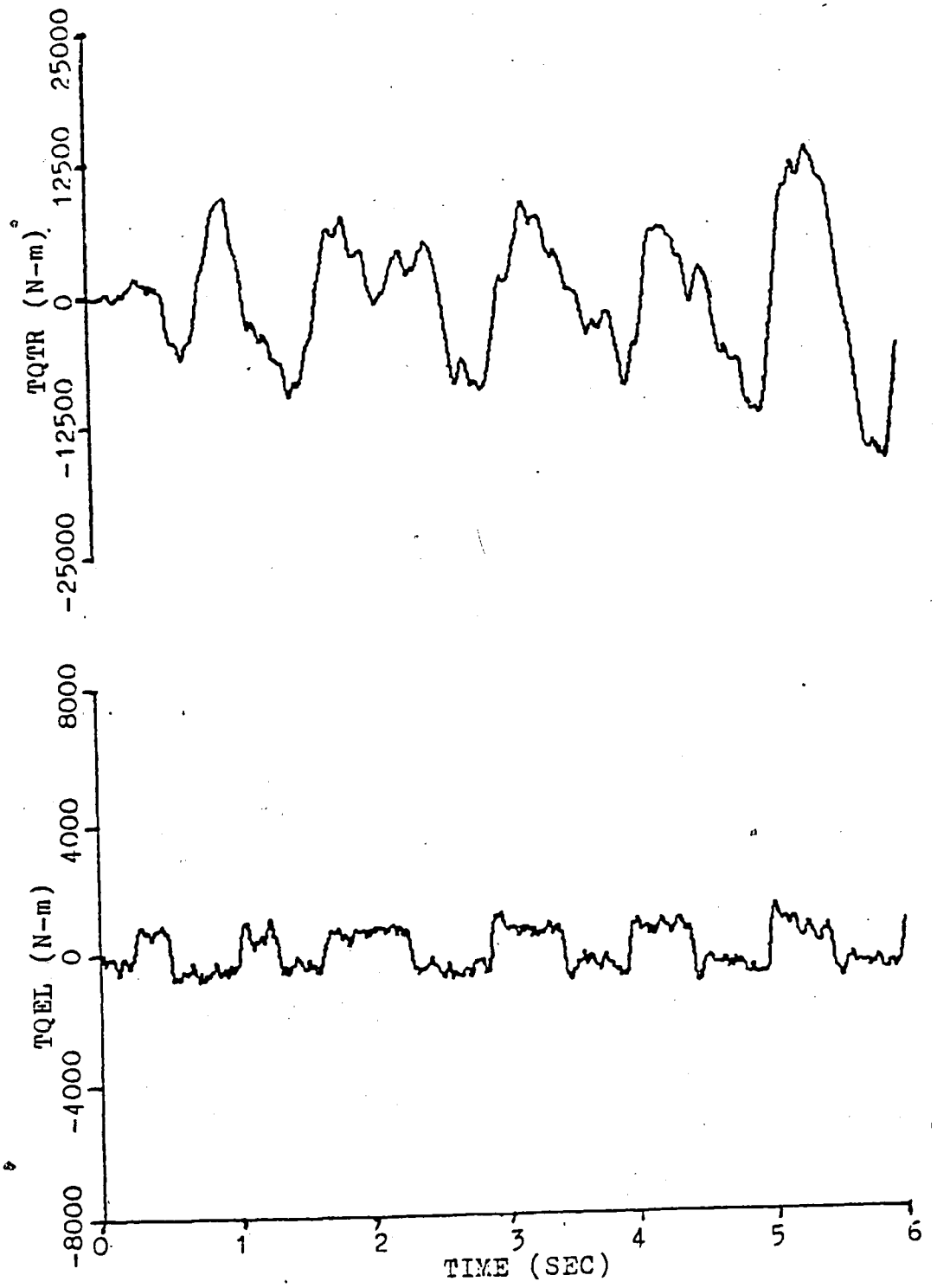

Fig. C1 Traverse (TQEL) and Elevation (TQEL) Controller Outputs, Conventional Control, Electric Gun Drives.

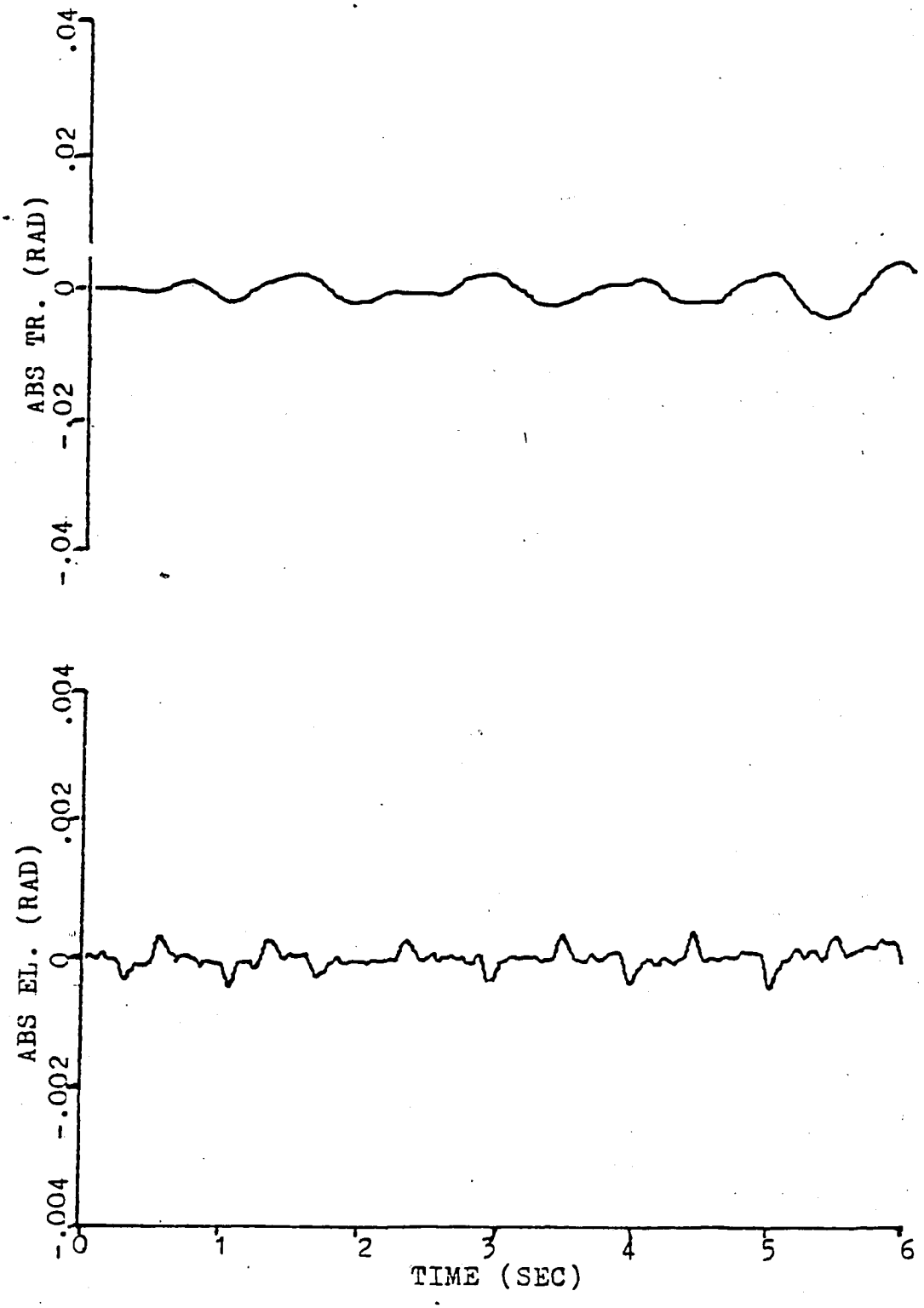

Fig. C2 Absoluate Traverse and Elevation Pointing Errors, Conventional Control, Electric Gun Drives.

APPENDIX D: Electric System with Stochastic Optimal Control

Note: Curves without diamonds are actual values.
Curves with diamonds are Kalman filter estimates.

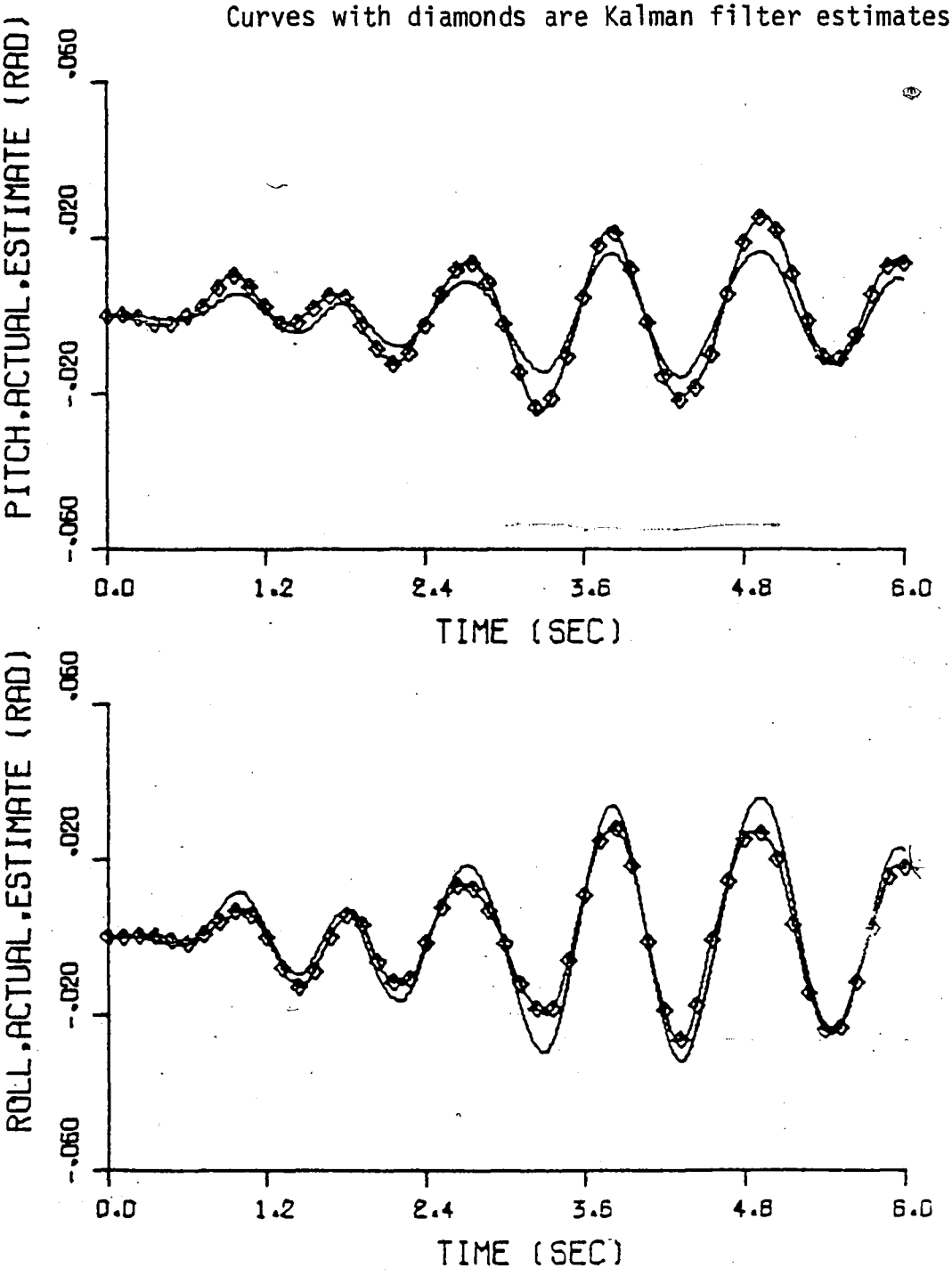

Fig. D1 Hull Pitch and Roll Angles, Stochastic Optimal Control, Electric Gun Drives.

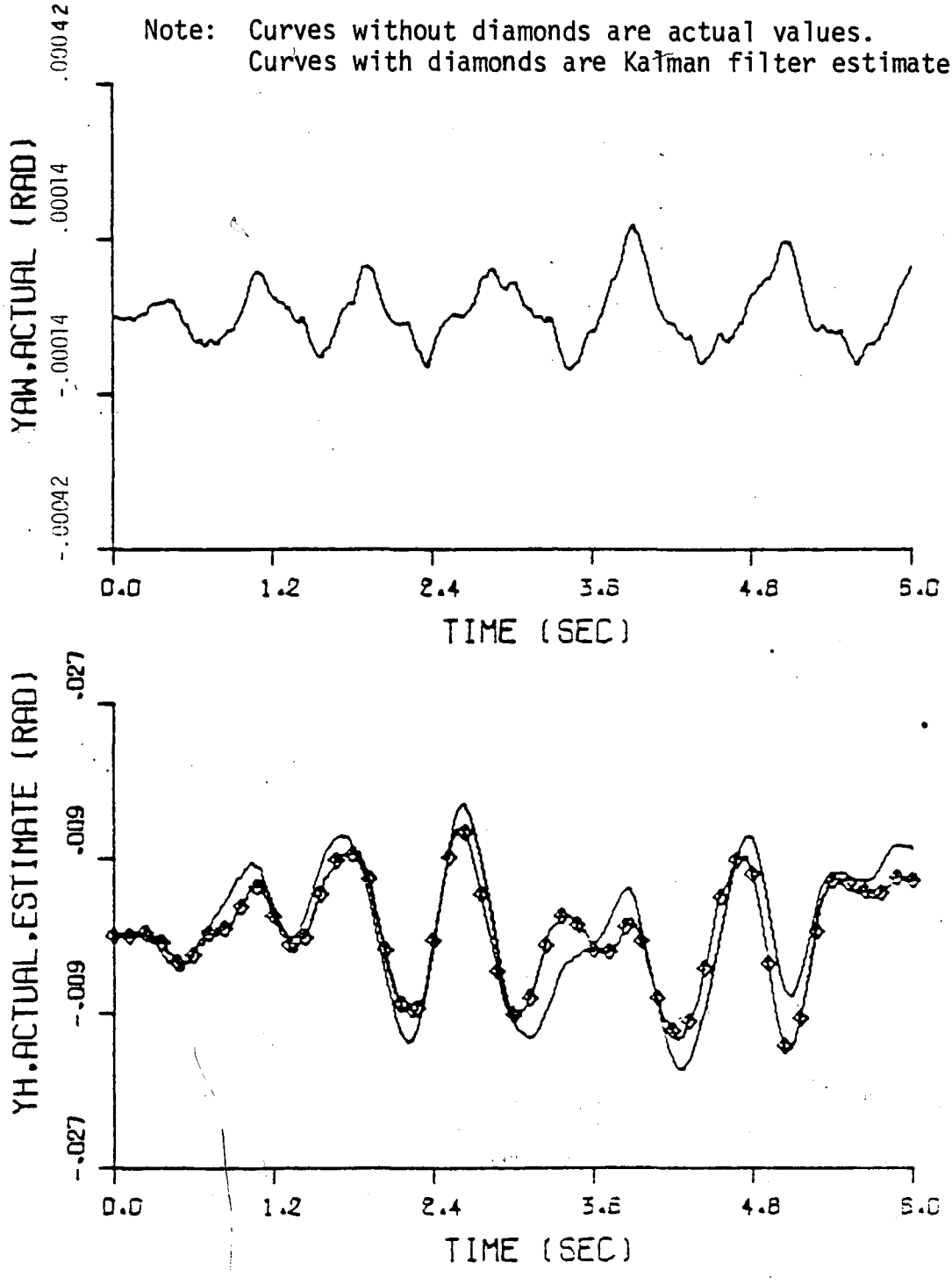

Fig. D2 Hull Yaw Angle and Vertical Position, Stochastic Optimal Control, Electric Gun Drives.

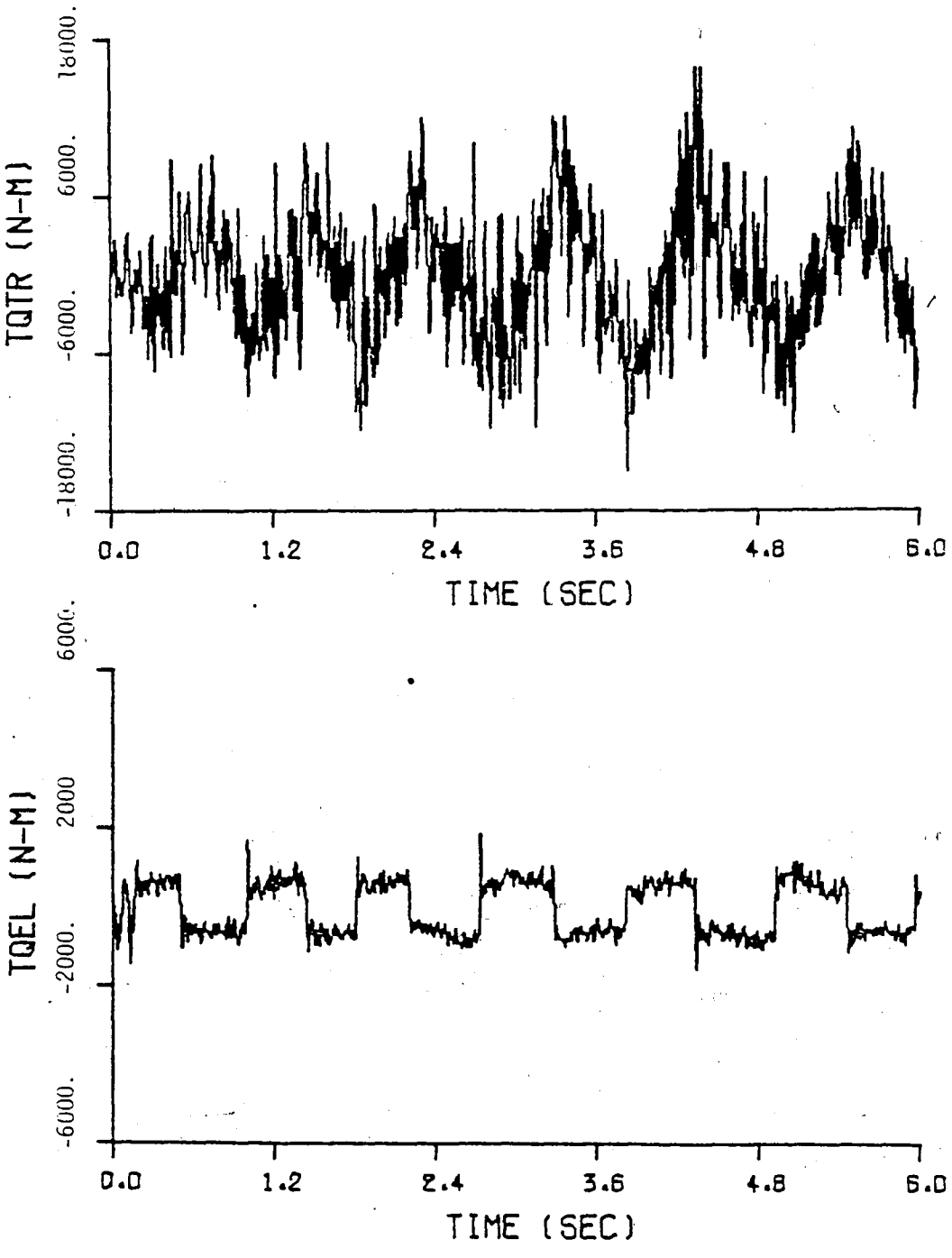

Fig. D3 Traverse (TQTR) and Elevation (TQEL) Controller Outputs, Stochastic Optimal Control, Electric Gun Drives.

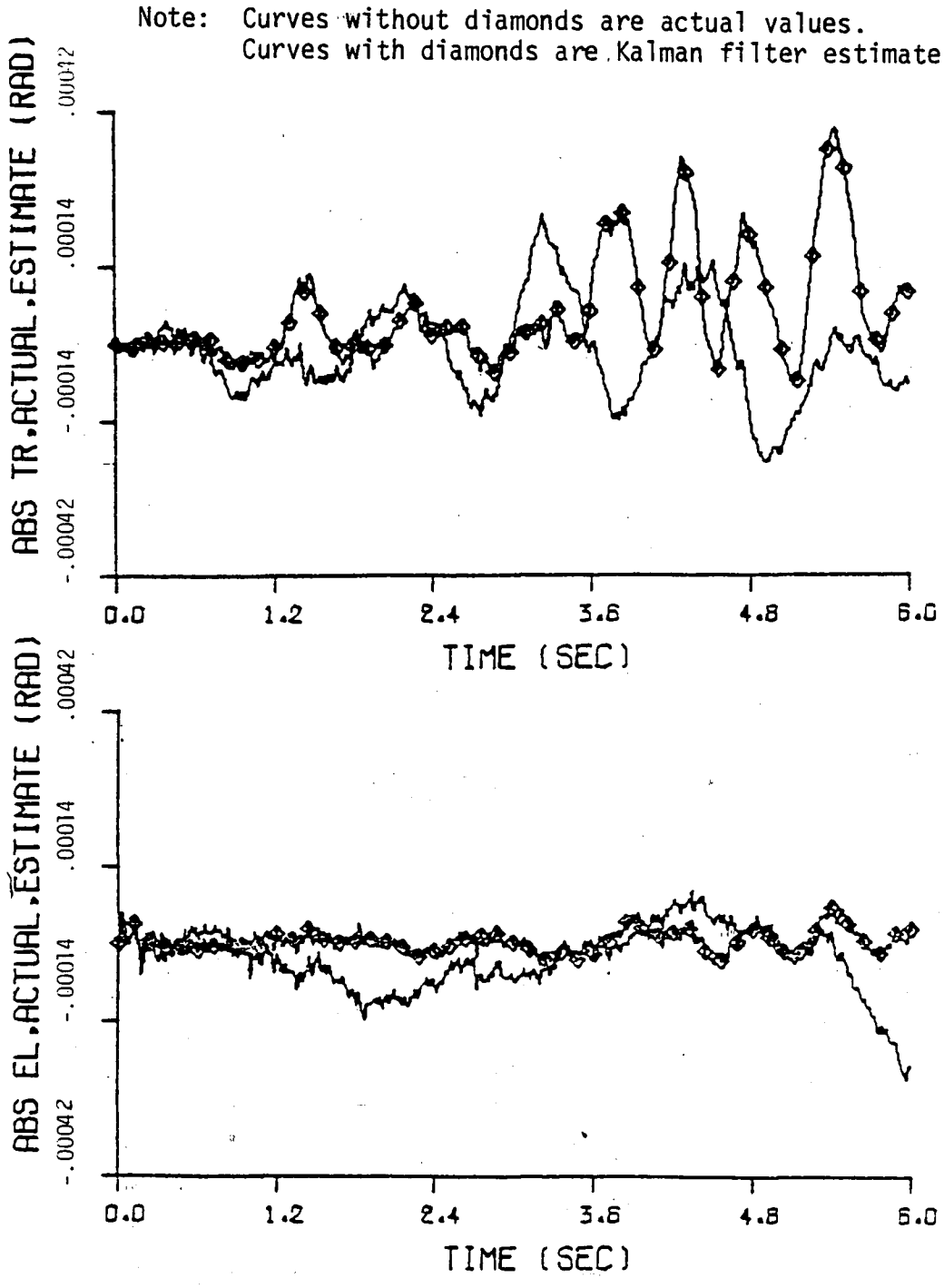

Fig. D4 Absolute Traverse and Elevation Pointing Errors, Stochastic Optimal Control, Electric Gun Drives.

VITA

David Alfred Haessig, Jr. was born on July 4, 1957 to David Alfred and Carolynn Vreeland Haessig in Boonton, New Jersey. David is the first of three children in his family. He grew up in Towaco, New Jersey, graduating from Montville High School, Montville, New Jersey in June 1975. Four years later he graduated with high honors from Lehigh University, Bethlehem, Pennsylvania receiving a B.S. in Mechanical Engineering.

During the summer of 1979, David was employed as a research assistant under Dr. S.H. Johnson, Lehigh University. As a result, he coauthored with Dr. Johnson the report "The Implementation of a Computer Model of the M60 Tank Stabilization System." At the end of the summer, he married Miss Kathleen M. Carroll, also of Towaco, New Jersey.

In September 1979, David enrolled as a master's candidate at Lehigh University. At this time he began employment as a research assistant under Dr. F.T. Brown to assist in the development of modern control schemes to improve tank turret stabilization. He remained in this capacity for eighteen months. During this period he coauthored with his advisor the report "Modern Control Concepts Applied to Disturbance Accommodation of Tank Turrets - Phase II."

Upon completion of his graduate studies in January 1981, David plans to begin employment with an industry involved in systems engineering and control.